Nouvelles méthodes de détermination des métaux dans les cendres volantes

Alice Stankova

N° d'ordre : 20-2010

Année : 2010

THESE DE L'UNIVERSITE DE LYON

Délivrée par

L'UNIVERSITE CLAUDE BERNARD LYON 1

ECOLE DOCTORALE DE CHIMIE

DIPLOME DE DOCTORAT

Spécialité : Chimie

(Arrêté du 7 août 2006)

par

Alice STAŇKOVÁ

TITRE :

Nouvelles méthodes de déterminations des métaux dans des déchets solides valorisables

Directeurs de thèse :

Mme Nicole GILON-DELEPINE

M Viktor KANICKÝ

JURY : M Didier LEONARD

M Karol FLORIÁN

M Ryszard LOBINSKI

Mme Nicole GILON-DELEPINE

M Viktor KANICKÝ

UNIVERSITE CLAUDE BERNARD - LYON 1

Président de l'Université	**M. le Professeur L. Collet**
Vice-président du Conseil Scientifique	M. le Professeur J-F. Mornex
Vice-président du Conseil d'Administration	M. le Professeur G. Annat
Vice-président du Conseil des Etudes et de la Vie Universitaire	M. le Professeur D. Simon
Secrétaire Général	M. G. Gay

COMPOSANTES SANTE

Faculté de Médecine Lyon Est – Claude Bernard	
Faculté de Médecine Lyon Sud – Charles Mérieux	Directeur : M. le Professeur J. Etienne
UFR d'Odontologie	Directeur : M. le Professeur F-N Gilly
Institut des Sciences Pharmaceutiques et Biologiques	Directeur : M. le Professeur D. Bourgeois
Institut des Sciences et Techniques de Réadaptation	Directeur : M. le Professeur F. Locher
Département de Formation et Centre de Recherche en Biologie Humaine	Directeur : M. le Professeur Y. Matillon Directeur : M. le Professeur P. Farge

COMPOSANTES SCIENCES ET TECHNOLOGIE

Faculté des Sciences et Technologies	Directeur : M. le Professeur F. Gieres
UFR Sciences et Techniques des Activités Physiques et Sportives	Directeur : M. C. Collignon
Observatoire de Lyon	Directeur : M. B. Guiderdoni
Institut des Sciences et des Techniques de l'Ingénieur de Lyon	Directeur : M. le Professeur J. Lieto
Institut Universitaire de Technologie A	Directeur : M. le Professeur C. Coulet
Institut Universitaire de Technologie B	Directeur : M. le Professeur R. Lamartine
Institut de Science Financière et d'Assurance	Directeur : M. le Professeur J-C. Augros
Institut Universitaire de Formation des Maîtres	Directeur : M. R. Bernard

ABSTRACT

Solid waste generated by our society are numerous, fly ashes are produced during the combustion of domestic or industrial waste in incinerators. Fly ashes are also produced through coal combustion in coal fired power plants. Fly ashes are results of these combustions and represent important quantity of wastes produced every year by our society. They have variable use – in construction, road industry, or they can be stocked for further use. As they are result of different origin, they have complex mineral and elemental composition. As a by-product or as a recycled product fly ashes fate is important to determine. In this view the determination of the elemental composition of fly ashes is the aim of this work.

Conventional methods of sample preparation are acid digestion or alkali fusion. These procedures are time and reagent consuming and complete digestion is not assured. The potential contamination of the reagents employed is important during these classical sample preparation methods.

During the past decade, development of direct solid sampling using laser ablation methods was important due to the need of reducing analysis time and also reducing reagent consumption. In this work, two methods based on laser ablation will be studied for fly ash analysis: Laser Induced Breakdown Spectroscopy (LIBS) and Laser Ablation Inductively Coupled Plasma Mass Spectrometry (LA-ICP-MS). LIBS will be studied for quantitative determination of major elements in fly ash samples while Laser ablation / ICP MS will be employed for trace element determination.

The sensitivity optimization and different calibration strategies are key problems of laser sampling methods. Sample preparation and condition optimisation were performed to determine major, minor and trace elements such as Al, As, Ba, Ca, Cr, Cu, Fe, Mg, Mn, Pb, Sr, V and Zn by both methods – LIBS for major elements and LA-ICP-MS for minor and trace elements.

Figures of merit such as detection limits, accuracy and calibration strategy were obtained following suitable developments and optimisation of instrument settings and a careful selection of binders and internal standards. Appropriate conditions were selected to determine the elements in fly ash samples.

In conclusion, direct solid sampling using laser ablation followed by LIBS or for solid introduction into ICP was found to determine major, minor and trace elements in fly ashes, improving pellets mechanical stability, high samples sensitivity and acceptable accuracy and detection limits.

KEY WORDS:

Laser ablation, fly ash, inductively coupled plasma (ICP), LIBS, LA-ICP-MS

RESUME

Les déchets solides générés par notre société sont nombreux. Les cendres volantes sont des déchets solides produits lors de la combustion de déchets domestiques ou industriels dans des incinérateurs. Les cendres volantes sont également produites par la combustion du charbon dans les centrales à charbon. Les cendres volantes sont le résultat de ces combustions et représentent une importante quantité de déchets produits chaque année par notre société. Les possibilités de recyclage de ces déchets sont nombreuses : dans la construction, l'industrie routière. Elles sont également stockées pour une utilisation ultérieure. Les origines différentes des charbons et déchets incinérés conduisent à une minéralogie et une composition élémentaire complexe. En tant que sous-produit le devenir des cendres volantes est important à déterminer, aussi la détermination de la composition élémentaire de ces cendres volantes est indispensable.

Les méthodes classiques de préparation des échantillons solides sont la minéralisation acide ou la fusion alcaline. Ces procédures prennent du temps et supposent l'utilisation de réactifs, de plus la digestion complète n'est pas toujours assurée. Le risque de contamination par les réactifs employés est important lors de ces méthodes classiques de préparation.

Au cours de la dernière décennie, le développement d'analyses directes d'échantillonnages des solides en utilisant des méthodes d'ablation laser a été important en raison de la nécessité de réduire le temps d'analyse ainsi que la consommation de réactifs. Dans ce travail, deux méthodes basées sur l'ablation par laser seront étudiées pour l'analyse des cendres: Laser Induced Breakdown Spectroscopy (LIBS) et Laser Ablation Inductively Coupled Plasma Mass Spectrometry (LA-ICP-MS). La spectrométrie LIBS sera étudiée pour la détermination quantitative des éléments majeurs dans les échantillons de cendres alors que le couplage ablation laser ICP / MS sera employé pour détermination des éléments traces.

L'optimisation de la sensibilité et les stratégies d'étalonnage sont les principaux problèmes traités dans ce travail. La préparation des échantillons et l'optimisation ont été effectuées pour déterminer les éléments tels que Al, As, Ba, Ca, Cr, Cu, Fe, Mg, Mn, Pb, Sr, V et Zn par les deux méthodes.

Les performances analytiques telles que les limites de détection, la justesse ont été obtenus à la suite d'optimisations instrumentales ainsi que d'une sélection des liants employés et de la sélection de l'étalon interne approprié.

En conclusion, l'analyse directe de solides en utilisant les techniques basées sur l'ablation laser développées dans ce travail conduisent à une justesse acceptable pour la détermination des éléments majeurs et traces dans les cendres volantes.

MOTS-CLES:

Cendres volantes, ablation laser, inductively coupled plasma mass spectroscopy (ICP-MS), LIBS

INTITULE ET ADRESSE DE L'U.F.R. OU DU LABORATOIRE :

UMR5180 Laboratoire des Science Analytique, Bat.CPE, Boulevard du 11 Novembre, 69 100 VILLEURBANNE, FRANCE

ABBREVIATIONS

OES: Optical Emission Spectrometry

CCD: Charge Coupled Device

EDS: Energy dispersive X-Ray spectroscopy

IS: Internal standard

eV: electron Volt

FX: Fluorescence X

ICP: Inductively Coupled Plasma

IR: Infra Rouge

LA: Ablation Laser (Laser Ablation)

LA-ICP: Laser ablation-Inductively Coupled Plasma

LA-ICP-AES: Laser Ablation Inductively Coupled Plasma Atomic Emission Spectroscopy

LA-ICP-MS: Laser Ablation Inductively Coupled Plasma Mass Spectroscopy

LASER: Light Amplification by Stimulated Emission of Radiation

LIBS: Laser Induced Breakdown Spectroscopy

LOD: Limit Of Detection

MS: Mass spectrometry

NIST: National Institute of Standards and Technology

PM: Photomultiplier

Ppm: Part Par Million (mg/kg)

Ppb: Part Per Billion (µg/kg)

RSD: Relative Standard Deviation

SEM: Scanning electron microscopy

Snet: Signal net

TOF-MS: Time Of Flight – Mass spectrometry

XPS: X-ray Photoelectron Spectroscopy

XRF: X-ray fluorescency

YAG: Yttrium Aluminum Garnet

I INTRODUCTION: LITERATURE SURVEY AND AIM OF THIS WORK

I.1 DEFINITION AND PRODUCTION OF FLY ASHES

The quantity of fly ashes produced after coal combustion in power plants or after domestic or industrial waste combustion in municipal waste incinerators increase every year. There are different possibilities how the fly ash can be valorised. First is the possibility to stock them or to use them in building or road industry. This is why is important to know their chemical composition. Several methods of fly ash sample preparation for analysis exist.

I.1.1 DESCRIPTION OF FLY ASHES

Fly ash is a fine particulate ash made by the combustion of a solid fuel such as coal or by combustion of domestic and industrial waste which is discharged as an airborne emission, or it can be recovered as a by-product for various commercial uses. It is only one of a variety of waste materials that is generated every year by the coal industry or by massive municipal waste incinerators.
There are two main groups of fly ash. These are produced by the coal industry and by municipal waste incinerators. The two main reasons why the production of fly ash has increased in recent years are the increasing consumption of fossil fuels and because people are increasing industrial and domestic waste production.

I.1.1.1 Fly ash produced by the coal industry

The combustion of fossil fuels, primarily coal, has increased in recent years because of increasing human population and higher demand for electrical energy. **Figure I. 1** shows the growth in U.S. and world coal combustion, predicted to the year 2040. As combustion has increased, the amount of waste materials produced by the coal industry has grown too. It is important to find a way of re-using waste materials and it is for this reason that it is very important to know the elemental composition of these waste products. The second reason is to avoid possible health risks. Coal contains trace amounts of heavy metal elements. The burning of coal means that some of these elements are oxidised in the production of coal ash. Typically, these heavy metals include arsenic, boron, cadmium, chromium, copper, lead, selenium and zinc. The U.S. Environmental Protection Agency (EPA) started an extensive study in 1988 about the possible hazardous risk that coal presents to the environment. The EPA concluded that the ash does not exhibit hazardous characteristics and does not require regulations because it is not a hazardous waste.

As stated earlier, coal ash contains varying concentrations of heavy metals. Despite the large volumes of ash produced, the total quantity of heavy metals is relatively small. An even smaller amount of these elements will be released into the environment. The largest quantities of heavy metals are in the form of manganese, barium and vanadium. Deposits of fuel ashes are a serious problem and a source of inorganic pollution. Knowledge of the chemical and physical properties of the ashes is important to assess the risk of potential environmental mobility of toxic trace metals [1]. Results of the content of heavy metals in samples coming from coal processing revealed that high concentrations of toxic elements in those materials could cause releasing them to the environment during unproper storage or application for agricultural or building purposes [2]. Although they are not hazardous, specially designed landfills are required to prevent the possible leaching of trace elements from fly ash that can reach drinking water sources. Coal contains naturally occurring radioactive elements, but studies show that the level of radioactivity in combustion products is about the same as the level found in surface rocks and soil. Another example of a potential health risk is the presence of mercury in combustion products, which can be potentially released into the environment. Studies show only tiny losses into the environment and a loss of only 1 percent of the initial concentration of mercury into the water when given a leaching test [3].

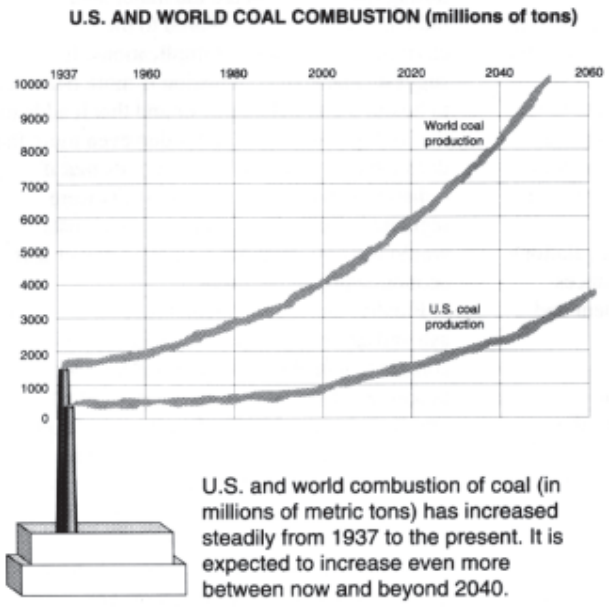

Figure I. 1: U.S. and world coal combustion growth [4].

I.1.1.2 Fly ash produced by industry and municipal waste incinerators

It is estimated that Europe annually produces over 250 million tonnes of municipal waste and more than 850 million tonnes of industrial waste. There are increasing amounts of discarded products which contain substances now recognised to be toxic or highly toxic which can be transported in the air or can accumulate in contaminated ashes. As in the case of coal fly ash, and also incinerator fly ash, these contain metals such as cadmium, lead, mercury, chromium, tin and zinc. When chemical substances in waste are not combusted properly, organic compounds are released as non combusted residues. Municipal and industrial fly ash is recycled and used as landfill as coal fly ash [5].

The possibility of contamination of ground water is the same in both cases of fly ash. The diagram of the mercury cycle in the environment, in **Figure I. 2**, shows the different forms of mercury, their concentrations in nature and the possibility of contaminating the water source or soil [6].

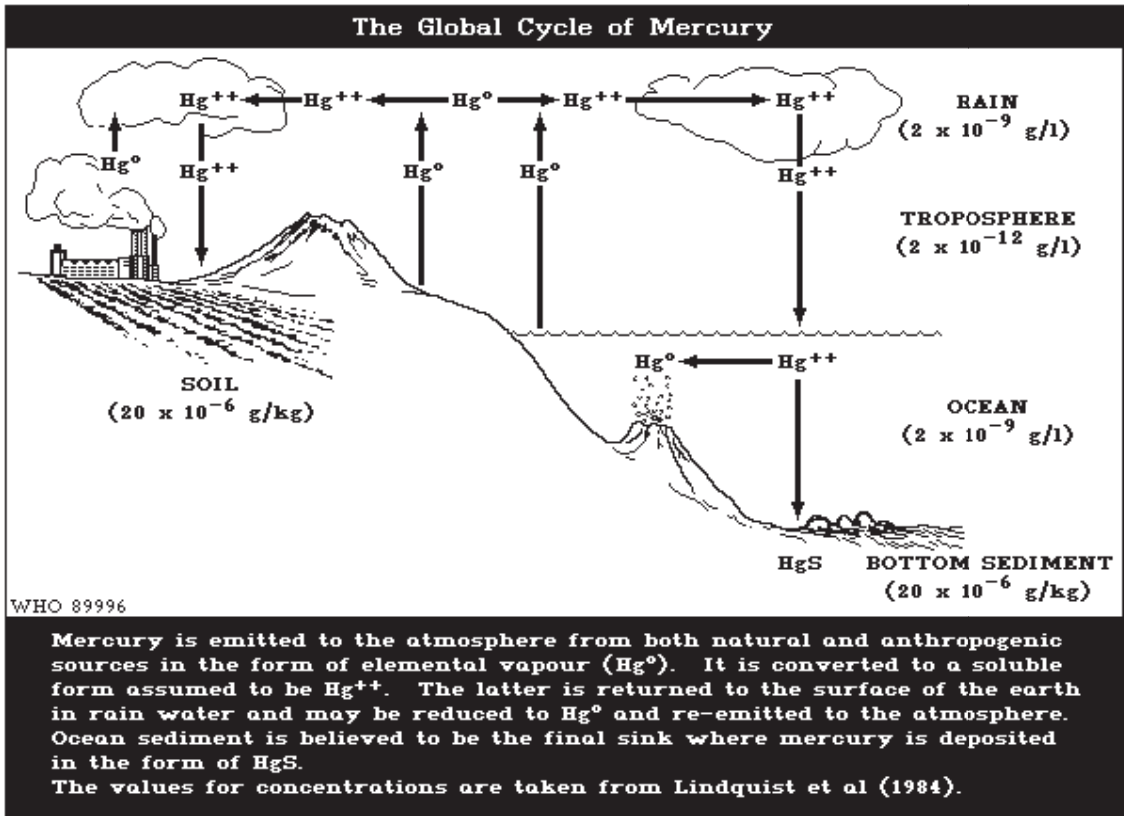

Figure I. 2: Diagram of the mercury cycle.

I.1.2 How is fly ash produced?

Fly ash is produced during the combustion of coal or domestic waste in incinerators. Different mechanisms are used for the combustion of coal and the combustion of domestic and industrial waste.

I.1.2.1 Production of coal fly ash

Coal fly ash is produced during coal combustion in a combustion chamber. Coal that has been pulverised is the most commonly used method in coal-fired power plant combustion which produces the very fine nature of fly ash.

There are three types of coal-fired boiler furnaces used in the electric utility industry. They are: dry-bottom boilers, wet-bottom boilers and cyclone furnaces. The resulting combustion by-products include wet-bottom boiler slag, dry-bottom ash, economiser ash and fly ash. The type of ash produced is dependent on both the boiler type and its design. Wet bottom boiler slag is produced when the molten coal residue material is released to a water filled hopper below the boiler – the resulting slag is glass-like. Dry-bottom ash is the ash product derived from burning coal in dry bottom boilers. The dry-bottom ash is the coarser coal residual material that falls through the bottom grates into hoppers, below the fire chamber. Dry-bottom ash is the largest of the ashes and can range in size from 19 to 75 mm. Economiser ash is composed of the larger, heavier portions of the fly ash that are collected bellow the economiser unit in electrostatic precipitators. Economiser ash is generally not used with the finer fly ash because it has poor chemical reactivity properties. Fly ash is the fine portion of the coal combustion chamber. It is collected by mechanical means, such as electrostatic precipitators.

When pulverised coal is combusted in a dry-ash, dry-bottom boiler, about 80 % of the ash escapes the furnace as fly ash, through the flue gas. When pulverised coal is combusted in a wet-bottom (or slag-tap) furnace, as much as 50 % of the ash stays in the furnace, with the other 50 % escaping in the flue gas. In a cyclone furnace, where crushed coal is used as the fuel, 70 to 80 % of the ash is retained as boiler slag and only 20 to 30 % escapes the furnace as dry ash in the flue gas [7]. A general schematic diagram of coal combustion and ash production is presented in **Figure I. 3**.

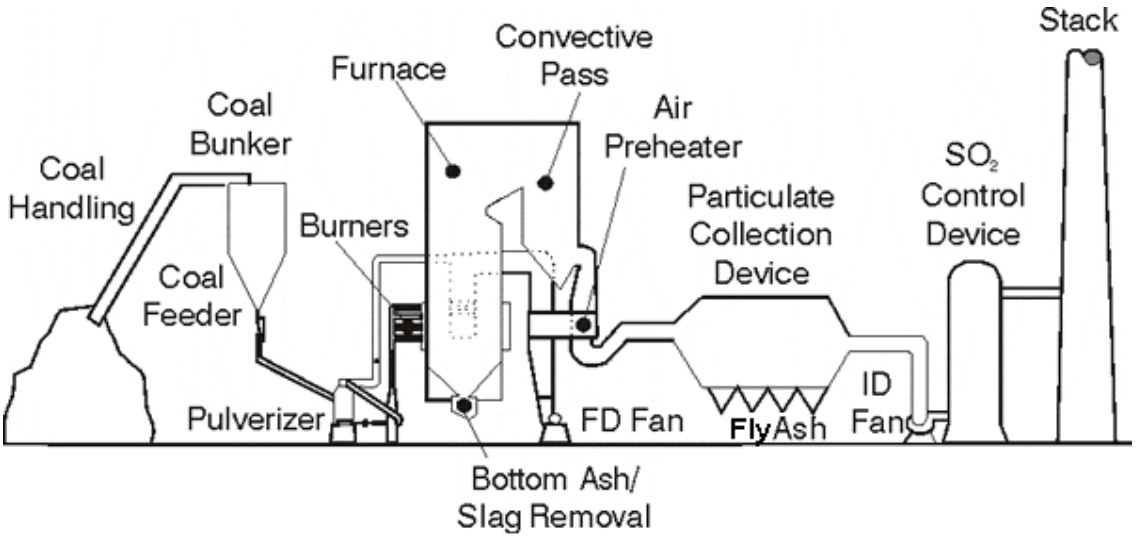

Figure I. 3: A schematic diagram of a typical pulverised coal combustion process. In this system, the coal is firstly ground to a fine powder and then combusted [8].

Fly ash is an incombustible mineral matter, a fine-grained, powdery particulate material that is carried off with the flue gas and collected by some cleaning equipment in the flue gas stack; there are usually electrostatic precipitators, baghouses, or mechanical collection devices such as cyclones. Fly ash generally ranges in size from 0.5 to 200 µm and is composed mostly of silicon, aluminium, iron and calcium oxide, along with unburned carbon portions. However, it can contain from 20 to 50 trace elements.

I.1.2.2 Production of domestic and industrial fly ash

The production of domestic and industrial fly ash is present in **Figure I. 4**. A truck discharges (1) its content into a storage silo (2). The air in the storage silo might be dusty and may contain combustible or explosive gases if they are allowed to accumulate. For this reason, the gases are constantly drawn off at a high volume (4) and fed into the incinerator to remove any dangerous emissions of greenhouse type gases. The fires which might accidentally be produced in the silo are avoided by constantly monitoring the infra-red radiation and by using other detection equipment. From the silo, a grabbing device (3) lifts the waste and transfers it into a hopper which is equipped with a screen and a mill to break up the large items.

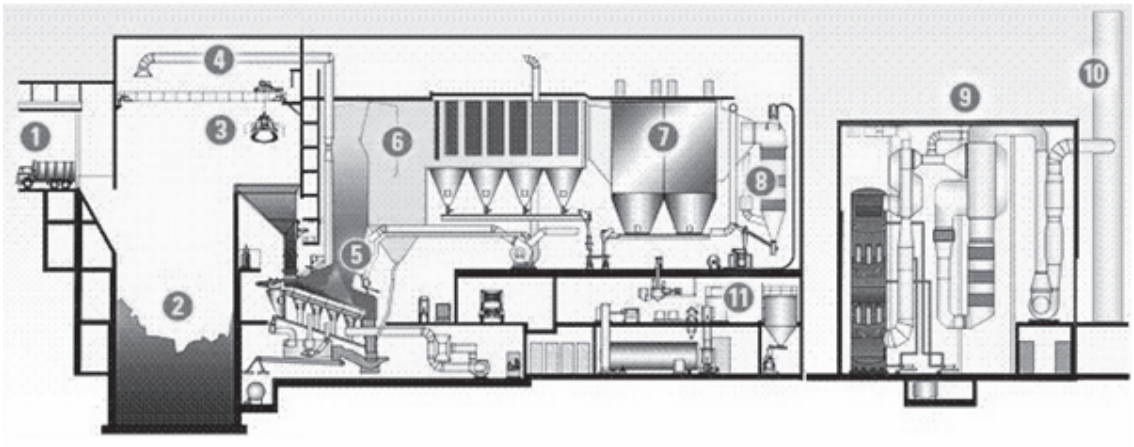

Figure I. 4: A diagram to enhance the value of waste [9].

The hopper pushes the rubbish into two incinerators and then it is put onto an inclined oscillating fire-bed (5). This has forced air fed from underneath to assist the combustion, which occurs at 1 000 to 1 200°C. The clinker (ash powder and rough hard remnants after coal has been burnt) falls through the fire-bed and to the bottom with a particle size of about 5 to 15 mm each, for further operating after cooling. A stream is generated in the boiler and superheated (6) through 40 km of pipe-work around which the flue gases circulate. The gases then go through an electrostatic precipitator (7) to eliminate most of the fly ash. They are then subjected to a series of treatments, starting with a water quench (8) where the pollutants are captured and treated, and residual fly ashes are removed (9), and they go through the chimney (10). Solids and water are treated to render them safe for the environment in a sophisticated series of operations. Waste water is treated with sodium hydroxide to precipitate heavy metals in the form of hydroxides, which are filtered out (11).

I.1.3 What are fly ash and its classification?

Determining the major and minor elements of fly ash is the first step for fly ash classification. The second step includes phase-mineral classification. Chemicals and minerals specify fly ash types and their properties. The third step evaluates potential industrial directions and environmental concerns of the fly ash, categorised according to its chemicals and minerals [10].

Fly ash is a pozzolanic material. Pozzolanic material is result of the process whereby coal is combusted, mineral matter transforms to fly ash and is then thermally altered into different forms, many of which are by themselves chemically very reactive, or which can be chemically activated. It is a siliceous material which in the presence of water will react with calcium hydroxide to produce a cement-type compound.

The possibility of characterising fly ash, useful for both the coal and industrial fly ash was proposed by the subcommittee of "Fly Ash Utilisation" at the United Nations. They suggested classification of fly ash into four groups according to chemical and physical characteristics.
These groups are:

- ☑ Group I – silico-aluminate fly ashes with SiO_2/Al_2O_3 ratio ≥ 2 and CaO < 15%;
- ☑ Group II – alumino-silicate fly ashes with SiO_2/Al_2O_3 ratio < 2, CaO < 15% and SO_3 < 3%;
- ☑ Group III – lime sulphate fly ashes with CaO > 15% and SO_3 < 3%;
- ☑ Group IV – basic fly ashes with CaO > 15% and SO_3 > 3%.

Fly ash from group I and II are acid and they do not have cement-like properties. Fly ash from group III and IV have high contents of CaO (including free CaO) and they belong to active or very active fly ash with cement-like properties.

The European Union countries use EN 450 standard (1995) for fly ash application as a common specification. However, almost every European country only uses a further specification.
The EN 450 standard includes:
-fineness (≤ 40.0% ± 10.0% on average value retained on 45 μm),
-loss on ignition (≤ 5.0% or ≤ 3-12% of national basis), and
-relative density (± 150 $kg.m^{-3}$ on nominal value), SO_3 (≤ 3.0%), free CaO (≤ 1.0% or ≤ 2.5% if soundness satisfactory), total CaO (≤ 10.0% only for sub-bituminous fly ash), reactive silica (≤ 25.0%), chloride (≤ 0.10%),
-there is no requirement about moisture, but fly ash should be stored and handled dry, or ≤ 0.5-1.5% on a national basis),
-and there are two classes of fineness, combustion of coal with biomass and waste, and fly ash processing.

Coal fly ash has been classified into three classes, C, F and N, based on a chemical composition of fly ash. According to ASTM C 618 (Standard Specification for Coal Fly Ash and Raw or calcified Natural Pozzolan for use in Concrete, ASTM International, American Society for Testing and Material Standards), the chemical requirements to classify fly ash are shown in **Table I. 1**.

Composition	C	F	N
$SiO_2 + Al_2O_3 + Fe_2O_3$ (min %)	50	70	70
SO_3 (max %)	5	5	4
Moisture content (max %)	3	3	3
Loss on ignition (max %)	6	6	10

Table I. 1: Chemical Requirements for Coal Fly Ash Classification.

Class C is pozzolanic and a cement-type fly ash normally produced from burning lignite or sub-bituminous coal. It usually contains significant amounts of Calcium Oxide (CaO) or lime.

Class F is a pozzolanic fly ash normally produced from burning anthracite or bituminous coal. This fly ash has siliceous or aluminous material, which itself possesses little or no cement-like value but will, when in powder form and in the presence of moisture, reacts chemically with calcium hydroxide at ordinary temperature to form cement-type compounds.

Class N is raw or calcifined natural pozzolan such as some diatomaceous earths, opaline cherts, and shales; tuffs, volcanic ashes, and pumicites; calcined clays and shales.

I.1.4 Physical and chemical properties

During the combustion process, the temperature in the furnace is from 1000 to 1700 °C depending on the type of fly ash. Fly ash is generated from various organic and inorganic constituents who are present in feed coals or waste. They have a complex composition; have a fine size and variable particle morphology and properties. This makes it difficult to identify and characterise how to use fly ash and its constituents.

Fly ash has a complex mixture of organic and inorganic materials with heterogeneous and variable composition. Fly ash contains closely associated and finely dispersed solid, liquid and gaseous components.

The phase and mineral composition of fly ashes includes:

- ☑ An inorganic constituent – composed of non-crystalline (amorphous) matter of different glass particles, and crystalline (mineral) matter such as crystals, grains and aggregates of various minerals;
- ☑ An organic constituent – composed of charred materials (slightly changed, semi-coked and coked particles) and organic minerals;

- ☑ A fluid constituent – composed liquid (moisture), gas and gas-liquid associated both with organic and inorganic matter.

Fly ash is composed mostly of silicon, aluminium, iron and calcium oxides and nearly all particles are spherical in shape as **Figure I. 5** shows.

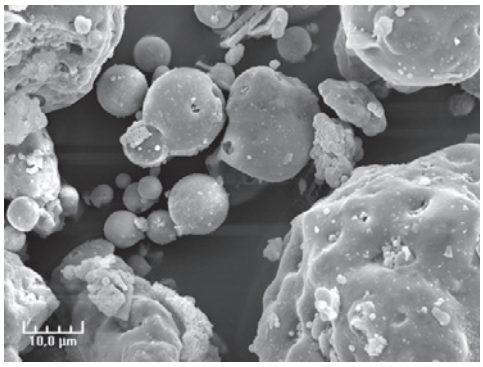

Figure I. 5: Fly ash powder (sample CW10) observed by a scanning electron microscope (SEM), x1500 magnification.

The chemical composition includes the content of major (> 1%), minor (1-10%), and trace (< 0.1%) elements. The major and minor elements are mostly expressed as oxides. These elements are commonly (in order of decreasing amounts): O, Si, Al, Ca, Fe, C, K, Mg, H, Na, Ti, N, P, Ba and occasionally Mn, Sr, F and Cl. The other elements are mostly trace elements. Most elements in fly ash occur in both organic and inorganic matter. Each element in fly ash is combined in different minerals and phase with variable proportions and distinctive properties and behaviour.

Each mineral or phase in fly ash has individual and/or synergetic active, semi-active, pozzolanic and also inert or inactive behaviour during the hydration-dehydration and hydroxylation and de-hydroxylation processes of fly ash.

Bulk chemical analyses and classification systems of fly ash always include data for loss of ignition. The losses of ignition are not equivalent to the organic matter concentrations. The utilisation of fly ash in some construction materials (mostly for cement and concrete) is determined by the organic matter in fly ash.

The particle size is an important characteristic of fly ash. We need information about the distribution of active, pozzolanic and inert inorganic phases and the charring of different particle fractions. Also, specific surface area is commonly related to the particle size of fly ash.

Colour is one of the important physical properties of fly ash in terms of estimating the lime content quality. Lighter colour indicates the presence of high calcium oxide and darker colours suggest high organic content [11]. Lighter colour also indicates lower carbon content, and darker colours indicate higher carbon content as **Figure I. 6** shows.

Figure I. 6: Fly ash is generally light tan in colour and consists mostly of silt-sized and clay-sized glassy spheres. This gives fly ash a consistency somewhat like talcum powder [12].

The chemical constituency of coal and solid waste fly ash mostly depends on the chemical composition of the burned coal or solid waste (domestic or industrial), and also depends on the techniques used for their storage and handling. The different ash mineralogy depends on the coal and also the solid waste combustion technology used. The bulk chemical composition can be generally correlated with the rank of the coal that was the source for the ash. The rank reflects the different particulars of the coal, both temporal and spatial. In the case of solid waste fly ash, the bulk chemical composition depends on the material which was burned and is very different between cases of domestic waste and cases of industrial waste.

The amount of crystalline material versus glassy phase (which is cenospheres) material depends on the combustion and glassification process used at particular power plants. When the maximum temperature in the combustion process is above approximately 1200 ^{0}C and the cooling time is short, the ash produced is mostly glassy phase material. Where boiler design or operation allows a more gradual cooling of the ash particles, crystalline phase calcium compounds are formed.

The factors that can affect the hydration and leaching properties of fly ash are such things as the relative proportion of the spherical glassy phase and crystalline materials, the size distribution of the ash, the chemical nature of the glass phase, the type of crystalline material and the nature and the percentage of unburned carbon [13]. The primary factors that influence the mineralogy of a **coal fly ash** are [14]:

- ☑ The chemical composition of the coal;
- ☑ The coal combustion process including coal pulverisation, combustion, flue gas clean up, and fly ash collection operations;
- ☑ The additives used including oil additives for flame stabilisation and corrosion control additives.

These same factors – chemical composition of waste, the combustion process and additives, influence the chemical composition of domestic and industrial fly ash. The minerals present in the

coal and solid waste dictate the elements composition of the fly ash. The mineralogy and the crystal qualities of the ash though, are dictated by the boiler design and operation.

The minerals in fly ashes can be divided into three categories:

- ☑ Primary minerals originate from the initial components of the combustion fuels/waste;
- ☑ Secondary minerals originate from phases that were formed during combustion;
- ☑ Ternary minerals originate from material formed during hydration of the fly ash.

From mineralogical point of view, three types of components are present in fly ashes. They are crystalline minerals, unburn carbon particles and non-crystalline alumino-silicate and other oxides glass. The most important minerals found in fly ashes are:

- ☑ Magnetite (Fe_3O_4) – 0.8-6.5%. Magnetite has a cubic hex-octahedral structure commonly striated with triangular markings on the octahedron faces;
- ☑ Hematite (Fe_2O_3) – 1.1-2.7%. The structure of hematite is hexagonal scalenohedral;
- ☑ Quartz (SiO_2) – 2.2-8.5%. Quartz has hexagonal-Trigonal trapezohedral structure;
- ☑ Mullite ($3Al_2O_32SiO_2$) – 6.5-9.0%. The fundamental building unit in mullite is the chain of edge-sharing AlO_6-octahedra, the crystal structure is orthorhombic;
- ☑ Free calcium oxide – up to 3.5%.

Other minerals have elements which range from trace amounts to 2.5%, such as wüstite (FeO), goethite (FeO(OH)), pyrite (FeS_2), calcite anhydride ($CaCO_3$) and periclase (MgO) [15], **Figure I. 7**.

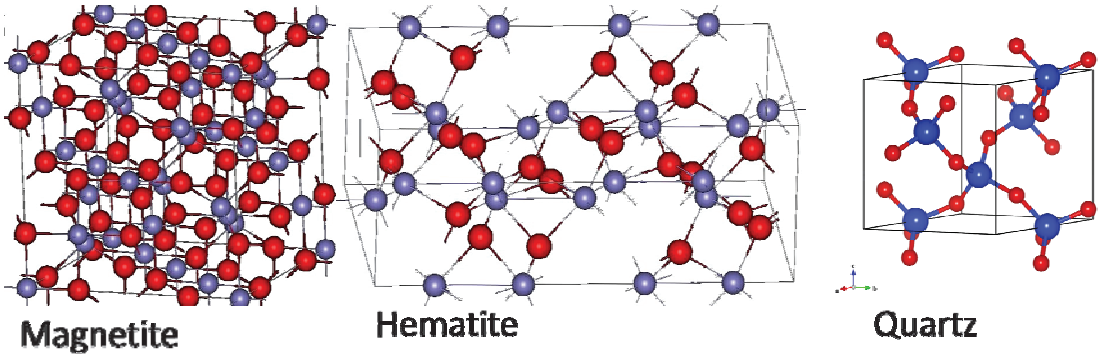

Figure I. 7: The crystal structure of major minerals presents in the fly ash samples.

I.2 APPLICATION OF FLY ASH

There are different areas of use for fly ashes: for example, in industrial coating, in concrete products, as the fill material for structural applications and also used for embankments.

I.2.1 In industrial coating

It is common practice to apply coatings of fly ash to components in fossil fuel energy generation to provide thermal insulation, corrosion and wear resistance. It is used also in chemical processes to protect the surface of structural steel against the surface degradation processes of wear, oxidation, corrosion and erosion [16].

Plasma spraying provides increased design flexibility, so a combination of materials with widely differing physical and chemical properties can be employed. However, atmospheric plasma sprayed coatings tend to have highly defective microstructures, with lamellar micro-cracks, non-molten particles, weak interfaces and gaps between solidified splats. The microstructure and mechanical properties depend on the spraying conditions. The result is that shrouded plasma spray processes can be used to deposit fly ash coatings on the steel in specific parameters. It is effective in increasing the oxidation and salt corrosion resistance of carbon steel at 900 °C. The fly ash coating on carbon steel has higher values than base steel. Porosity is slightly higher than the range of porosity for plasma spray coatings. The coating was effective in increasing the oxidation and salt corrosion resistance of carbon steel.

I.2.2 In concrete products

Fly ash can be used as a raw material in concrete products and grout. This is the largest single use of fly ash as a mineral admixture in Portland Cement Concrete. Fly ash used in concrete must have sufficient pozzolanic reactivity and must be in consistent quality [17-19].

Fly ash as an additive has a number of positive effects on the resulting concrete:

- ☑ It decreases the demand of water and decreasing the water to cement ratio;
- ☑ It improves the particle size packing (due to the smaller size of fly ash particles, in comparison to the aggregate) thus decreases the air entrainment in the concrete;
- ☑ Fly ash increases resistance to corrosion and ingress of corrosive liquids by reacting with calcium hydroxide in the cement to become a stable, cement-type compound of calcium silicate hydrate;
- ☑ Use of fly ash (in correct proportions) will ultimately result in stronger concrete than straight Portland cement;
- ☑ Use of fly ash as an additive in Portland cement will generally reduce the water demand of the mix.

I.2.3 Fill material for structural applications and embankments

Fly ash can be used as a backfill material for wall retainers and bridge abutments, or fly ash ground can be used to fill abandoned rock quarries. Qualities to be considered before an ash is used as a structural fill or cover material are such things as the particle size of the ash, compaction characteristics, density, permeability and compressive strength of the ground matter.

Particle size is one of importance when considering the consolidation characteristics of the material. The smaller the particle size, the easier and more quickly will be the physical consideration of the ash. By using the fly ash as a lighter weight cover material compared to soil, excessive settlement or landslide of the sub-soil is avoided. Fly ash can be used as a substitute for natural soils [20].

I.2.4 Others applications

Fly ash can also be used as:

- ☑ An ingredient in soil modification or / and stabilisation [21-23];
- ☑ A component in moveable landfill – moveable landfill is a slurry mixture consisting of sand and other aggregate material and a cement-type binder. Fly ash is used as a fine aggregate and for its pozzolanic properties and is also used as a supplement to, or a replacement for the cement [24-25];
- ☑ A component of road bases, sub-bases and pavement. Fly ash increases the strength, bearing capacity and durability of pavement mixture. It is part of a binder which stabilizes base construction applications [26-27];
- ☑ Mineral filler in asphalt. It serves to improve the cohesion of the binder (asphalt cement) and the stability of the mixture [28];
- ☑ And also as passive protection against fire [29].

I.3 METHODS OF ANALYSIS OF FLY ASH

There are two ways of characteristics of fly ashes. The first is the characterisation of fly ash by surface analysis techniques. The second category is the elemental determination of fly ashes in the form of powder or in solution.

There are different techniques used for the fly ash analysis. The mineralogical composition of fly ashes can be determined for example by quantitative or semi-quantitative X-ray diffraction, X-ray photoelectron spectroscopy (XPS). The X-ray fluorescence, inductively coupled plasma – atomic emission spectroscopy can be used for determination the chemical composition.

The methods are divided into those oriented to the elemental analysis and those oriented to the surface analysis. Detailed information about methods is presented in next chapters.

I.3.1 Mineralogy

The complex mineralogy associated with fly ash includes several processes such as vaporisation, melting, crystallisation, nitrification, condensation and precipitation which occurs during flue gas combustion and treatment [30]. Mineralogy is established using methods of surface analysis. Surface analysis provides information about the morphology, particle size distribution and also the mineral and chemical composition.

X-Ray diffraction with coherent scattering of the incidental radiation is used to analyse the crystal structure, the chemical composition, the geometrical distribution of the atoms in the crystal mesh and to identify the parameters of the crystal lattice. The empirical formula and elemental composition can be determined by use of X-Ray Photoelectron Spectroscopy (XPS) based on the irradiation of material with X-Rays and then the simultaneous measuring of the kinetic energy and the number of electrons escaping from the material. The Scanning Electron Microscope (SEM) uses high-energy electron beams that interact with the atoms from the sample. This produces signals that contain information about the sample topography and composition. Information about the atomic lattice can be obtained by using the Transmission Electron Microscope (TEM). This uses beams of electrons which interact with the sample as the beam is transmitted through it. Secondary Ion Mass Spectrometry (SIMS) is a technique used on surface science to analyse the composition of solid surfaces. This is done by sputtering the sample surface with a focused primary ion beam and then collecting and analysing ejected secondary ions. These secondary ions are measured to determine the elemental, isotopic and molecular composition of the surface.

Several methods are used to do this measuring and their principles are listed above. The Scanning Electron Microscopy (SEM), X-Ray diffraction (XRD), the Transmission Electron Microscopy (TEM), Neutron Activation Analysis (NAA), Secondary Ion Mass Spectrometry (SIMS) and Synchrotron Microprobe Technique (SMP) all give detailed imaging information about the morphology and the surface texture of individual particles, as well as their elemental composition. Both the surface and internal structure can be analysed. The main components of fly ash are the iron rich spheres, which are mostly present as oxide, and also the alumina-silicate spheres which are amorphous and are well mixed in whole sample [31-40]. The other major elements present in fly ash were also analysed and their distribution and association with other elements was proved [31, 41-43]. Calcium is generally associated with oxygen, sulphur and phosphorous but it is not associated with silicon or aluminium.

Silicon and aluminium are generally associated with one another. Another strong correlation is between the content of Hg, Se, As and the carbon content in fly ash. The size of the particles which compose fly ash varies from 1 µm to more than 200 µm [31-32]. The information about ultrafine particles (<100 nm) and their distribution are reported by TEM [44].

I.3.2 Elemental determination in fly ash

Information about the elementary particle composition can be obtained after fly ash is digested with the help of acid, or by direct solid analysis.

I.3.2.1 Analysis in a digest form

Analysis of a digested form is one of the most common types of analysis. There are various techniques used for determining elementary particles (also known as trace elements) in fly ash. These techniques are such methods as microwave-acid digestion followed by inductively coupled plasma-atomic emission spectrometry (MW-AD ICP-AES), Graphite Furnace Atomic Absorption Spectrometry (GFAAS), and Hydride Generation Atomic Absorption Spectrometry (HGAAS). Other techniques are Inductively Coupled Plasma-Mass Spectrometry (ICP-MS), Inductively Coupled Plasma-Atomic Emission Spectrometry (ICP-AES), Hydride Generation Inductively Coupled Plasma-Mass Spectrometry (HG-ICP-MS), ultrasound-assisted digestion followed by Inductively Coupled Plasma Optical Emission Spectrometry (ICP-OES) and Electro-Thermal Vaporisation Inductively Coupled Plasma Mass Spectrometry with Slurry sampling (FETV-ICP-MS) [30-32, 45-54]. A summary of the digestion procedures is shown in **Table I. 2**.

Table I. 2: Summarised digestion procedures of fly ash samples.

System	Reagent	Elements	Recovery/Method	Reference
Open system	HNO_3-$HClO_4$-HF	Ba, Co, Ce, Cs, Cu, Dy, Ga, Ge, La, Lu, Mn, Ni, Rb, Sr, Tb, Th, Y, Yb, Zn, Zr	Recovery 37-178%, ICP-MS, ICP-AES	[43, 55-56]
	HNO_3-$HClO_4$-HCl	Al, As, Cr, Cu, Fe, Mn, Ni, Pb, Ti, V Zn	Recovery 4-104%, ICP-OES	[57]
	Aqua regia-NH_4F-HNO_3-H_2SO_4	Al, Ba, Cd, Co, Cr, Cu, Fe, Mn, Mo, Ni, Pb, Sr, Ti, V, Zn	ICP-OES	[58]
	HF-$HClO_4$-H_3BO_3-HCl	Al, Ba, Cd, Co, Cr, Cu, Fe, Mn, Mo, Ni, Pb, Sr, Ti, V, Zn	ICP-OES	[58]
Close system – microwave digestion	HNO_3-HCl-HF	As, Sb, Se, Cr, Cu, Pb, Co	ICP-MS, ICP-OES, AAS Recovery 91-103%	[59-60]
	Aqua regia-HF-H_2O_2	Sb, Cs, Cr, Co, Fe, U, Zn	ICP-MS, error ±10%	[61]
	HNO_3-H_2O_2-HF	V, Cr, Mn, Fe, Co, Ni, Cu, Zn, As, Se, Cd, Sb, Pb, 38 elements (Ag-Zr)	Recovery 9-109%, ICP-MS, ICP-AES	[45, 62-64]
	HNO_3-HF	Cu, Ga, Ge, As, Sb, Se, Ba, Co, Ni, Pb, Sr, V, Zn, Cd, Mn, Cr	Recovery 40-264%, ICP-MS, ICP-OES	[54, 56, 58, 65-67]
	HNO_3-$HClO_4$-HF	Ti, Zn, V, Mo, Cr, La, Cu, Ni, As, Cd, Pb, Y, Ce, Pr, Nd, Sm	Recovery 10-109%, ICP-OES, ETV-ICP-MS, ICP-MS	[32, 68-69]
	HNO_3-HCl	As, Al, Cr, Cu, Fe, Ni, V, Pb, Zn, U	Recovery 96-118%, ICP-MS	[70]
	HCl-HNO_3-H_2O_2	Al, Ba, Cd, Co, Cr, Cu, Fe, Mn, Mo, Ni, Pb, Sr, Ti, V, Zn	ICP-OES	[58]
	HF-aqua regia-HNO_3	As, Cd, Co, Cr, Cu, Mn, Ni, Pb, Se, V, Zn	Recovery 93-255%, ICP-OES	[56]
Alkali fusion	Lithium tetraborate	Ca, Si, Al, Fe, Mg, Ti, S, P	Dissolution of beads in HCl or HNO_3, ICP-OES	[34, 71]

For traditional ICP-AES and ICP-MS analyses, a wet digestion of fly ash is generally achieved using HNO_3 and a mixture of acids. These acids are such as $HNO_3/HF/H_3BO_3$, aqua regia or two-step digestion with or without the assistance of microwave-acid digestion [30, 45-46, 49]. Another way to analyse fly ash is by lithium tetraborate fusion, which is then decomposed by acid. The acid decomposition is not the same for all types of fly ash. The decomposition procedure is selected according to the origin of the fly ash. After decomposition by acid, the recovery is not 100 percent. Various authors [31-32, 45-46, 54] found that the recovery varied from 24% to 270 % depending on the procedure. This is not sufficient recovery in order to control how much the environment is polluted. Another disadvantage of solution analysis is the many hours needed to prepare the sample. There are specific methods used to determine particular elements. One method is Hydride Generation Atomic Absorption Spectrometry (HGAAS), which determines specific elements such as As, Se and Sb. With HGAAS, the limits of detection for some elements are comparable to those of ICP-MS, and HGAAS is generally a single element measurement [45-46]. The articles cited here show the difficulties of sample preparation, which is longer than the case of laser ablation, where the sample preparation takes only minutes.

I.3.2.2 Direct solid analysis

XRFS (X-Ray Fluorescence Spectrometry) is a non-destructive analytical technique used to determine the concentrations of elements present in solid, powdered and liquid samples.

The advantage of powder material analysis is the gain of time and less risk of contamination during the decomposition of the sample. The techniques used for direct solid analysis are: X-Ray Fluorescence (XRF) for determining the trace elements [10, 32, 47, 72], and X-Ray Photoelectron Spectroscopy (XRPS) for studying the molar ratio of the elements like Al, As, Ca, Fe and S normalised to Si [73]. In this study, it was proved that there was high As enrichment on the surface of prepared discs. Other methods are:

- ☑ Neutron activation analysis (NAA) [61, 74-75];
- ☑ Ultrasonic slurry sampling electro thermal vaporization inductively coupled plasma-mass spectrometry (USS-ETV-ICP-MS) [66, 76];
- ☑ Scanning electron microscopy energy dispersive spectrometry (SEM-EDS) [34, 39, 54];
- ☑ Laser ablation inductively coupled plasma-mass spectrometry (LA-ICP-MS) [34, 41, 77-79] and
- ☑ Laser-induced breakdown spectroscopy (LIBS) [80].

Direct solid analysis can be performed by analysing the powder or powder compacted into the form of pellets with binders (e.g. cellulose, mixture of cellulose and paraffin). The laser ablation technique

can be performed on the powder directly placed on the tape [77] or on the pellet. The results show good agreement (5 to 10 %) with reference values. There are few publications regarding Laser Ablation Inductively Coupled Plasma-Mass Spectrometry (LA-ICP-MS) and Laser Induced Breakdown Spectrometry (LIBS) for fly ash analysis. The interest in these analyses was determining the elements and also locating the elements. The work of Spears *et* al [77] used LA-ICP-MS for element location within fly ash. Van Heuzen *et al.* [78], Coedo *et al.* [79] and Piispanen *et al.* [34] investigated the possibility of quantitative elemental analysis of the fly ash by LA-ICP-MS. Noda *et al.* [80] used laser induced breakdown spectrometry (LIBS) to detect the carbon content in fly ash. In this article, the authors used the intensities of other elements with their variable correction factors (plasma temperature and pressure correction factors), to determine the carbon content in fly ash samples. Plasma temperatures and pressure parameters had to be determined in the experimental operating conditions.

All these techniques were used to determine the chemical and physical properties of fly ash, and also to determine the possibilities of applying fly ash to different areas of industry and the environment. All these applications and studies show that researchers have huge interest in fly ash and they explain why, in this particular work, we turned our attention to analysing the elements of fly ash. The problems with the recovery, which were shown in the previous chapter, explain the need to develop new methods without digestion, and laser ablation is the possible solution.

Laser Ablation Inductively Coupled Plasma-Mass Spectrometry (LA-ICP-MS) and Laser Induced Breakdown Spectrometry (LIBS) are of interest because of their easy sample preparation, fast analysis and because they are able to cover whole concentration ranges using just these two techniques.

I.4 NEW METHODOLOGY FOR DIRECT SOLID ANALYSIS

There has been a huge increase in the number of articles concerning the utilisation and understanding of Laser Ablation Inductively Coupled Plasma-Mass Spectrometry (LA-ICP-MS) and Inductively Coupled Plasma Optical Emission Spectroscopy (ICP-OES), as shown in, **Figure I. 8**.

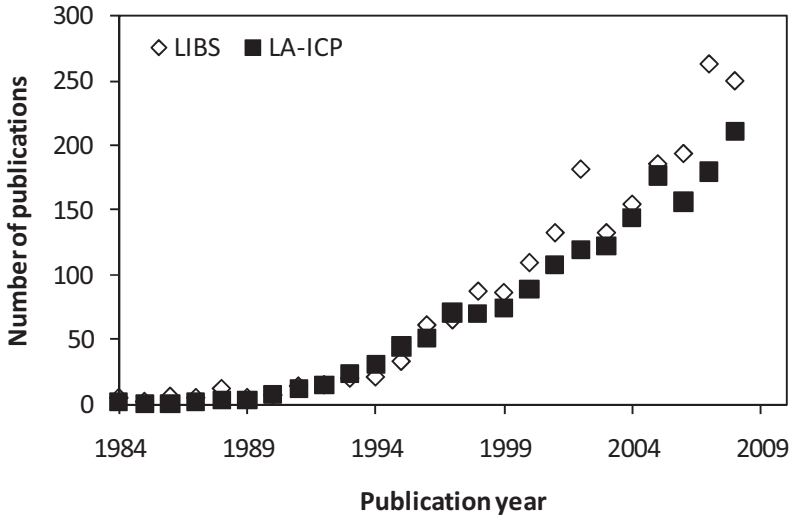

Figure I. 8: Number of publications in LA-ICP-MS and ICPOES since 1984 [81].

The common process used here is the laser ablation method. The experimental parameters of laser ablation determine the amount, the composition, and the particle size distribution released by a given sample. The influence of these parameters was investigated in recent years in order to better understand and minimise the limitations of the parameters cited here. Several reviews were written about Laser Ablation Inductively Coupled Plasma-Mass Spectrometry (LA-ICP-MS), its problems, features and application [82-85]. The main problems of laser ablation were described such as elemental fractionation (the main limitation of laser-based sampling techniques), particle transport efficiency, spatial distribution and the element composition of produced particles. The possible solutions were reported elsewhere. Several authors focused on such things as the sampling process of laser wavelengths (IR vs. UV) [86-87], pulse duration (ns vs. fs) [88-90], laser ablation carrier gas (Ar vs. He vs Ne) [91-92] and the laser ablation cell design were studied and reported by several authors. All these processes play important roles in the properties of laser generated aerosols. The applications of fs-LA-ICP-MS in the biological and medical fields was described by Günther [95]. The applications in the field of spatial research, i.e. meteorites, were reported by Horn [96-97]. Short laser pulses (fs) directly deposit their energy on the sample, while longer laser pulses may also heat the expanding plasma by inverse Bremsstrahlung. At high laser frequencies, plasma heating may affect an electron density increase which makes the plasma opaque and reduces the interaction of the laser with the sample. As a result, there is less ablation by the sample [98-101].

There are only a few good reviews that describe the problems of Laser Induced Breakdown Spectroscopy (LIBS). The applications of LIBS are in other reviews such as in semi-quantitative or quantitative analysis, depth profiling, archaeology, cultural heritage [102], and environment or in the

detection of explosive residues and landmine detection [103]. The analysis can be of solid, liquid, gas samples and aerosols [104-115] and can be made under different atmosphere – air, He, Ar. Using Argon as the atmosphere gives more emission signal than air [116-117]. The important bearing of this technique were explained in two specialised books [114, 118], where the instrumentation and research applications are well described. Recent developments are focused on the portable LIBS, analysis in distance and double-pulse analysis. The utilisation of portable LIBS and analysis in distance is used by army personnel to detect residues of explosives. The review explaining this topic shows its importance to the security services [119-120]. The portable LIBS and analysis in distance can also be used in the field of archaeology and for on-line analysis of environmental samples like contamination of soils. The double-pulse LIBS reduces the amount of air entrained in laser induced plasma and improves the distinction between energetic and non-energetic materials [119-121]. Two laser pulses are used to generate the micro-plasma which is separated by a few µs. Collinear and orthogonal laser schemes utilising both fs and ns pulses are used. The advantage of these systems is the increase in signal. The ablation pulse is separated from the analytical pulse thus, in most cases, improving how the pulse reproduces. Also, the triple pulse was tested and compared with the single and double pulse [106]. Attention was also turned to the portable LIBS and its industrial application. Contrary to the instruments used in laboratory research, the instrument must be robust, stable, reliable, quick and available for operation when applied to the industrial field [102, 106, 122].

I.4.1 Pellets preparation

Analysing powder material has both advantages and disadvantages. The main advantage of this analysis is the gaining of time, minimal risk of contamination during digestion, and less probability of losing information about the element during digestion. Analysis in the powder form allows us to obtain information about the element distribution from a whole sample.

The main disadvantage can be in the pellet preparation itself. Several parameters must be checked and optimised before analysis. One of these parameters is the need to have the particle sizes homogenised in order to obtain uniform particle size distribution. Another parameter is the possible utilisation of a binder. In the case of fly ash, the presence of a binder is necessary. Without any binder, we will not have a pellet that is able to resist laser ablation. The binder must be very pure, easy to manipulate, have good mechanical properties, have a small and uniform particle size (10-40 µm), with easy spectrum and it must also be cheap. Many of the binders were tested by Mitchell *et al.* [123] in order to prepare pellets made from copper powder. The first tested binder was cellulose, but after homogenisation (shaking) the pellets produced spurious signals that could not be reproduced, which were attributed to non-homogenised analyte distribution. In order to improve

analyte distribution, copper nitrate solution in absolute ethanol was prepared and added into a known amount of cellulose. It was then mixed and dried so the ethanol could evaporate. An improvement in signal RSD% was observed, but the preparation was very time consuming. Finally, copper powder and cellulose were homogenised in a ball mill and it was found to be the best solution, with the RSD% increase usually 2 to 6%. Other binders were also tested, and the resulting pellets were observed and compared. Pellets with potassium bromide (hygroscopic) showed fracturing and cracking around the laser sparked area because the sample was not homogenised. Carbon black pellets would not form as solid pellets. Utilisation of graphite also did not make the pellet mechanically strong. Hydrolysed casing formed a firm pellet which became sticky after exposure to air. Cellulose would not form a solid pellet. Cellulose acetate also formed firm and smooth pellets. The last binder tested was boric acid and this formed hard, slightly brittle and smooth pellets.

It must be stressed that this information is quite old. No other work was published with so many binders tested for preparation. Other binders which were tested for pellet preparation by different authors, were silver [117, 124], polyvinylpyrollidone-methyl cellulose [125], KBr [126] and also α-cyano-4-hydroxy-cinnamic acid used commonly as a matrix for MALDI analysis [127].

To increase the mechanical stability of the pellets, Polyvinyl Alcohol (PVA) powder can simultaneously be fixed to the back of the pellet [128]. Another way to prepare the pellets is the glue technique. With this, the powder is mixed with a glue solution such as methyl methacrylate resin Elvacite 3000 which is dissolved in acetone, and then analysed [129]. The homogeneous sample distribution in the glue is required.

Lithium tetraborate fusion was the last type of sample prepared [130]. This procedure eliminates the effects of minerals and results in a highly homogeneous sample. The disadvantages of this are the dangers of contamination, loss of volatile elements, dilution of the sample and the amount of time spent. The basic preparation of the pellets, when possible, is without a binder. This type of preparation is possible for soil, sediments or geological samples [125-126, 131-133].

I.4.2 Calibration strategies

There are several mechanisms by which this data can be presented. The qualitative and semi-quantitative analyses using laser ablation are quite routine. The main mechanisms will be discussed in two separated chapters Laser ablation – ICP and the second for Laser induced breakdown spectroscopy (LIBS) I.4.2.1. The traditional model is with external calibration, where the *x-axis* shows the concentration and the *y-axis* shows the intensity in arbitrary units. The problem with this type of

calibration method is the need for reference materials which have the same matrix as the samples. This is not always easy to assure.

I.4.2.1 Laser ablation – ICP

The main difficulties with calibration are the sample and reference materials. If the sample and reference materials do not have the same matrix, then the response to the ablation is different. The reference material must be homogeneous and well-characterised at trace element level. The background measurement must be correlated with the reference material and this is important for the calibration, which is used to correct the signal from the ablation of a sample. The background signals are usually obtained from measurements of a gas blank. This is the measurement without laser ablation and is performed separately, before or after the ablation.
Generally, four main calibration strategies are used:

- ☑ External calibration using a solid reference standard;
- ☑ External calibration using a solid reference standard with internal standardization;
- ☑ Calibration using solution;
- ☑ Direct liquid ablation,
- ☑ Isotope dilution.

I.4.2.1.1 External calibration using a solid reference standard

External calibration is mostly used in cases when the matrix of the sample is the same, or close to, that of the standard reference material. It is used with success on various alloys, metals, glass, geological samples [134] or biological samples [135]. We must pay attention though, that there is no fractiousness, or that it is similar to the sample fractiousness. In the case of powder samples, being homogenised and the sample matrix are both important.
Another possibility is the matrix matching calibration method. Here, in the case of non- existing reference materials, it is possible to prepare specific matrix matched standards. These include a mixture of an appropriate matrix material with an analyte. The techniques by which the matrix matched standards can be prepared are:

- ☑ Addition of compounds to a powder matrix;
- ☑ Mixing and pressing with or without a binder;
- ☑ Addition of standard solutions to a powdered matrix;
- ☑ Co-precipitation of elements into a matrix with single element solution;

☑ Drying and pressing glass fusion and the production of sintered compacts.

Other technique is the external calibration using previously digested and analysed materials, as it is made by Elish *et al.* [136] in the case of hair samples. A new approach is the in-situ analysis of major elements and trace elements without applying an internal standard [137]. The ablation yield correction factor based on the sum of oxides and multiple calibration standards can be used to analyze elements of anhydrous glasses and minerals.

I.4.2.1.2 External calibration using a solid reference standard with internal standardization

The use of an Internal Standard (IS) was studied by many authors such as Leach and Hiefje [138]. IS produces a much more robust calibration method by allowing application of a correction for different ablation yield, between the sample and reference material. It can also partially correct the matrix effect and the signal drift. The internal standard can be added during preparation, i.e. while pressing pellets or fusing glasses. Two of the common elements used as an internal standard is indium [138-139], germanium [132, 139]. The use of internal standards is limited by the need to have one element present which has a known concentration, and the need for it to be homogenised in the sample. Fitzpatrick *et al.* [140] used a standard prepared with the sol-gel process which had selenium as the known element with a known sulphur concentration. The sol-gel process is the preparation of ceramic materials by first preparing of a sol, gelling the sol, and then removing the solvent. These sol-gels were used as standards for NIST 610 and NIST 612. Their determination and sulphide reference materials are used as calibration standards to verify the method. The sulphur concentration was calculated from the slope of the calibration curve, the x-intercept and the known concentration of selenium. The sol-gel process is suitable to use similarly to solution calibration standards.

One interesting possibility of internal standardisation is particle size distribution. Aerosol particles that are <100 nm were used as the internal standard [141]. In the same article, external calibration with glass CRMs was discussed, using calcium as the internal standard. The mass that was transported could be used for non-matrix-matched analysis of unknown non-metal samples. This uses particle size distribution as the internal standard as long as the sample density is known. Isotope dilution is also one of the common techniques used for internal standardisation. It is used, for example, to analyse glass samples [142], road dust and rocks [143] and coal using LINA-Spark Atomiser system [144]. The principal disadvantage of isotope dilution is the cost of spike solutions.

I.4.2.1.3 Calibration using solution

The principle of calibration using solution is the simultaneous introduction of reference material (using solution nebulisation) with the laser ablated material in order to obtain matched plasma conditions. Using two sample channels to obtain matched plasma conditions was developed by Thomson *et al*. [145]. One channel is for the ablated material, and the other is for nebulised aqueous solution standards. This principle was also proposed by Günther *et al.* [146] and it was described by Günther *et al.* [147], Cromwell and Arrowsmith [148], Pickhardt *et al.* [149]. This principle is used for bulk, local, distribution and semi-quantitative analyses.

However, some disadvantages were reported. Interferences were reported in the dual sample introduction system due to oxide formation, i.e. wet solution nebulisation in ICP-MS and lowered sensitivity. Halicz and Günther [150] proposed a nebulisation solution based calibration for analysing major, minor and trace elements. Quantification strategies were applied. They used Ca as an internal standard and they determined Ca using a normalisation of all matrix-containing elements to 100%. The advantage of this normalization is that it allows the analysis of solid samples without knowing its concentration on an internal standard element. This is usually required when using naturally occurring matrix elements for internal standardisation. However, it also means that all analysed elements have the same sensitivity.

Mao and Russo [151] proposed how to optimise and calibrate LA-ICP-AES by measuring vertical spatial intensity profiles. The authors found that due to the excitation mechanism and ICP, the response was different between aqueous solution nebulisation and laser ablation sampling. Mao and Russo found that this phenomenon can be minimised by changing the gas flow rate.

Masters and Sharp [152] introduced universal calibration strategies using aqueous standards with modified absorption coefficients. They used polymer additive (poly sodium 4-styrene sulfonate) which was absorbed by the wavelength of the laser used. The principle is to vary the absorption coefficient of the standard by a different polymer concentration. It should be possible to match the mass of the ablation yield of the standards and samples. This matching should produce equivalent count rates from the standards and samples to make equal concentrations of the analytes. The NIST 613 was used as the sample to be analysed by this method. The internal standard was calculated by using a correction factor for the concentration of elements in the NIST 613 sample. The concentration found was in good agreement with the reference values.

I.4.2.1.4 Direct liquid ablation

The direct liquid ablation calibration strategy is mostly used for LA-ICP-MS measurements. It was first demonstrated by Günther *et al.* [147] by the quantitative analysis of NIST 610 and NIST 612 glass, using different solutions, with the use of internal standards (Na and Yb). The particle size distribution is very important in explaining the ablation behaviour of liquids and solids. The particle size from ablation was mostly quite small. Broader particle size distribution was measured for solution ablation. Because of the similar signal of liquid and solid ablation, the concentration was calculated using the following equation: $(C_A)_{solid} = (C_{IS})_{solid} \cdot \frac{[I_A/I_{IS}]_{solid} \cdot (C_a)_{liquid}}{[I_A/I_{IS}]_{liquid} \cdot (C_{IS})_{liquid}}$, where I_A is the measured intensities of analyte in the liquid and solid, I_{IS} is the intensities of the internal standard in the liquid standard and the solid sample, C_A is the concentration of the analyte in the liquid standard and C_{IS} is the concentrations of the internal standard in the liquid standard and the solid sample.

Boué-Bigne *et al.* [153] later added a chromophore to modify the optical absorption characteristics of the solutions in order to obtain the desired degree of ablation. Several conditions were studied to evaluate the role of chromophore such as the plasma conditions, optimisation of modified standard solutions, ablation mechanism of solutions, and also the application of this method to the analysis of NIST 613 and low density polyethylene. The purpose of the chromophore was to improve laser energy coupling to the aerosol solution in such a way, that the threshold ablation fluency was reached within the surface layers of the liquid. The ideal chromophore should strongly absorb at the laser wavelength, should not precipitate when in contact with the analytes, and should be non-toxic.

I.4.2.1.5 Isotope dilution

Isotope dilution can be considered a special case of the internal standard method. It is a method of elemental analysis. The basis of this technique is to add a known quantity of spike which is enriched in an isotope and then measure the change of the isotope ratio of signal intensities for two selected isotopes of an element. This allows us to calculate the concentration of the element in the sample. The internal standard that is used is an isotope (isotopomer) of the compound to be measured. All compounds to be measured must have their internal standard, so five different elements must have five different spike solutions. The importance of the standard with the sample is that its mass is different. This technique is mostly used for the characterisation of reference materials. The concentration C can be calculated as follows:

$$C = \frac{M_s K(A_s - B_s R)}{W(BR - A)}$$

Where M_s is the mass of the spike (usually expressed in ng or µg; W is the weight of the sample; K is the ratio of the natural atomic weight and the atomic weight of the enriched material; A is the natural abundance of the reference isotope; B is the natural abundance of the spike isotope; A_s is the abundance of the reference isotope in the spike solution; B_s is the abundance of the spike isotope in the spike isotope enriched spike and the R is the measured $\text{reference isotope}/\text{spike isotope}$ ratio [154].

This uses the isotope ratios and it is a quasi-absolute method of analysis. The protocol of isotope dilution analysis is to prepare a solution which is NOT spiked in order to estimate the concentrations of the element in the sample. Thus, we can establish the appropriate values for M_s and we can also measure the ratio for the proposed pairs of isotopes. Once the non-spiked solution is prepared, we can prepare the solution with the addition of the enriched isotopic spike. This is normally added as a weighed aliquot of a known solution with known concentration which is prepared from the enriched material. Calibration strategies use the simple isotope dilution, where the certified spike is added to the sample and allowed to equilibrate before sample processing and analysis are performed. The double isotope dilution is also used for the trace element determination in the diverse matrix [155]. The performance of the isotope dilution used with the LA-ICP-MS method was proved by Tibi and Heumann [128]. Its precision was better than 10 % and the limit of detection was > 0.03 µg/g. Another utilisation of the LA-ICP-IDMS method was to determine sulphur in petroleum products [143], using double isotope dilution. The results were compared with those obtained by conventional ICP-IDMS and they show good accuracy. Isotope dilution is often used by combining the separation techniques (chromatography) coupled with ICP-MS [156-157]. The use of ID for the trace element analysis was reported by Botha et al. [155] and Ciceri et al. [158].

A critical review summarised the possibility of using the ICP-IDMS for routine analysis in connection with other techniques. The other techniques included HPLC, LA, and ETV-electro thermal analysis. This review was presented by Heumann [159]. The disadvantages of this procedure are that mono-isotopic elements are not used, and that it is a very time consuming analysis. This technique though, has several advantages as a partial compensation for the loss of analyte during the sample preparation and its immunity to physical and chemical interferences. The conclusion was that there was a good possibility to routinely use this technique.

I.4.2.2 Laser induced breakdown spectroscopy (LIBS)

For LIBS calibrations, the external calibration using solid reference materials, and external calibration using a solid reference standard with internal standardization are used. These two calibration strategies are describes in the chapters I.4.2.1.1 and I.4.2.1.2. On the contrary, the calibration strategy using liquid standards could not be used. But the calibration-free strategy is future calibration strategy for LIBS measurements.

I.4.2.2.1 Calibration-free LIBS

The calibration-free method was proposed in 1999 by Ciucci *et al.* [160-161]. It is an analysis without standards. This analysis applies the basic equations derived from the Local Thermodynamic Equilibrium (LTE) assumption to compensate for the matrix effect. This is done in order to make every measurement self-consistent and to avoid the need to compare this with calibration curves of reference samples. The method is based on the assumption of optically thin plasma, stochiometric ablation and local thermal equilibrium. The method requires measurements of at least two emission lines from the same specimen in order to calculate the plasma electron temperature. Also, at least one line needs to be measured for each element in plasma with known spectroscopic parameters. The Boltzmann plot that contains the points corresponding to all lines observed in the experimental spectrum is shown by the equation:

$$\overline{I_{ij}} = FC^s A_{ij} \frac{g_i e^{-\frac{E_j}{kT}}}{U^s(T)}$$

Where $\overline{I_{ij}}$ represents the measured integral line intensity (counts), C^s is the concentration of the emitting species in the plasma. The experimental parameter F takes into account the optical efficiency of the collection system, as well as the total plasma number density and its volume. The spectral response of the collecting optics, spectrometer and detector, which is characteristic of the experimental apparatus, should be measured once radio metrically, for all determinations. The spectral intensity values are then normalised by the efficiency curve. Only the relative response of the system must be determined, because the information of absolute intensity of the lines is included in the parameter F. The C^s and T values must be determined from the experimental data. The partition function of each species can be calculated from the known spectroscopic data once the plasma temperature has been determined. By defining the quantities:

$y = ln\frac{\overline{I_{ij}}}{g_i A_{ij}}, = E_i, m = -\frac{1}{k_B T}, q^s = ln\frac{C^s F}{U^s T}$.

Taking the logarithm of both sides, we can write: $y = mx + q^s$.

A similar equation can be written for each specimen in the plasma. Using the definitions of the quantities, the intensity value of each experimental LIBS line can be represented as a point on the Boltzmann plane. The data presented in the spectrum can be graphically represented as a Boltzmann plot. Here, the different points lie on several straight parallel lines, with slope m (related to the plasma temperature) and intercept q^S (proportional to the logarithm of the species concentration times the experimental factor F. This takes account of the efficiency of the detection system, the plasma volume and the experimental geometry, each of which correspond to a different atomic specimen.

Experimental data is available for each specimen in the plasma. The concentration of the specimen and consequently the concentration of the corresponding element (multiplied by the experimental factor F) can be calculated as the sum of the concentrations of the neutral and single ionized species. The F factor can be determined by normalising to unite the sum of the species concentration C_s: $\sum_s C_s = \frac{1}{F}\sum_s U_s(T)e^{q_s} = 1$, since the sum of the relative concentrations of all the element must equal unity. Finally, the concentration of all the atomic species of the sample can be obtained as: $C_s = \frac{U_s(T)}{F}e^{q_s}$ [114, 160, 162].

By applying this method, we obtain the concentrations for all the components of the emission, including the trace elements in concentrations up to the detection limit of the technique (which is several mg/kg) without the need for calibrations. There are wide-ranging applications for the calibration-free LIBS method. The application to determine metallic alloy elements was reported by several authors [163-166], The semi-quantitative analysis of soil and brass samples was reported by Herrera *et al.* [165]. The comparison between the CF-LIBS and Monte Carlo simulated annealing optimisation method in vacuum was reported by Herrera *et al.* [166]. The results obtained by CF-LIBS are closer to the certified values than those obtained with MC-LIBS. Sun and Yu [167] reported an improvement in self absorption by an internal reference method with results closer to the reference values.

I.4.3 Performance characteristics

The analytical method can by characterised by criteria as the limit of detection, sensitivity, precision and accuracy.

Limit of detection is the smallest concentration c_L that can be detect with reasonable certainty. The concentration is shown by: $c_L = \frac{x_L - \bar{x}_b}{S}$, where x_L is the limiting detectable including the blank, and $\bar{x}_b$ is the average blank measure. The limiting detectable is defined as $x_L = x_b + ks_b$, where k is a numerical factor chosen according the confidence level desired and s_b is the standard deviation of

the blank measures. Generally k is taken as 3, so we can write: $c_L = \frac{3s_b}{S}$. This means that any concentration resulting in three times the background standard deviation is considered to be just barely detectable.

Sensitivity is defined as the slope of the analytical calibration curve. This curve plots the measure versus the concentration of the analyte in a series of standards where the analyte concentrations are known. That is, $S = dx/dc$ if it is a straight line over the entire concentration ranges of interest. If c is plotted versus x, the plot is called an analytical evaluation curve.

Accuracy is defined by how close the agreement is between the result of a measurement and the true value of the accepted reference value.

Precision is defined by how close the agreement is among independent test results obtained by applying the experimental procedure under stipulated conditions. When the random part of the experimental errors (which affects the results) is small, it shows the procedure is reasonably precise. A measure of precision is the standard deviation.

The difference between accuracy and precision is present on the **Figure I. 9**.

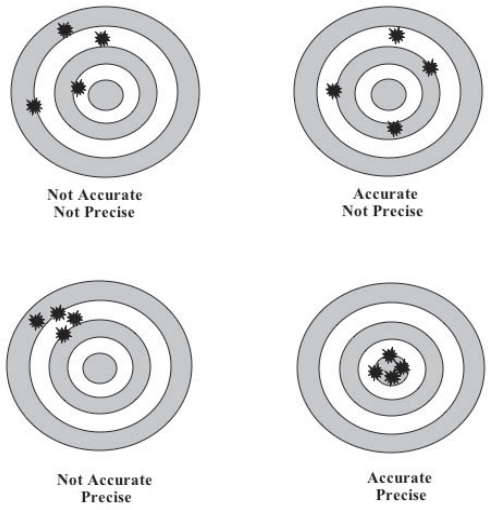

Figure I. 9: Accuracy versus precision [168].

Standard deviation (SD) is the positive square root of the sum of the squares of the deviations between the observations and the mean of the series, divided by one less than the total number in the series. The standard deviation is the positive square root of the variance, a more fundamental statistical quantity: $s = \sqrt{\sum_{i=1} \frac{(x_i - \bar{x})^2}{n-1}}$, where x_i represent the individual measure, and $\bar{x}$ is the mean of n measurements.

Relative standard deviation (RSD) is the standard deviation divided by the mean of the series: $RSD = \frac{s}{\bar{x}}$.

Relative standard deviation % (RSD%) is the $RSD = \left(\frac{s}{\bar{x}}\right) 100$. [169]

I.5 CONCLUSION

As it can be seen from this introduction into the problematic, the fly ashes are produced in big quantity and their use is very variable – road constructions, part of cement concrete. As they are produced form different materials – coal, domestic or industrial waste, their chemical composition vary from ppb to %w/w for many elements, which some can be dangerous for environment and human health.

The disadvantage of these samples is, that they have very complex matrix which is not easy to digest by the use of classical methods. This is why new methodology of direct solid sampling is introduced. Selected methods of fly ash characterisation were discussed to understand the complexity of problematic and to select the appropriate sampling methodology and conditions of analysis.

I.6 REFERENCES

1. Smeda, A. and W. Zyrnicki, *Application of sequential extraction and the ICP-AES method for study of the partitioning of metals in fly ashes.* Microchemical Journal, 2002. **72**(1): p. 9-16.
2. Baranowska, I., A. Slaczka, and K. Srogi, *Differential pulse polarography in the analysis of products from coal treatment.* Polish Journal of Environmental Studies, 2001. **10**(1): p. 57-61.
3. *www.epa.gov*. June 2008.
4. *www.mindfully.org*. June 2008.
5. *www.eea.europa.eu*. June 2008.
6. *www.inchem.org*. June 2008.
7. *Babcock and Wilcox, Steam, Its Generation and Use, New York, 1978.*
8. *www.undererc.gov*. June 2009.
9. *www.cypenv.org*. June 2009.
10. Vassilev, S.V. and C.G. Vassileva, *A new approach for the classification of coal fly ashes based on their origin, composition, properties, and behaviour.* Fuel, 2007. **86**(10-11): p. 1490-1512.
11. Cockrell, C.F.M., R.B.; Leonard, J.W.; Anderson, R.E, *Potential for recovering unreacted lime from limestome-modified fly ash by agglomerate.* U.S. Clearinghouse Fed. Sci. Tech. Inform., 1970. **267**(No. 196779).
12. Association, A.F.A. *www.acaa-usa.org* June 2007].
13. Roy, D.M.L., K. Diamond S. , *Characterization of fly ash and its reactions in concrete.* Materials Research Society Symposium Proceeding, 1985. **43**: p. 3–20.
14. Baker, E.G. and L.K. Mudge, *Catalytic Tar Conversion in Coal-Gasification Systems.* Industrial & Engineering Chemistry Research, 1987. **26**(7): p. 1390-1395.
15. Wesche, K., *Fly ash in concrete: Properties and performance.* Rilem report 7, 1991.
16. Sidhu, B.S., et al., *Wear and oxidation behaviour of shrouded plasma sprayed fly ash coatings.* Tribology International, 2007. **40**(5): p. 800-808.
17. Chen, B. and J. Liu, *Experimental application of mineral admixtures in lightweight concrete with high strength and workability.* Construction and Building Materials, 2008. **22**(6): p. 1108-1113.
18. Chugh, Y., et al., *Development of construction materials using sulfite-rich scrubber sludge and fly ash.* Fuel, 2006. **85**(16): p. 2323-2329.
19. Krishnaiah, S. and D. Singh, *Determination of thermal properties of some supplementary cementing materials used in cement and concrete.* Construction and Building Materials, 2006. **20**(3): p. 193-198.

20. Goswami, R.K. and C. Mahanta, *Leaching characteristics of residual lateritic soils stabilised with fly ash and lime for geotechnical applications.* Waste Management, 2007. **27**(4): p. 466-481.
21. Yunusa, I.A.M., et al., *Fly-ash: An exploitable resource for management of Australian agricultural soils.* Fuel, 2006. **85**(16): p. 2337-2344.
22. Lee, H., et al., *Fly ash effect on improving soil properties and rice productivity in Korean paddy soils.* Bioresource Technology, 2006. **97**(13): p. 1490-1497.
23. Jala, S. and D. Goyal, *Fly ash as a soil ameliorant for improving crop production - a review.* Bioresource Technology, 2006. **97**(9): p. 1136-1147.
24. Taha, R.A., et al., *Evaluation of controlled low strength materials containing industrial by-products.* Building and Environment, 2007. **42**(9): p. 3366-3372.
25. Katz, A. and K. Kovler, *Utilization of industrial by-products for the production of controlled low strength materials (CLSM).* Waste Management, 2004. **24**(5): p. 501-512.
26. Francois, D. and C. Criado, *Monitoring of leachate at a test road using treated fly ash from municipal solid waste incinerator.* Journal of Hazardous Materials, 2007. **139**(3): p. 543-549.
27. Yarbasi , N., E. Kalkan, and S. Akbulut, *Modification of the geotechnical properties, as influenced by freeze thaw, of granular soils with waste additives.* Cold Regions Science and Technology, 2007. **48**(1): p. 44-54.
28. Lin, D., J. Lin, and S. Chen, *The application of baghouse fines in Taiwan.* Resources, Conservation & Recycling, 2006. **46**(3): p. 281-301.
29. Vilches, L., et al., *Insulating capacity of fly ash pastes used for passive protection against fire.* Cement and Concrete Composites, 2005. **27**(7-8): p. 776-781.
30. Chang, F. and M. Wey, *Comparison of the characteristics of bottom and fly ashes generated from various incineration processes.* Journal of Hazardous Materials, 2006. **138**(3): p. 594-603.
31. Chang, C., et al., *Application of methods (sequential extraction procedures and high-pressure digestion method) to fly ash particles to determine the element constituents: A case study for BCR 176.* Journal of Hazardous Materials, 2009. **163**(2-3): p. 578-587.
32. Zhang, Y.F., et al., *Determination of trace rare earth elements in coal fly ash and atmospheric particulates by electrothermal vaporization inductively coupled plasma mass spectrometry with slurry sampling.* Environmental Pollution, 2007. **148**(2): p. 459-467.
33. Smith, K., et al., *Investigation of Fly Ash Particulates Using SEM, TEM and Synchrotron Microprobe Techniques.* Microscopy and Microanalysis, 2005. **11**(S02): p. 1686-1687.

34. Piispanen, M.H., et al., *A Comparative Study of Fly ash Characterization by LA-ICP-MS and SEM-EDS.* Energy & Fuels, 2009. **23**(7): p. 3451-3456.

35. Zevenbergen, C., et al. *Clay formation during weathering of alkaline coal fly ash*. in *International Ash Utilisation Symposium*. 1999.

36. Chen, Y., et al., *Characterization of ultrafine coal fly ash particles by energy-filtered TEM.* Journal of Microscopy, 2005. **217**(3): p. 225.

37. Pattanaik, S., et al., *X-ray absorption fine structure spectroscopy and X-ray diffraction study of cementitious materials derived from coal combustion by-products.* Cement and Concrete Research, 2004. **34**(7): p. 1243-1249.

38. Sobczak, N., et al., *TEM characterization of the reaction products in aluminium fly ash couples.* Materials Chemistry & Physics, 2003. **81**(2-3): p. 296-300.

39. Kutchko, B. and A. Kim, *Fly ash characterization by SEM EDS.* Fuel, 2006. **85**(17-18): p. 2537-2544.

40. Nuhoglu, Y. and F. Bulbul, *Elemental analysis of the ashes of main thermal power plants in Turkey.* Journal of Trace and Microprobe Techniques, 2003. **21**(4): p. 721-728.

41. Bartoòová, L., Z. Klika, and D. Spears, *Characterization of unburned carbon from ash after bituminous coal and lignite combustion in CFBs.* Fuel, 2007. **86**(3): p. 455-463.

42. Li, Z., et al., *Partitioning behaviour of trace elements in a stoker-fired combustion unit: An example using bituminous coals from the Greymouth coalfield (Cretaceous), New Zealand.* International Journal of Coal Geology, 2005. **63**(1-2): p. 98-116.

43. Pires, M. and X. Querol, *Characterization of Candiota (South Brazil) coal and combustion by-product.* International Journal of Coal Geology, 2004. **60**(1): p. 57-72.

44. Silva, L., T. Moreno, and X. Querol, *An introductory TEM study of Fe-nanominerals within coal fly ash.* Science of the Total Environment, 2009.

45. Iwashita, A., et al., *Determination of trace elements in coal and coal fly ash by joint-use of ICP-AES and atomic absorption spectrometry.* Talanta, 2007. **71**(1): p. 251-257.

46. Iwashita, A., et al., *Effect of pretreatment conditions on the determination of major and trace elements in coal fly ash using ICP-AES.* Fuel, 2006. **85**(2): p. 257-263.

47. Halmos, P., et al., *Direct analysis of fly ash materials by inductively coupled plasma atomic emission spectrometry using slurry nebulization.* Microchemical Journal, 2005. **79**(1-2): p. 25-28.

48. D az-Somoano, M., M. Antonia López-Antón, and M. Rosa Martinez-Tarazona, *Determination of selenium by ICP-MS and HG-ICP-MS in coal, fly ashes and sorbents used for flue gas cleaning.* Fuel, 2004. **83**(2): p. 231-235.

49. Alvarez-Ayuso, E., X. Querol, and A. Tomas, *Environmental impact of a coal combustion-desulphurisation plant: abatement capacity of desulphurisation process and environmental characterisation of combustion by-products.* Chemosphere, 2006. **65**(11): p. 2009-17.

50. Bettinelli, M. and U. Baroni, *Icp-Ms Multielemental Characterization of Coal Fly-Ash.* Atomic Spectroscopy, 1995. **16**(5): p. 203-210.

51. Skodras, G., et al., *Quality characteristics of Greek fly ashes and potential uses.* Fuel Processing Technology, 2007. **88**(1): p. 77-85.

52. Burton, L. and M. Blades, *Computer simulation of spectral interferences in inductively coupled plasma-optical emission spectroscopy.* Spectrochimica Acta, 1988. **43**.

53. Botto, R., *Quality assurance in operating a multielement ICP emission spectrometer.* Spectrochimica acta. Part B: Atomic spectroscopy, 1984. **39**(1): p. 95-113.

54. Ilander, A. and A. Vaisanen, *The determination of trace element concentrations in fly ash samples using ultrasound-assisted digestion followed with inductively coupled plasma optical emission spectrometry.* Ultrasonics Sonochemistry, 2009. **16**(6): p. 763-768.

55. Llorens, J.F., J.L. Fernandez-Turiel, and X. Querol, *The fate of trace elements in a large coal-fired power plant.* Environmental Geology, 2001. **40**(4-5): p. 409-416.

56. Marrero, J., et al., *Characterization and determination of 28 elements in fly ashes collected in a thermal power plant in Argentina using different instrumental techniques.* Spectrochimica Acta Part B-Atomic Spectroscopy, 2007. **62**(2): p. 101-108.

57. Gomez, D., et al., *Fractionation of metals and metalloids by chemical bonding from particles accumulated by electrostatic precipitation in an Argentine thermal power plant.* Microchemical Journal, 2007. **85**(2): p. 276-284.

58. Szymczycha-Madeja, A. and W. Mulak, *Comparison of various digestion procedures in chemical analysis of spent hydrodesulfurization catalyst.* Journal of Hazardous Materials, 2009. **164**(2-3): p. 776-780.

59. Bettinelli, M., et al., *Determination of trace elements in power plant emissions by inductively coupled plasma mass spectrometry, comparison with other spectrometric techniques.* Microchemical Journal, 1998. **59**(2): p. 203-218.

60. Koukouzas, N., et al., *Mineralogical and elemental composition of fly ash from pilot scale fluidised bed combustion of lignite, bituminous coal, wood chips and their blends.* Fuel, 2007. **86**(14): p. 2186-2193.

61. Das, A.K., et al., *ICP-MS multielement determination in fly ash after microwave-assisted digestion of samples.* Talanta, 2001. **54**(5): p. 975-981.

62. Swami, K., et al., *Microwave assisted digestion of atmospheric aerosol samples followed by inductively coupled plasma mass spectrometry determination of trace elements.* Fresenius Journal of Analytical Chemistry, 2001. **369**(1): p. 63-70.

63. Pentari, D., A.E. Foscolos, and V. Perdikatsis, *Trace element contents in the Domeniko lignite deposit, Elassona Basin, Central Greece.* International Journal of Coal Geology, 2004. **58**(4): p. 261-268.

64. Depoi, F.S., D. Pozebon, and W.D. Kalkreuth, *Chemical characterization of feed coals and combustion-by-products from Brazilian power plants.* International Journal of Coal Geology, 2008. **76**(3): p. 227-236.

65. Liu, H.T. and S.J. Jiang, *Determination of copper in coal fly ash in the presence of excess titanium by dynamic reaction cell inductively coupled plasma mass spectrometry.* Analytical and Bioanalytical Chemistry, 2003. **375**(2): p. 306-309.

66. Ni, J.L., C.C. Liu, and S.J. Jiang, *Determination of Ga, Ge, As, Se and Sb in fly ash samples by ultrasonic slurry sampling electrothermal vaporization inductively coupled plasma mass spectrometry.* Analytica Chimica Acta, 2005. **550**(1-2): p. 144-150.

67. Ilander, A. and A. Vaisanen, *An ultrasound-assisted digestion method for the determination of toxic element concentrations in ash samples by inductively coupled plasma optical emission spectrometry.* Analytica Chimica Acta, 2007. **602**(2): p. 195-201.

68. Zhang, Y.F., Z.C. Jiang, and B. Hu, *Determination of refractory elements in atmospheric particulates using slurry sampling electrothermal vaporization inductively coupled plasma optical emission spectrometry and inductively coupled plasma mass spectrometry with polyvinylidene fluoride as chemical modifier.* Rapid Communications in Mass Spectrometry, 2006. **20**(14): p. 2091-2098.

69. Xie, H.L., et al., *Determination of trace multi-elements in coal fly ash by inductively coupled plasma mass spectrometry.* Journal of Central South University of Technology, 2007. **14**(1): p. 68-72.

70. Hassan, N.M., et al., *Analysis of environmental samples using microwave-assisted acid digestion and inductively coupled plasma mass spectrometry: Maximizing total element recoveries.* Water Air and Soil Pollution, 2007. **178**(1-4): p. 323-334.

71. Renfrow, M.B., J.M. Riley, and J.T. Riley, *Inductively coupled plasma-atomic emission spectrometric analysis of aqueous slurries of solids.* Microchemical Journal, 1997. **56**(1): p. 30-39.

72. Dogan, O. and M. Kobya, *Elemental analysis of trace elements in fly ash sample of Yatagan thermal power plants using EDXRF.* Journal of Quantitative Spectroscopy & Radiative Transfer, 2006. **101**(1): p. 146-150.

73. Ohki, A., et al., *Analysis of arsenic and some other elements in coal fly ash by X-ray photoelectron spectroscopy.* Journal of Hazardous Materials, 2005. **119**(1-3): p. 213-7.

74. Bettinelli, M., et al., *Microwave oven digestion of power plant emissions and ICP-MS determination of trace elements.* Atomic Spectroscopy, 1998. **19**(3): p. 73-79.

75. Eighmy, T.T., et al., *Comprehensive Approach toward Understanding Element Speciation and Leaching Behavior in Municipal Solid-Waste Incineration Electrostatic Precipitator Ash.* Environmental Science & Technology, 1995. **29**(3): p. 629-646.

76. Bettinelli, M., S. Spezia, and S. Roberti, *Determination of mercury in coal using FI-CVAAS and FI-CV-ICP-MS.* Atomic Spectroscopy, 1999. **20**(1): p. 13-19.

77. Spears, D.A., *The use of laser ablation inductively coupled plasma-mass spectrometry (LA ICP-MS) for the analysis of fly ash.* Fuel, 2004. **83**(13): p. 1765-1770.

78. Vanheuzen, A.A. and J.B.W. Morsink, *Analysis of Solids by Laser Ablation Inductively Coupled Plasma Mass-Spectrometry (La-Icp-Ms) .2. Matching with a Pressed Pellet.* Spectrochimica Acta Part B-Atomic Spectroscopy, 1991. **46**(14): p. 1819-1828.

79. Coedo, A., I. Padilla, and M. Dorado, *Determination of minor elements in steelmaking flue dusts using laser ablation inductively coupled plasma mass spectrometry.* Talanta, 2005. **67**(1): p. 136-143.

80. Noda, M., et al., *Detection of carbon content in a high-temperature and high-pressure environment using laser-induced breakdown spectroscopy.* Spectrochimica Acta Part B-Atomic Spectroscopy, 2002. **57**(4): p. 701-709.

81. SciFinder, *http://scifinder.cas.org*.

82. Becker, J.S., *Applications of inductively coupled plasma mass spectrometry and laser ablation inductively coupled plasma mass spectrometry in materials science.* Spectrochimica Acta Part B-Atomic Spectroscopy, 2002. **57**(12): p. 1805-1820.

83. Mokgalaka, N.S. and J.L. Gardea-Torresdey, *Laser ablation inductively coupled plasma mass spectrometry: Principles and applications.* Applied Spectroscopy Reviews, 2006. **41**(2): p. 131-150.

84. Beauchemin, D., *Inductively coupled plasma mass spectrometry.* Analytical Chemistry, 2008. **80**(12): p. 4455-4486.

85. Garcia, C.C., et al., *Elemental fractionation and stoichiometric sampling in femtosecond laser ablation.* Journal of Analytical Atomic Spectrometry, 2008. **23**(4): p. 470-478.

86. Motelica-Heino, M., P. Le Coustumer, and O.F.X. Donard, *Micro- and macro-scale investigation of fractionation and matrix effects in LA-ICP-MS at 1064 nm and 266 nm on glassy materials.* Journal of Analytical Atomic Spectrometry, 2001. **16**(6): p. 542-550.

87. Hattendorf, B., C. Latkoczy, and D. Günther, *Peer Reviewed: Laser Ablation-ICPMS.* Analytical Chemistry, 2003. **75**(15): p. 341-347.

88. Poitrasson, F., et al., *Comparison of ultraviolet femtosecond and nanosecond laser ablation inductively coupled plasma mass spectrometry analysis in glass, monazite, and zircon.* Analytical Chemistry, 2003. **75**(22): p. 6184-6190.

89. Koch, J., et al., *Particle size distributions and compositions of aerosols produced by near-IR femto-and nanosecond laser ablation of brass.* Journal of Analytical Atomic Spectrometry, 2004. **19**(2): p. 267-272.

90. González, J., et al., *UV-femtosecond and nanosecond laser ablation-ICP-MS: internal and external repeatability.* Journal of Analytical Atomic Spectrometry, 2006. **21**(8): p. 778-784.

91. Horn, I. and D. Gunther, *The influence of ablation carrier gasses Ar, He and Ne on the particle size distribution and transport efficiencies of laser ablation-induced aerosols: implications for LA-ICP-MS.* Applied Surface Science, 2003. **207**(1-4): p. 144-157.

92. Wang, Z., B. Hattendorf, and D. Günther, *Analyte response in laser ablation inductively coupled plasma mass spectrometry.* Journal of the American Society for Mass Spectrometry, 2006. **17**(5): p. 641-651.

93. Pisonero, J., D. Fliegel, and D. Gunther, *High efficiency aerosol dispersion cell for laser ablation-ICP-MS.* Journal of Analytical Atomic Spectrometry, 2006. **21**(9): p. 922-931.

94. Feldmann, I., et al., *Optimisation of a laser ablation cell for detection of hetero-elements in proteins blotted onto membranes by use of inductively coupled plasma mass spectrometry.* Journal of Analytical Atomic Spectrometry, 2006. **21**(10): p. 1006-1015.

95. Günther, D. and B. Hattendorf, *Solid sample analysis using laser ablation inductively coupled plasma mass spectrometry.* Trends in Analytical Chemistry, 2005. **24**(3): p. 255-265.

96. Horn, I., et al., *In situ iron isotope ratio determination using UV-femtosecond laser ablation with application to hydrothermal ore formation processes.* Geochimica Et Cosmochimica Acta, 2006. **70**(14): p. 3677-3688.

97. Horn, I. and F. von Blanckenburg, *Investigation on elemental and isotopic fractionation during 196 nm femtosecond laser ablation multiple collector inductively coupled plasma mass spectrometry.* Spectrochimica Acta Part B: Atomic Spectroscopy, 2007. **62**(4): p. 410-422.

98. Garcia, C.C., H. Lindner, and K. Niemax, *Laser ablation inductively coupled plasma mass spectrometry-current shortcomings, practical suggestions for improving performance, and*

experiments to guide future development. Journal of Analytical Atomic Spectrometry, 2009. **24**(1): p. 14-26.

99. Russo, R., et al., *Laser ablation in analytical chemistry a review.* Talanta, 2002. **57**(3): p. 425-451.
100. Russo, R., et al., *Laser assisted plasma spectrochemistry: laser ablation.* Journal of Analytical Atomic Spectrometry, 2004. **19**(9): p. 1084-1089.
101. Fernández, B., et al., *Direct analysis of solid samples by fs-LA-ICP-MS.* Trends in Analytical Chemistry, 2007. **26**(10): p. 951-966.
102. Goujon, J., et al., *A compact and portable laser-induced breakdown spectroscopy instrument for single and double pulse applications.* Spectrochimica Acta Part B-Atomic Spectroscopy, 2008. **63**(10): p. 1091-1096.
103. Harmon, R.S., et al., *LIBS for landmine detection and discrimination.* Analytical and Bioanalytical Chemistry, 2006. **385**(6): p. 1140-1148.
104. Giakoumaki, A., K. Melessanaki, and D. Anglos, *Laser-induced breakdown spectroscopy (LIBS) in archaeological science-applications and prospects.* Analytical and Bioanalytical Chemistry, 2007. **387**(3): p. 749-760.
105. Fantoni, R., et al., *Methodologies for laboratory Laser Induced Breakdown Spectroscopy semi-quantitative and quantitative analysis-A review.* Spectrochimica Acta Part B-Atomic Spectroscopy, 2008. **63**(10): p. 1097-1108.
106. Noll, R., et al., *Laser-induced breakdown spectroscopy-From research to industry, new frontiers for process control.* Spectrochimica Acta Part B-Atomic Spectroscopy, 2008. **63**(10): p. 1159-1166.
107. Gottfried, J.L., et al., *Laser-induced breakdown spectroscopy for detection of explosives residues: a review of recent advances, challenges, and future prospects.* Analytical and Bioanalytical Chemistry, 2009. **395**(2): p. 283-300.
108. Rusak, D., et al., *Fundamentals and applications of laser-induced breakdown spectroscopy.* Critical Reviews in Analytical Chemistry, 1997. **27**(4): p. 257-290.
109. Rusak, D., et al., *Recent trends and the future of laser-induced plasma spectroscopy.* Trends in Analytical Chemistry, 1998. **17**(8-9): p. 453-461.
110. Song, K., et al., *Determination of trace elements in zinc-base alloys and rock samples using laser-induced breakdown spectroscopy (LIBS).* Journal of the Korean Physical Society, 1997. **30**(2): p. 463-468.
111. Sneddon, J. and Y. Lee, *Novel and recent applications of elemental determination by laser-induced breakdown spectrometry.* Analytical Letters, 1999. **32**(11): p. 2143-2162.

112. Winefordner, J.D., et al., *Novel uses of lasers in atomic spectroscopy.* Journal of Analytical Atomic Spectrometry, 2000. **15**(9): p. 1161-1189.

113. Winefordner, J.D., et al., *Comparing several atomic spectrometric methods to the super stars: special emphasis on laser induced breakdown spectrometry, LIBS, a future super star.* Journal of Analytical Atomic Spectrometry, 2004. **19**(9): p. 1061-1083.

114. Miziolek, A., V. Palleschi, and I. Schechter, *Laser-induced breakdown spectroscopy (LIBS): fundamentals and applications*. 2006: Cambridge Univ Press.

115. Pasquini, C., et al., *Laser induced breakdown spectroscopy.* Journal of the Brazilian Chemical Society, 2007. **18**(3): p. 463-512.

116. Lee, Y.L. and J. Sneddon, *Quantitative Elemental Analysis of Solid Samples by Arf-Excimer Laser-Ablated Atomic Emission-Spectrometry.* Spectroscopy Letters, 1992. **25**(6): p. 881-891.

117. Novotny, K., et al., *Analysis of powdered tungsten carbide hard-metal precursors and cemented compact tungsten carbides using laser-induced breakdown spectroscopy.* Spectrochimica Acta Part B-Atomic Spectroscopy, 2007. **62**(12): p. 1567-1574.

118. Cremers, D. and L. Radziemski, *Handbook of laser-induced breakdown spectroscopy*. 2006: John Wiley.

119. Gottfried, J.L., et al., *Double-pulse standoff laser-induced breakdown spectroscopy for versatile hazardous materials detection.* Spectrochimica Acta Part B-Atomic Spectroscopy, 2007. **62**(12): p. 1405-1411.

120. Gottfried, J.L., et al., *Strategies for residue explosives detection using laser-induced breakdown spectroscopy.* Journal of Analytical Atomic Spectrometry, 2008. **23**(2): p. 205-216.

121. De Lucia, F.C., et al., *Double pulse laser-induced breakdown spectroscopy of explosives: Initial study towards improved discrimination.* Spectrochimica Acta Part B-Atomic Spectroscopy, 2007. **62**(12): p. 1399-1404.

122. Noll, R., et al., *Laser-induced breakdown spectrometry - applications for production control and quality assurance in the steel industry.* Spectrochimica Acta Part B-Atomic Spectroscopy, 2001. **56**(6): p. 637-649.

123. Mitchell, P.G., J. Sneddon, and L.J. Radziemski, *Direct Determination of Copper in Solids by Direct-Current Argon Plasma Emission-Spectrometry with Sample Introduction Using Laser Ablation.* Applied Spectroscopy, 1987. **41**(1): p. 141-148.

124. Musil, P., et al., *Determination of elements in agricultural soils using IR laser ablation inductively coupled plasma atomic emission spectrometry.* Spectrochimica Acta Part B-Atomic Spectroscopy, 2000. **55**(11): p. 1747-1758.

125. Ramsey, M.H., et al., *An Objective Assessment of Analytical Method Precision - Comparison of Icp-Aes and Xrf for the Analysis of Silicate Rocks.* Chemical Geology, 1995. **124**(1-2): p. 1-19.

126. Kleiber, L., et al., *Strategies for the analysis of coal by laser ablation inductively coupled plasma mass spectroscopy.* Analytical and Bioanalytical Chemistry, 2002. **374**(1): p. 109-114.

127. Petkovic, M., et al., *Application of flavonoids - quercetin and rutin - as new matrices for matrix-assisted laser desorption/ionization time-of-flight mass spectrometric analysis of Pt(II) and Pd(II) complexes.* Rapid Commun Mass Spectrom, 2009. **23**(10): p. 1467-75.

128. Tibi, M. and K. Heumann, *Isotope dilution mass spectrometry as a calibration method for the analysis of trace elements in powder samples by LA-ICP-MS.* Journal of Analytical Atomic Spectrometry, 2003. **18**(9): p. 1076-1081.

129. Klemm, W. and G. Bombach, *A simple method of target preparation for the bulk analysis of powder samples by laser ablation inductively coupled plasma mass spectrometry (LA ICP MS).* Fresenius'Journal of Analytical Chemistry, 2001. **370**(5): p. 641-646.

130. Arrowsmith, P., *Laser ablation of solids for elemental analysis by inductively coupled plasma mass spectrometry.* Analytical Chemistry, 1987. **59**(10): p. 1437-1444.

131. Bousquet, B., J. Sirven, and L. Canioni, *Towards quantitative laser-induced breakdown spectroscopy analysis of soil samples.* Spectrochimica Acta Part B: Atomic Spectroscopy, 2007.

132. Arroyo, L., et al., *Optimization and validation of a LA-ICP-MS method for the routine analysis of soils and sediments.* Spectrochim. Acta B, 2009. **64**: p. 16 25.

133. Moenkeblankenburg, L., T. Schumann, and J. Nolte, *Direct Solid Soil Analysis by Laser-Ablation Inductively-Coupled Plasma-Atomic Emission-Spectrometry.* Journal of Analytical Atomic Spectrometry, 1994. **9**(9): p. 1059-1062.

134. Pearce, N.J.G., et al., *A compilation of new and published major and trace element data for NIST SRM 610 and NIST SRM 612 glass reference materials.* Geostandards Newsletter-the Journal of Geostandards and Geoanalysis, 1997. **21**(1): p. 115-144.

135. Jackson, B., et al., *Elemental mapping and quantitative analysis of Cu, Zn, and Fe in rat brain sections by laser ablation ICP-MS.* Analytical and Bioanalytical Chemistry, 2006. **384**(4): p. 951-957.

136. Elish, E., Z. Karpas, and A. Lorber, *Determination of uranium concentration in a single hair strand by LAICPMS applying continuous and single pulse ablation.* Journal of Analytical Atomic Spectrometry, 2007. **22**(5): p. 540-546.

137. Liu, Y.S., et al., *In situ analysis of major and trace elements of anhydrous minerals by LA-ICP-MS without applying an internal standard.* Chemical Geology, 2008. **257**(1-2): p. 34-43.

138. Leach, A.M. and G.M. Hieftje, *Methods for shot-to-shot normalization in laser ablation with an inductively coupled plasma time-of-flight mass spectrometer.* Journal of Analytical Atomic Spectrometry, 2000. **15**(9): p. 1121-1124.

139. Craig, C., K. Jarvis, and L. Clarke, *An assessment of calibration strategies for the quantitative and semi-quantitative analysis of calcium carbonate matrices by laser ablation-inductively coupled plasma-mass spectrometry (LA-ICP-MS).* Journal of Analytical Atomic Spectrometry, 2000. **15**(8): p. 1001-1008.

140. Fitzpatrick, A., et al., *Fabrication of solid calibration standards by a sol gel process and use in laser ablation ICPMS.* Journal of Analytical Atomic Spectrometry, 2008. **23**(2): p. 244-248.

141. Kuhn, H.R. and D. Gunther, *A quantification strategy in laser ablation ICP-MS based on the transported aerosol particle volume determined by optical particle size measurement.* Journal of Analytical Atomic Spectrometry, 2006. **21**(11): p. 1209-1213.

142. Pickhardt, C., et al., *On-line isotope dilution in laser ablation inductively coupled plasma mass spectrometry using a microflow nebulizer inserted in the laser ablation chamber.* International Journal of Mass Spectrometry, 2006. **248**(3): p. 136-141.

143. Boulyga, S., J. Heilmann, and K. Heumann, *Isotope dilution ICP-MS with laser-assisted sample introduction for direct determination of sulfur in petroleum products.* Analytical and Bioanalytical Chemistry, 2005. **382**(8): p. 1808-1814.

144. Boulyga, S.F., et al., *Development of an accurate, sensitive, and robust isotope dilution laser ablation ICP-MS method for simultaneous multi-element analysis (chlorine, sulfur, and heavy metals) in coal samples.* Analytical and Bioanalytical Chemistry, 2007. **389**(3): p. 697-706.

145. Thompson, M., S. Chenery, and L. Brett, *Calibration Studies in Laser Ablation Microprobe - Inductively Coupled Plasma Atomic Emission-Spectrometry.* Journal of Analytical Atomic Spectrometry, 1989. **4**(1): p. 11-16.

146. Gunther, D., et al., *Capabilities of an Argon Fluoride 193 nm excimer laser for laser ablation inductively coupled plasma mass spectrometry microanalysis of geological materials.* Journal of Analytical Atomic Spectrometry, 1997. **12**(9): p. 939-944.

147. Günther, D., et al., *Direct liquid ablation: a new calibration strategy for laser ablation-ICP-MS microanalysis of solids and liquids.* Fresenius'Journal of Analytical Chemistry, 1997. **359**(4): p. 390-393.

148. Cromwell, E. and P. Arrowsmith, *Semiquantitative analysis with laser ablation inductively coupled plasma mass spectrometry.* Analytical chemistry, 1995. **67**: p. 131-131.

149. Pickhardt, C., J. Becker, and H. Dietze, *A new strategy of solution calibration in laser ablation inductively coupled plasma mass spectrometry for multielement trace analysis of geological samples.* Fresenius'Journal of Analytical Chemistry, 2000. **368**(2): p. 173-181.

150. Halicz, L. and D. Günther, *Quantitative analysis of silicates using LA-ICP-MS with liquid calibration.* Journal of Analytical Atomic Spectrometry, 2004. **19**(12): p. 1539-1545.

151. Mao, X.L. and R.E. Russo, *Optimization and calibration of laser ablation inductively coupled plasma atomic emission spectrometry by measuring vertical spatial intensity profiles.* Journal of Analytical Atomic Spectrometry, 1997. **12**(2): p. 177-182.

152. Masters, B. and B. Sharp, *Universal calibration strategy for laser ablation inductively coupled plasma mass spectrometry based on the use of aqueous standards with modified absorption coefficients.* Analytical Communications, 1997. **34**(9): p. 237-239.

153. Boue-Bigne, F., et al., *A calibration strategy for LA-ICP-MS analysis employing aqueous standards having modified absorption coefficients.* Journal of Analytical Atomic Spectrometry, 1999. **14**(11): p. 1665-1672.

154. Jarvis, K., et al., *Handbook of inductively coupled plasma mass spectrometry*. 1992: Blackie Glasgow.

155. Botha, A., A. Barzev, and J. Fischer, *Isotope dilution ICP-MS analysis of trace elements in a Syenite rock reference material.* Journal of Analytical Atomic Spectrometry, 2007. **22**(5): p. 578-581.

156. Yang, L., et al., *Application of double-spike isotope dilution for the accurate determination of Cr(III), Cr(VI) and total Cr in yeast.* Analytical and Bioanalytical Chemistry, 2006. **386**(6): p. 1673-1680.

157. Point, D., et al., *Simultaneous determination of inorganic mercury, methylmercury, and total mercury concentrations in cryogenic fresh-frozen and freeze-dried biological reference materials.* Analytical and Bioanalytical Chemistry, 2007. **389**(3): p. 787-798.

158. Ciceri, E., et al., *Validation of an isotope dilution, ICP-MS method based on internal mass bias correction for the determination of trace concentrations of Hg in sediment cores.* Talanta, 2008. **74**(4): p. 642-647.

159. Heumann, K., *Isotope-dilution ICP MS for trace element determination and speciation: from a reference method to a routine method?* Analytical and Bioanalytical Chemistry, 2004. **378**(2): p. 318-329.

160. Ciucci, A., et al., *New procedure for quantitative elemental analysis by laser-induced plasma spectroscopy.* Applied Spectroscopy, 1999. **53**(8): p. 960-964.

161. Ciucci, A., et al., *CF-LIPS: A new approach to LIPS spectra analysis.* Laser and Particle Beams, 1999. **17**(4): p. 793-797.

162. Corsi, M., et al., *Double pulse, calibration-free laser-induced breakdown spectroscopy: A new technique for in situ standard-less analysis of polluted soils.* Applied Geochemistry, 2006. **21**(5): p. 748-755.

163. Aguilera, J., et al., *Application of calibration-free laser-induced breakdown spectroscopy to radially resolved spectra from a copper-based alloy laser-induced plasma.* Spectrochimica Acta Part B: Atomic Spectroscopy, 2009. **64**(7): p. 685-689.

164. Sun, L.X. and H.B. Yu, *Correction of self-absorption effect in calibration-free laser-induced breakdown spectroscopy by an internal reference method.* Talanta, 2009. **79**(2): p. 388-395.

165. Herrera, K., et al., *Semi-quantitative analysis of metal alloys, brass and soil samples by calibration-free laser-induced breakdown spectroscopy: recent results and considerations.* Journal of Analytical Atomic Spectrometry, 2009. **24**(4): p. 413-425.

166. Herrera, K., et al., *Comparative study of two standard-free approaches in laser-induced breakdown spectroscopy as applied to the quantitative analysis of aluminum alloy standards under vacuum conditions.* Journal of Analytical Atomic Spectrometry, 2009. **24**(4): p. 426-438.

167. Sun, L. and H. Yu, *Correction of self-absorption effect in calibration-free laser-induced breakdown spectroscopy by an internal reference method.* Talanta, 2009.

168. *http://celebrating200years.noaa.gov/magazine/tct/accuracy_vs_precision.html*. Septembre 2009.

169. *IUPAC. Compendium of Chemical Terminology, 2nd ed. (the "Gold Book"). Compiled by A. D. McNaught and A. Wilkinson. Blackwell Scientific Publications, Oxford (1997). XML on-line corrected version: http://goldbook.iupac.org (2006-) created by M. Nic, J. Jirat, B. Kosata; updates compiled by A. Jenkins. ISBN 0-9678550-9-8. doi:10.1351/goldbook*. July 2009.

II Part II

Experimental Part

II.1 Introduction to laser spectrochemistry

The word LASER is an acronym for **L**ight **A**mplification by **S**timulated **E**mission of **R**adiation. It is a quantum mechanical device that produces coherent radiation. The origins of laser theory are dating by the year 1916, where Albert Einstein has for the first time defined stimulated emission. The first laser was made in 1960 and the big laser development started in the 1970s [1].

The principle is based in the quantum mechanics, which is closely related with the transfer of energy among atoms and molecules. The energy of a particular level is measured relative to the ground level, which is marked zero level with zero energy. The changing of the level from one to another is called transition. This transition can be from the lower energy level to the higher energy level, this phenomenon is called excitation, or it can be the transition from the higher energy level to the lower energy level, and this has name deexcitation. Excitation into the excited state requires the absorption of an amount of energy equal to the differences in energy between the two levels. The deexcitation is accompanied by the release of the transition energy. Atoms and molecules can absorb or release the energy in the form of photons, quanta or electromagnetic radiation. There are three different cases that can be observed, **Figure II. 1**.

The first is, when the atom is in excitation, after some period of time, it may spontaneously return to the ground level by releasing the energy in form of photon. This process is called spontaneous emission. In the second case the photon emission is stimulated by incoming photons, and this process is called as a stimulated emission. The third case is called absorption. This occurs when the photons are absorbed by the atoms in excited electronic state.

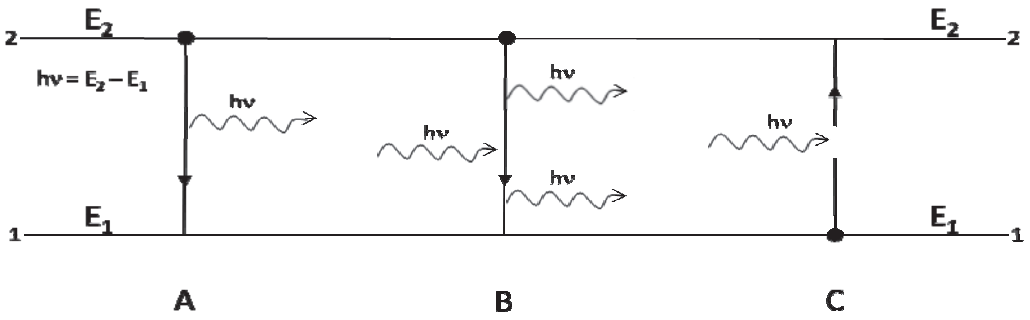

Figure II. 1: Schematic illustration of spontaneous emission (A), stimulated emission (B) and absorption (C).

II.1.1 Spontaneous emission

Spontaneous emission takes place when the atoms are in excited state. There is no external radiation required to initiate the emission. When an atom is in excited state E_2, it gives up spontaneously its energy and falls down to a lower energy level E_1. In the same time the photon of energy is released: $h\nu = E_2 - E_1$. We can write the equation which describes the change in the population density N_2 of level E_2 as the population which is transferred to the zero level. The rate of decrease is proportional to the population of any time:

$$\frac{dN_2}{dt} = -A_{21}N_2$$

Where the $A_{21}$is the Einstein coefficient of spontaneous emission, and can be also called as the spontaneous transition probability. Its reciprocal $\tau = 1/A_{21}$ is the radiative lifetime and is a characteristic parameter of transition.

In the case, when only the spontaneous emission takes place, the solution of the before mentioned equation is:

$$N_2(t) = N_{20}e^{-A_{21}t}$$

The relation between the Einstein coefficient of spontaneous emission and the Einstein coefficient for absorption B_{12} is

$$A_{21} = \frac{8\pi h\nu^3}{c^3}B_{12}$$

Where $\nu = \nu_{12} = \nu_{21}$ is the frequency of the spectral line resulting from the transition between the two states.

The spontaneous emission is the type of non-coherent light emission which is produced for example by the bulb or sun.

II.1.2 Absorption

Absorption takes place when the radiation containing photons of energy $h\nu = (E_2 - E_1)$ is incident on the material with ground state energy E_1 and arbitrary excited state energy E_2. After this stimulus, the atom in the ground level is released in the level E_2. In the process, the photon is absorbed. The energy differences $E_2 - E_1$ which is required by the atom to make the transition is obtained from the energy of the incident electromagnetic wave.

We can define the rate at which the N_1 atoms are raised from energy level E_1 to E_2 using the equation:

$$\left(\frac{dN_1}{dt}\right)_{st} = -B_{12}N_1\rho(\nu)$$

Where $(dN_1/dt)_{st}$ is the rate at which transitions 2→1 occur as a result of stimulated emission and B_{12} is a constant characteristic of the atom (Einstein coefficient of absorption) and $\rho(\nu)$ is the radiation field. This rate of stimulated emission is not depended only on the particular transition, as it is in the case of A, but it depends also on the intensity of the incident electromagnetic wave.

II.1.3 Stimulated emission

Stimulated emission requires the presence of external radiation. When an incident photon with of resonant energy $h\nu = E_2 - E_1$ passes by atom in excited state E_2, it stimulates the atom to drop to the lower state E_1. In this process the atom releases the same energy, direction, phase and polarization as the incident photon. The result is then two identical photons in the place of one, or an increase in the intensity of the incident beam. In this process the rate at which the N_2 atoms are stimulated by the radiation field (photons) to decrease from the level E_2 to the lower level E_1 is proportional both to the number of atoms present and to the density of the radiation field:

$$\left(\frac{dN_2}{dt}\right) = -B_{21}N_2\rho(\nu)$$

Where the B_{21} is the Einstein coefficient of stimulated emission and the photon density is expressed as a function of frequency with a factor $\rho(\nu)$.

This is the process of stimulated emission which makes possible the laser function.

Using the absorption, spontaneous and stimulated emission and the Einstein coefficients A and B, we can focus to the Einstein´s assumptions and their implications:

- ☑ Between radiation fields and the atoms exist the thermodynamic equilibrium with the arbitrary temperature T.
- ☑ The radiation field $\rho(\nu)$ has the spectral distribution characteristic of a blackbody at temperature T.
- ☑ The atom population densities N_2 and N_1 at energy levels E_2 and E_1 are distributed according to the Boltzmann distribution at the temperature.
- ☑ Population densities N_2 and N_1 are constant in time [2].

II.2 BASIC LASER COMPONENTS

The laser instrument is an optical oscillator that emits an intense, highly collimated narrow and monochromatic beam of coherent radiation. A laser has three basic components: an external energy source or pump, an optical amplifier medium and an optical cavity or resonator. These three elements are shown schematically in **Figure II. 2**.

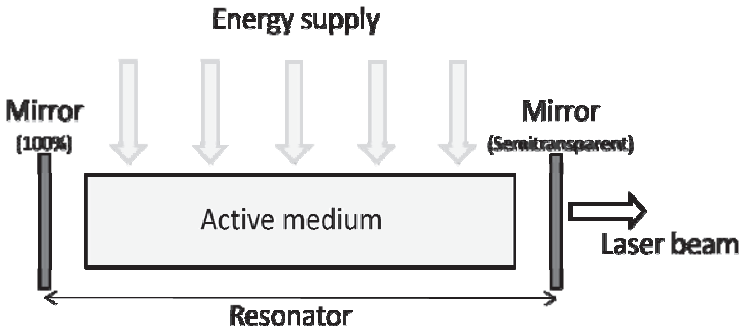

Figure II. 2: The basic elements of the laser.

II.2.1 Energy source (pump)

The **pump** (energy source) produces the inversion population in the laser medium. Several types of pumping are used for different types of lasers:

- ☑ Optical pumping;
- ☑ Electrical pumping;

The two mainly used pumping are optical and electrical. It difference depends on the origin of the source of energy. In the case of the **optical pumping**, the energy is emitted by a powerful lamp or a laser beam. In the case of **electrical pumping**, the energy is done by radio-frequency, or pulsed current flowing in a conductive medium, such as an ionized gas or a semiconductor. The important parameters are the electron excitation cross section and the lifetime of the various energy levels. The type of pumping depends on the laser. Generally, in the case of solid-state or liquid lasers, the optical pumping produced by incoherent source is used. This incoherent source can be a powerful lamp, which is absorbed by the active medium, so that the atoms are pumped into the upper level. In the case of laser pumping where the laser wavelength fall to the absorption bands of the active medium, the narrow light beam is absorbed by the active medium. In the case of gas and semiconductor lasers, the electrical pumping with a sufficiently intense electrical discharge is generally used.

II.2.2 Active medium and population inversion

Other important part of laser is the **active medium** (or amplifying medium), which can be a gas, liquid or solid, and which determines the wavelength of the laser radiation. The requirement of active medium is its ability to support a population inversion between two energy levels of the laser atoms. This is made by pumping more atoms into the higher energy level than exist in the lower energy level. In the case, when there is no pumping present, there is no the **population inversion**

between any two energy levels of a laser medium. Active medium can amplify light by means of the process of stimulated emission.

The **population inversion** is the essential condition for laser operation. Once a population inversion is established in the medium, it can be used to amplify the light. According to the Boltzmann distribution, $N_2/N_1 = e^{-\Delta E/kT}$, where $\Delta E = E_2 - E_1$, the higher level E_2 will always be less populated than the lower level E_1. The population inversion in the medium is creating by the pumping process, which drives the population distribution far from thermal equilibrium. But pumping alone is not sufficient to obtain the population inversion. Because the probability of absorption and stimulated emission is the same, the molecules drop back by photon emission as fast as they are pumped to the upper level. The gain of the optical resonator has to be greater than the losses. The magnitude of the gain which overcomes the losses is called laser threshold. The population inversion is achieved when the gain is larger than the losses in the optical resonator. Then the light can be emitted from the optical cavity.

II.2.3 Resonator (optical cavity)

The goal of this part of laser is to concentrate the light and to stimulate the emission of laser radiation. We can explain is principle using the **Figure II. 3**.

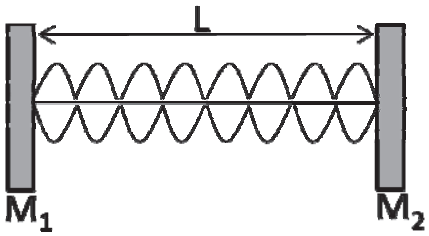

Figure II. 3: Scheme of optical resonator.

If we place a source of radiation emitting at a wavelength λ between the mirrors M_1 and M_2 separated by the distance L, the standing wave can be creates as a result of reflection of the mirrors surfaces. The standing wave can be generated only when this condition is fulfilled:

$$L = n\frac{\lambda}{2}$$

This condition indicates that the standing wave can be generated only when the integer multiple of the wavelengths between this two mirrors is comprised. For the wavelengths that do not fulfil this condition, destructive interference can occur and the intensity of the standing wave may decrease to

zero. The mirror M_1 is almost entirely non-transparent for the radiation inside the cavity; we can assume that the reflectivity is $R{\sim}100\%$, and we can call this mirror as the high reflector. The second mirror M_2 has a larger transparency (with the reflectivity $R = 90 - 99\%$), which allows to the generated radiation to be emitted out of the optical cavity. This mirror is called output coupler. Light propagated along the cavity axis and passing through the pumped active medium is reflected back through it, stimulating further emission in the same direction. This means that laser photons which made multiple reflections within the cavity are amplified at each pass through the active medium.

Optical resonator operates when we deliver the energy by the pumping to the active medium. This energy is not sufficient to affect the system equilibrium; that is the energy level´s does not differ very much from the Boltzmann distribution.

Laser resonator has two types of modes: transverse and longitudinal. Transverse mode represent in the cross sectional profile of the beam, in its intensity pattern. Longitudinal mode corresponds to different resonance along the length of the optical cavity which occurs at different frequencies or wavelengths within the gain bandwidth of a laser. Transverse modes are classified according to the number of nulls than appear across the beam cross section in two directions. The fundamental mode, where intensity peaks at the centre is known as TEM_{00}. A mode with single null along one axis and no null in the perpendicular direction is TEM_{01} or TEM_{10} depending to the orientation. The TEM_{00} is desirable. On the **Figure II. 4** the schematic illustration of the transverse mode which can be achieved is demonstrated.

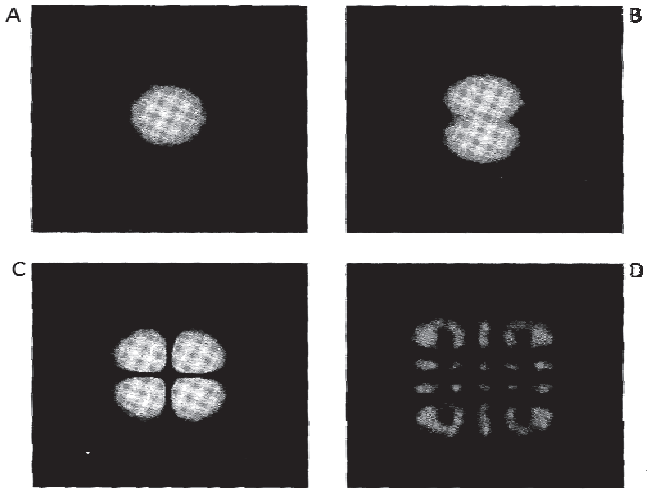

Figure II. 4: Laser transverse-mode patterns: A – 00 mode; B – 01 mode; C – 11 mode; D – coherent superposition of two or more transverse modes [3].

When the laser is oscillating in the TEM_{00} mode, it emits a beam with Gaussian intensity distribution, which is called Gaussian beam. This Gaussian beam can be described as a light beam where the electric field profile in a plane perpendicular to the beam axis can be described with a Gaussian function, possibly with an added parabolic phase profile [4]. In this case, the beam divergence is relatively small and we have the Gaussian intensity profile at any location along the beam axis and this beam is not influenced by the passing throw the simply optics elements (lenses).

After the description of three basic laser elements, we can summarise how these elements work together. Photons of certain resonant energy must be created in optical cavity, they must interact with atoms, and then they must be amplified using stimulated emission, while bouncing back and forth between the mirrors of the resonator. The laser beam is formed using coupling a certain fraction of laser light wave out of the cavity through the output coupler mirror [5-6].

On the **Figure II. 5** is the explication of laser operation. On the two energy levels we are not able to produce the population inversion, for this reason we must use system with more energy levels. On three or four energy levels we can understand what happens to an atom in the laser medium during the creation of a laser photon. In the case of three energy levels, the medium is pumped from the lowest level to the highest level. Populating the middle (metastable state) from the highest level is very fast. Inversion occurs when the middle level population exceeds the population of the lowest level. In the case of four energy levels, pumping occurs from the level 1 to the level 4. Conversion to the level 3 is very fast; the level 2 is populated from the level 3 by photon emission at the lasing wavelength. The population inversion is obtained between the level 3 and level 2. For continuous wave operation, there is necessary that the transition from the level 2 to the level 1, which must be also very fast.

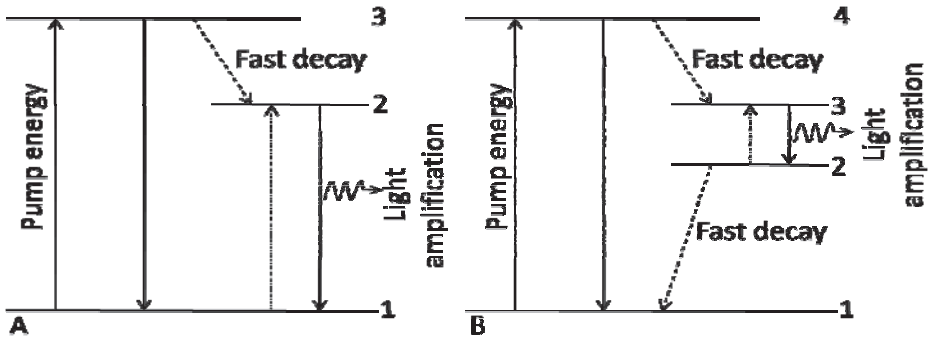

Figure II. 5: Three (A) and four (B) energy laser levels.

II.3 CHARACTERISTICS OF LASER BEAM

After the generation of laser beam we can turn attention of its properties. They are:

- ☑ Directionality;
- ☑ Monochromaticity;
- ☑ Coherence.

II.3.1 Directionality

They are two ways how to measure directionality, also called divergence of the laser beam. The first way is to measure the degree of beam spreading at very large distance from the source. The second way is to measure the radial intensity distribution of the focused beam in the focal plane of a lens. Degree of directionality of a laser beam is due to the geometrical design of the optical cavity and to the monochromatic and coherent nature of light generated in the cavity. Directionality is limited by optical diffraction and the presence of non-desirable off-axis mode. The directional properties of a laser beam are related to its spatial coherence. The laser beam can be with perfect spatial coherence or with the case of partial spatial coherence. In the case of perfect spatial coherence, a beam of finite aperture has unavoidable divergence due to diffraction. The value of divergence can be obtained from diffraction theory. For amplitude distribution we obtain:

$$\Theta_d = \frac{\beta\lambda}{D}$$

Where λ and D are the wavelength and the diameter of the beam. The factor β is a numerical coefficient of the order of unity whose value depends on the shape of the amplitude distribution and how both the divergence of the beam are defined. A beam with the diffraction which can be obtained by this way is called diffraction limited.

II.3.2 Monochromaticity

Monochromaticity means that the laser beam covers only a narrow range of frequencies or wavelengths. The monochromaticity of light is determined by the emission process where atoms in excited states decay to lower energy states and emit light. Monochromaticity is possible when a two

mirror arrangements forms a resonant cavity, oscillation can occur at the resonance frequencies of this cavity.

II.3.3 Coherence

Each light source has a finite coherence length, or distance over which the light they produce is in phase. Coherence is a property that the light wave it contains is in phase with another. They are two concept of coherence: spatial (measure of the uniformity of phase across the optical wave front) and temporal (measure of the degree of monochromaticity of the light). Coherence is a measure of the degree of phase correlation that exists in the radiation field of a light source at different locations and different times. The spatial coherence of a single mode laser beam extends across the full width of the beam. The temporal coherence is many orders of magnitude above that of any ordinary light source.

Laser light can be focused because of its properties described above. It is coherent light that appears to come from a distant point source. The laser beam can be focused using the lens to a small diameter. Laser beam with beam divergence (Θ_d) incident on a lens of focal length (f), whose diameter is several times larger than the width of the incident laser beam, is focused to a diffraction limited spot of diameter approximately equal to:

$$d \cong f\Theta$$

A focus size spot d_0, which is created after the laser beam cross by the focusing lens, can be determined using the focal length of the focus lens f, beam wavelength λ and the entrance beam diameter D as it is shown on the **Figure II. 6**:

$$d_0 = \frac{2f\lambda}{D}$$

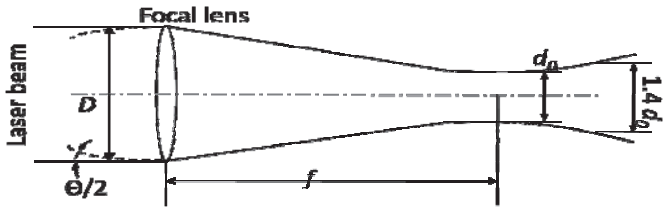

Figure II. 6: Focusing a Gaussian beam.

We can also estimate the Depth of Focus (DOF) that is the range along which the size of the beam is no more than 1.4 times minimum spot size:

$$DOF = 2.5\lambda\left(\frac{f}{D}\right)^2$$

Focusing laser light down to small spot can be achieved by lenses with short focal lengths and laser beam with small divergence. The beam divergence of a laser can be reduced with the additional optics found in beam expander.

There are several temporal operating modes of lasers. **Continuous wave** operation can be achieved only if the lifetime of the upper energy level is longer than that of the lower level. The modes which allow creation of short laser pulses are **Q-switch** mode and **gain switch** mode. Q-switching is technique which allows one to generate laser pulse with duration comparable to a photon decay time and high peak power. The resonator quality (Q) of the cavity is reduced by introducing an intensity-dependent or time-varying loss so that lasing will not take place until the gain of the inverted population has been pumped to a very high value. In the case of Q-switching, the losses are rapidly switched to a low value, in the case of gain switching; it is the laser gain which is rapidly switched to a high value. Gain switching is achieved by using a pumping pulse that is so fast, that the laser gain (and then population inversion) reaches a value which is considerably above the threshold before the number of cavity photons has had time to build up a sufficiently high level to depopulate the inversion. In the case of **locking mode**, we can suppose the oscillating mode with comparable amplitudes which oscillate with some definite relation between their phases. They are two mode locking mode: active mode locking, in which the mode-locking element is driven by an external source, and passive mode locking, in which the element that induce mode-locking is not driven externally but instead exploits some nonlinear optical effect – saturation or a saturable absorber change in a suitable material.

After description how the lasers works and what they consist, we can turn our attention of the different laser types [7-8].

II.4 LASER EMPLOYED IN LIBS AND LASER ABLATION SPECTROSCOPY

Lasers can be classified according its laser medium. The basic laser types are:

- ☑ Solid state lasers;
- ☑ Gas lasers.

In this work, principally the solid state lasers were used, so in this chapter, the main attention will be turned to their description and utilisation.

An example of **solid state laser** is the *ruby laser* working on 694.3 nm. The first ruby laser was demonstrated in the 1960 by Maiman [1]. Ruby laser rods are grown from sapphire (Al_2O_3) doped with about 0.01 to 0.5 percent chromium to form a synthetic ruby crystal having red or pink colour with about 10^{19} chromium atoms per cubic centimetres. There are some limitations in performance because it is three level laser, and the self-absorption can be observed in the un-pumped regions. The main application has been in holography or in the atmospheric ranging, scattering and LIDAR measurements. The *neodymium laser* is the most common laser from solid state lasers. The active medium is usually made from nonconductive solid, typically a glass or crystalline doped by neodymium, chromium, erbium or other ions which provide required energetic conversion. Many of the common dopants are rare earth element and they have been added to improve the optical pumping efficiency of laser ions via fluorescence sensitization. The most used type is the triply ionised neodymium doped yttrium aluminium garnet (YAG) which emit light typically at 1064 nm or using frequency doubled or tripled it emit at 532 or 266 nm. The energy level diagram is showed on the **Figure II. 7**. The alternative of YAG is the YLF – yttrium lithium fluoride laser (oscillate from 1047 to 1053 nm depending on polarization) which is not as hard as YAG and has lower thermal conductivity. The description of lasers, their wavelengths, also with the operating modes (pulse, continuous) is well presented in the Handbook of Lasers [4] or in Industrial Applications of Lasers [9]. The commercially available lasers are listed in the **Table II. 1**.

Table II. 1: Commercially available solid state lasers [9].

Commonly employed in LIBS and LA-ICP		
Laser		**Pulsed wavelength (µm)**
Nd: YAG		1.06, 0.266, 0.355, 0.532, 1.32
Laser		**Pulsed wavelength (µm)**
Ruby		0.694
Nd: Glass		1.06, 0.266, 0.355, 0.532
Alexandrite	Beryllium aluminium oxide	Tuneable 0.72-0.78
Ti: Sapphire	Aluminium oxide	Tuneable 0.7-1.1
Nd: YLF	Yttrium Lithium Fluoride	1.047, 1.31, 0.51, 0.523
Ho: YAG	Yttrium Aluminium Garnet	2.1
Er: YAG	Yttrium Aluminium Garnet	2.4
Uncommon		
Laser		**Pulsed wavelength (µm)**
Co:MgF_2		Tuneable 1.75-2.5
Cr: Th: Ho: YAG	Yttrium Aluminium Garnet	2.09
Er: Glass		1.54
Er: Cr: YSGG	Yttrium Scandium Gallium Garnet	2.79
Er: YSGG	Yttrium Scandium Gallium Garnet	2.79
Ho: YSGG	Yttrium Scandium Gallium Garnet	2.1
Nd: Cr: GSGG	Gadolinium Scandium Gallium Garnet	1.06
Tm: YAG	Yttrium Aluminium Garnet	2.01

The energy range which can be achieved with Nd:YAG laser working on 1064 nm in continuous operations is from 10-20 W, in multi mode operation the energy range can be from 50-100 W. In pulse operations, the energy range is to 100 J, but typical repetition rates is few hertz with rates to 300 Hz at reduced energy and pulse duration in 0.2 to 20 ms range. In Q-switched operations, the pulse energy is to 2 J at low repetition rate and typical pulse duration is in 7-10 ns range.

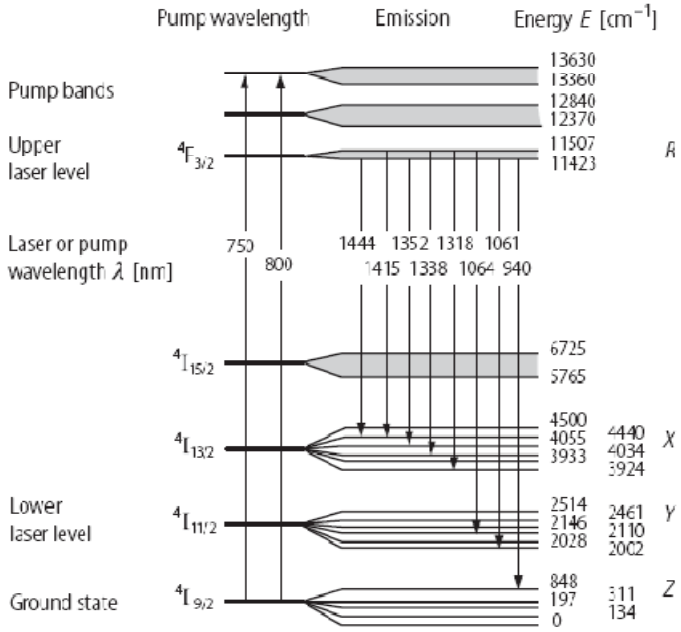

Figure II. 7: Energy level diagram for Nd^{3+} in YAG .

The applications of solid state lasers are very large, in industry, pharmacology, medicine, chemistry, archaeology, and environment.

The helium-neon laser (HeNe) is an example of **gas laser**. As a gain medium is a mixture of helium and neon gases in a 5:1 to 20:1 ratio contained in a glass envelope. The active mediums are helium atoms in excited state that were excited in the electrical discharge. Collision of the excited helium atoms with the ground-state neon atoms results in transfer of energy to the neon atoms. The number of neon atoms entering the excited states builds up as further collisions between helium and neon atoms occur, causing a population inversion. It emits mainly at 632.8 nm, 1152.3 nm and 3391.3 nm.

The carbon dioxide laser (CO_2 laser), argon-ion laser and nitrogen laser are the other example of the gas lasers. The CO_2 molecule is the active medium and is used usually with other gases – He, N_2, H_2. The CO_2 laser emits the infrared light with the principal wavelength around 9.4 and 10.6 µm. this laser is used primarily for cutting and welding.

The argon-ion laser uses an ionised gas (Ar) as an active medium. It provides generation in ultraviolet (multiple charge), visible and infrared (neutral charge) range. It emits at 458 nm, 488 nm or 514.5 nm in the visible range.

The nitrogen molecules are used as a gain medium in the nitrogen laser. It is a pulse laser with pulse duration 5-7 ns operating at 337 nm.

Excimer lasers use a mixture of gases with a composition 0.05-0.3 % of reactive gas (fluorine or chlorine), 1-10 % of inert gas (argon, krypton or xenon) and 90-99 % of carrier gas (helium or neon). The examples are ArF (emits at 193 nm), KrCl (emits at 222 nm), KrF (emits at 248 nm), XeCl (emits at 308 nm) and XeF (emits at 351 nm). The excimers (non stable excited molecules) are the active medium. It is a pulses laser, where the high energy pulses are produced by an electrical discharge or high-energy electron beams.

The important effect which must be described before the experimental description is the interaction of the laser beam with the sample surface which allows the microplasma creation and plasma emission with the excited atoms and ions.

II.5 LIBS EXPERIMENTAL SETUP USED FOR MEASUREMENTS

The reason why the LIBS technique is more and more use is the facility of sample preparation, fast analysis, qualitative, semi-quantitative or quantitative results and easy instrumentation. There are not many commercially available LIBS systems. In the research laboratories; the self-built system in which the laser, spectrograph and detector are assembled according the analysis is more in use.

The principle of the technique is that after the interaction of the laser beam with the sample surface, the plasma with the evaporate particles, ions and atoms is created above the sample surface. The light of plasma is captured by the fibre optics and transported onto the spectrometer with the camera and detector. Result is the spectrum of the elements present in the sample.

The Nd:YAG lasers with different characteristic were used for fly ash analysis. The neodymium laser is the most common solid-state laser which is used. The principal of this type of laser is that atoms presents in impurity-level concentrations in crystalline or glass host material are excited optically by light from an external source, producing a population inversion in a rod of laser material. The rod is mounted in an optical cavity which provides the optical feedback needed to the laser action. Neodymium lasers can generate continuous beams of few milliwatts to over kilowatt, short pulses with peak powers in the gigawatt range or pulsed beams with average powers in the kilowatt range. The active medium in lasers used in this work is a synthetic crystal yttrium aluminium garnet (YAG) which is a garnet like structure with the chemical formula $Y_3Al_5O_{12}$. Main advantage of this type of laser material is its thermal characteristics which allow a production of a good quality laser beam. As it is a four level laser, it is more efficient than the three level laser. The Nd:YAG laser works on its 1064 nm harmonic frequency, but this wavelength can be changed using non linear optics to obtain the second (532 nm), third (335 nm) and fourth (266 nm) harmonics [1].

II.5.1 Instrumental set-up

Three instrumental set-ups with different lasers and focalising lenses were employed. The sample position makes the difference between the two first set-ups. The sample was positioned and fixed vertically to the laser firing when the 50 mm lens was used. In the case of 80 mm lens, the sample was positioned vertically to the laser firing without fixation. The changing of sample position was to facilitate the focus of the optical fibre to the microplasma created on the sample surface. The instrumental setups 1&2 are shown on the **Figure II. 8**.

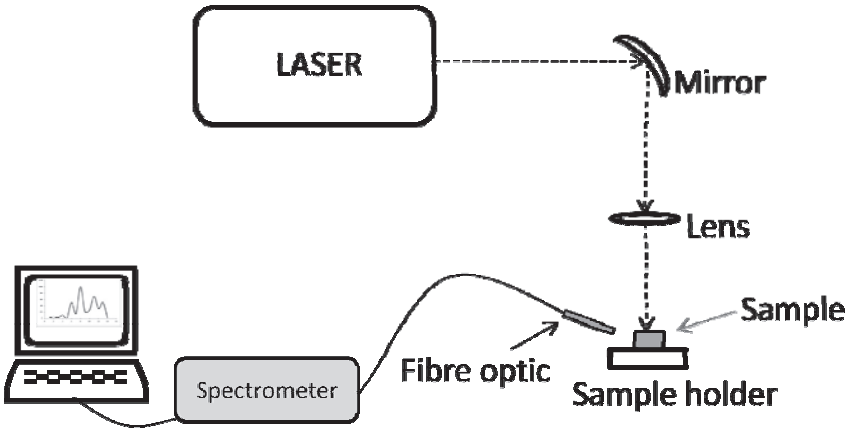

Figure II. 8: Experimental set up.

II.5.2 Laser Minilite I (Continuum)

It is a Nd:YAG Q-switch laser, which is solid state laser and in our work was operated at the third wavelength 355 nm. Maximal pulse laser energy is 4 mJ and the pulse duration 3-5 ns. The laser pulse repetition rate varies from 1-15 Hz.

II.5.3 Laser Brilliant (Quantel)

Also this laser is a Nd:YAG pulsed laser in our work was operated at 532 nm with the pulse duration of 4 ns and the repetition rate 10 Hz. The maximal pulse energy is 180 mJ. The LIBS system consists the lasers, lens optics, optical fibre and spectrometer with camera and detector.

II.5.3.1 Light collection system

Different light collections and also spectrographs were employed in our work. The light collection system is used to focus the laser pulses on the sample and then to transport the plasma light into the detection system (spectrograph and detector). Light collection system contains the lenses, mirrors and/or fibre optics. The **simple lenses** are use to focus the laser beam onto the sample surface to achiev an analytically useful plasma. Typically, spherical optics are used to focus the laser beam – usually radially symmetric for an Nd:YAG laser. This result in a circular spot focused on the sample resulting that the plasma is radially symmetric with respect to the optical axis of the laser beam. Important parameters for the lens are the focal length, diameter and material. Typical focal lengths for in situ measurements are from 50 to 150 mm with lens diameters of either 25 to 50 mm. The resulting diameter of the laser beam for a majority of solid state lasers and their harmonic are in the order of 6 to 8 mm. More sophisticated, multi lens focusing systems are needed to focus the laser pulse over the distance of many meters and to achieve the minimum spot size (= highest power density on the target).

The **fibre optic cables** (FOCs) simplify the collection of the plasma light. They are useful in the case, when the detection system cannot be positioned close to the target. The position of the FOC is important; small changes in the position of the plasma will affect the intensity of observed light because the intensity and relative intensities of emissions are strongly depended on position in the plasma. Typically, the fused silica is used for FOC. The fibre transmits the light using total internal reflection and those light rays entering the fibre within the acceptance cone angle will be reflected down the fibre with high efficiency. The acceptance angle of fused silica fibre optics is about 26° so that light can be collected from all parts of the plasma if positioned a few centimetres distant. Fibre optic consists from shielding, buffer, cladding and core.

Fibre core diameters range typically from 50 μm to 1 mm for fused silica. A cladding material (typically fluorine-doped silica) of lower refractive index than the core fibre is used to enhance the light guiding effect. The role of buffer is to protect the cladding from scratchers and other damage than will cause the fibre to break. The composition of the buffer determines the operating environment of the fibre. The typical material of buffer is polyamide and it can be used in a wide temperature range from -100°C to 400°C. For the extremes of temperature (-90°C to 750°C) the gold buffer is used.

Using FOC, the plasma light can either be focused onto the fibre end to increase light collection, or how it is in our case; the fibre can simply be pointed at the plasma, which can in contrast reduce the alignment sensitivity. The FOC can also be used to deliver laser pulses to a remotely located sample.

The pulse energy leaving the fibre can be focused with a lens system to form the laser plasmas [2, 11].

II.5.3.2 Dispersion system

The basis of a LIBS measurement is a collection and analysis of emission spectrum. Important properties of a spectrometer are:

- ☑ The resolution – the minimum wavelength separation at two adjacent spectral features which can be observed at two separated lines;
- ☑ The width of spectrum that can be observed.

Spectral component can be an acousto-optic tuneable filter, monochromator, spectrograph or echelle spectrograph which can monitor one or several wavelength. The **acousto-optic tuneable filter** (AOTF) is a spectral bandpass filter. It can be used either as a spectral line selection device or for imagining the light of a specific wavelength. The AOTF consist of crystal of tellurium dioxide or quartz with a piezoelectric transducer bonded to one side. Radiofrequency wave is applied to the crystalline material and adjusting this radiofrequency wave the bandpass wavelength can be varied continuously over a range. There are different designs of **spectrograph**. They are: Czerny-Turner, Paschen-Runge and crossed-Czerny-Turner.

More often, the **echelle spectrograph**, **Figure II. 9**, is used for LIBS measurement. In general, the diffraction grating disperses the light. A prism with its dispersion at right angles to that of the grating, stacks orders vertically over one another so as to create a two dimensional display of wavelength vs. order. The advantage of echelle spectrograph is wide wavelength range which can be monitored in same time.

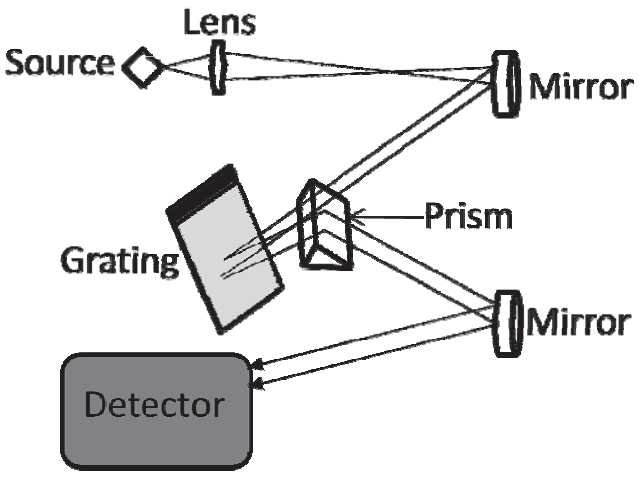

Figure II. 9: Design of Echelle spectrograph.

II.5.3.3 Detectors

The type of detector which is used depends on the spectral resolution device. Charge coupled device (CCD) or intensified charge coupled device (ICCD). They are used with spectrograph to record the continuous spectrum presented at the focal plane of the instrument. The **CCD** is two-dimensional device, so the x-y spatial distribution of light incident on the device can be recorded. A charge transfer device must transform a photon into the charge that can be transport and measured by an electric arrangement. The principle is that incoming light creates electrical charge (electron particles) in the silicon chip. Free electron cannot travel trough the chip freely – the chip is designed, so the grid of potential negative walls and electrodes keep them in area called potential wells. Each potential well represents one pixel. Number of pixel in horizontal and vertical direction as well as physical dimensions of one pixel comprises basic CCD characteristics [12-13].
In this work, the Ocean Optics spectrometer with the CCD detectors was used for detection.

II.5.4 Operation conditions LIBS

As mentioned before, two of the three LIBS set ups employed were employing the Minilite Nd:YAG laser, in this case, the micro plasma emission was directly imaged at the optical fibre entrance (solar resistant, core diameter 600 µm, IDIL Fibres Optiques, France). Optical fibre was connected to an Ocean Optics HR 2000 (Ocean Optics, USA) spectrometer equipped with a CCD detector (spectral range 100 nm, i.e. 228 to 330 nm) with a spectral resolution of 100 picometers (FWMH). The OOLIBS software (Ocean Optics, USA) was used for signal treatment (background and net signal intensity measurements).
A third LIBS setup was employed using the Brilliant laser; in this case, the sample was placed in sample holder inside the ablation chamber (TESCAN s.r.o., Czech Republic). Detection is achieved using a TRIAX 320 spectrometer (Horiba Jobin Yvon, Longjumeau France) equipped with ICCD camera detection (Horiba Jobin Yvon, Longjumeau France). A 20 nm detection window was used. The camera was triggered by the Q-switch signal of the laser, the delay time and gate width were optimized at 1µs and 10µs respectively.

II.6 LASER ABLATION – INDUCTIVELY COUPLED PLASMA (LA-ICP) SETUP DESCRIPTION

Laser ablation combined with inductively coupled plasma with mass spectrometer or atomic emission spectrometer allows rapid and precise analysis of solids. With such source, the sample is positioned in the ablation cell prior to the ICP source. The argon gas at atmospheric pressure flows through the cell towards the ICP source. The sample is irradiated by the laser beam, and the ablated material is transported with the argon stream to the plasma, where the analyte species are ionised and in the case of mass spectrometer separated by the mass analyser.

The system composed by the Laser UP-213 from New Wave coupled with ICP-MS Thermo or Agilent was used. There is a common use of New Wave´s UV lasers in recent years because of its reduction of matrix effect in comparison with IR lasers (1064 nm lasers) [14] and also due the easy manipulation and simple interface between the laser and ICP. The shorter wavelengths reduce also the inter-element fractionation [15], [16]. Many researchers use this assembly for the analysis of matrix which are close to fly ashes as it is for example soils.

II.6.1 Laser UP-213 (New Wave)

The UP 213 is a Nd:YAG solid state laser which operates in deep UV region 213 nm and it construction is shown on the **Figure II. 10**. The beam from the fundamental 1064 nm to the final output 213 nm is flat-topped for the flattest craters at the sample surface.

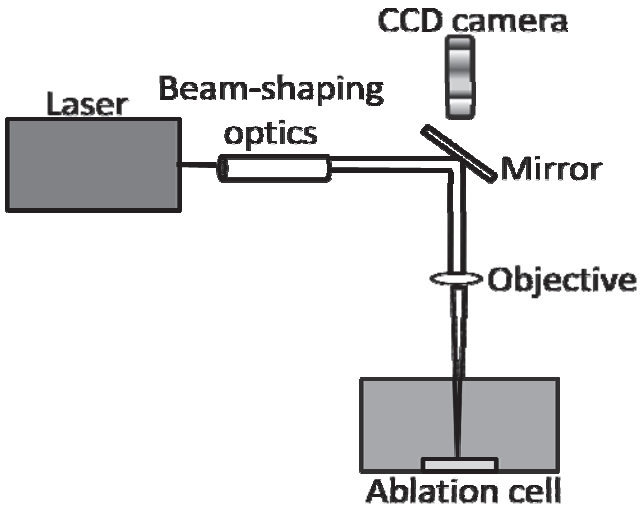

Figure II. 10: Principal setup of the laser system the UP-213 laser from New Wave society.

The body of the laser is created by the Tempest 213 nm 20 Hz laser which works on its fifth harmonic with the laser pulse duration < 4 ns. The repetition rate varies from 1 to 20 Hz, the fluence can be up to 30 J/cm^2 and the energy on the surface can be greater than 3 mJ. This laser was coupled with inductively coupled plasma mass spectrometers from Thermo or Agilent society (LA-ICP-MS).

II.6.2 Description of ICP-MS system

The principal constituents of an ICP-MS instrument are the plasma source which allows the creation of ions, the reaction/collision cell (optional) to eliminate the spectral interferences, mass analysers which sort the ions according their mass to charge (m/z) ratio and the detectors.

II.6.2.1 Ion source

The ion source is inductively coupled plasma. The ICP torch is placed horizontally, so the ions are extracted from the ICP. After the ions creation, the gaseous ion beam is sampled and transported through the series of small orifice: the interface, to the ion optics and further to the quadrupole mass analyser. The sampling cone is typically made from nickel because of its high thermal conductivity and resistance to corrosion, although platinum, copper and aluminium can be used for certain applications. The region behind the sampling cone is maintained at a moderate pressure (2 - 2.5 mbar) using the rotary vacuum pump. A skimmer cone is placed behind the sampling cone and it is generally made from the same material as the sampler. The pressure behind the skimmer cone is typically ≈ 10^{-4} mbar. The schematic diagram of the interface is shown of the **Figure II. 11**.

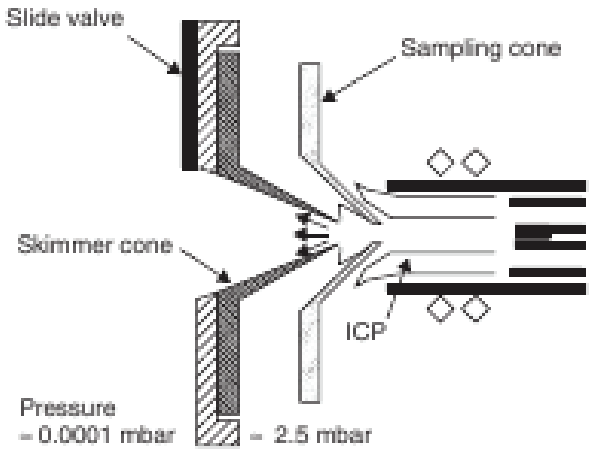

Figure II. 11: Schematic diagram of inductively coupled plasma – mass spectrometry interface [6].

Ion beam is focused to the mass analyser entrance using ion optics. First role of the ion optics is to obtain a collinear beam which is required for efficient ion filtering and transmission by the quadrupole filter and also to trap the photons emitted by the plasma in order to suppress the noise contribution that they could cause if they arrived on the detector. Within this ion guide a system called "collisions/reactions cells" may be employed in order to neutralise some interfering polyatomics created in the plasma or in the interface.

II.6.2.2 Reaction/collision cell

Main limitation of the quadrupole mass filter is its low resolution, allowing some poly-atomic interference. The polyatomics are formed from elements frequently present in complex matrices and also from argon. For instance, ^{56}Fe and ^{80}Se may be interfered by ^{40}Ca^{16}O and ^{64}Zn^{16}O produced from ^{40}Ca and ^{64}Zn but also by ^{40}Ar^{16}O and ^{40}Ar^{40}Ar. The use of a "collisions/reactions cells" has several interests:

- ☑ Neutralisation of the chemical ionisation species;
- ☑ Interferent or analyte m/z ratio shifts.

The so called "collisions/reactions cells" are multipoles placed within the ion optics of the ICP-MS and generally only operated with a dc current. The cell is operated with gas, typically a buffer gas and a reactive gas. Several reaction mechanisms have been proved to take place:
(i); (ii); (iii); and (iv) atom transfer.

(i) Charge transfer reactions

$$C^+ + B \rightarrow B^+ + C$$

Where C represent the interferent and B represent the reagent. The practical example of this type of reaction is the example of $Ar^+ + NH_3 \rightarrow NH_3^+ + Ar$, where the Ar is uncharged, so non-detected.

(ii) Proton transfer

$$CH^+ + B \rightarrow BH^+ + C$$

Proton transfer can remove the interference from ArH^+. The result is the creation of Ar which is neutral and so non-detected: $ArH^+ + H_2 \rightarrow H_3^+ + Ar$.

(iii) Hydrogen atom transfer

$$C^+ + BH \rightarrow CH^+ + C$$

The example is of this type of transfer is: $Ar^+ + H_2 \rightarrow ArH^+ + H$.

Last type of atom transfer is the *hydride-atom transfer* which can remove interference by forming the hydride of an element with no charge:

$$A^+ + BH \rightarrow B^+ + AH$$

Where A represent the analyte.

(iv) Atom transfer:

$$A^+ + B \rightarrow AB^+$$

The example is the case of NH_3, where the mass/charge ratio increase by 17 amu:

$$Ni^+ + NH_3 \rightarrow Ni^{+\cdot}NH_3$$

Last type is the **condensation reaction**, where we also increase the mass/charge ratio:

$$A^+ + BO \rightarrow AO^+ + B$$

The example is the oxide creation of the element, which will increase the mass/charge ratio by 16 amu:

$$Ce^+ + N_2O \rightarrow CeO^+ + N_2$$

The reagent gases using in reaction/collision cell varies depending the utilisation of the cell. As an example He is used as a collision gas, H_2 and NH_3 are used as charge-exchange gases, O_2 and N_2O are used as oxidation-reaction gases, H_2 is used as a reduction-reagent gas and CH_4 is other gas which can be used as a reaction gas.

On the **Figure II. 12** the schematic diagram of the multipole reaction/collision cell from Thermo X-series II are present.

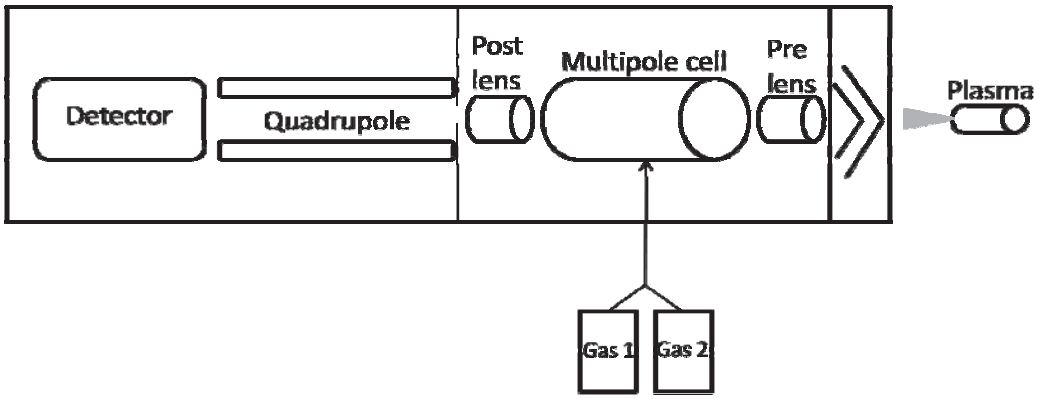

Figure II. 12: Schematic diagram of the ICP-MS Thermo X-series II with the dynamic collision cell [17].

In this work, two different ICP-MS instruments with different collision/reaction system were used. The ICP-MS from the Thermo society is equipped a hexapole collisions/reactions cell and the ICP-MS from Agilent, series 7500 is equipped with Octopole collisions/reactions system. This hexapole is part

of the Thermo lens system and is present in the ion path. Both hexapole and octopole reaction system uses only helium or hydrogen.

II.6.2.3 Mass analysers

The mass analyser sorts the ions extracted from the ICP source according their m/z ration. Mass analysers perform:

- ☑ Separation of ions according to their mass to charge (m/z) ratio;
- ☑ They measure the relative abundance of ions at each mass.

The most common type of analyser which was also used in this work is the **quadrupole mass analyser**. It consists four parallel electrically conducting rods, which are arranged parallel to each other in a symmetrical configuration, **Figure II. 13**. When a mixture of ions with different mass/charge values passes through the centre of rods and travel parallel to the length of the rods, only a single m/z ion species is permitted to traverse unimpeded and exit at the opposite end. All other m/z species are rejected from the quadrupole. Selection of the ions with a specific m/z that will traverse through the quadrupole is determined by the reproducible application of the electrical potentials to the rods.

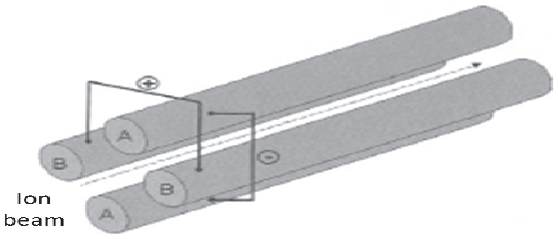

Figure II. 13: Quadrupole mass filter [18].

There are two important performance specifications of mass analyser which influence its ability to separate an analyte peak from a spectral interference. The first is the resolving power R, which is represented by equation $R = m/\Delta m$, where m is the nominal mass and Δm is the mass differences.
The second important performance of mass analyser is the abundance sensitivity, which is the signal contribution of the tail of an adjacent peak at one mass lower and one mass higher than the analyte peak.
In a quadrupole, the ability to separate different masses is determined by a combination of factors including shape, diameter and length of the rods, frequency of quadrupole power supply, operating vacuum, applied RF/DC voltage (RF radiofrequency, DC direct-current), motion and kinetic energy of the ions entering and exiting the quadrupole. The stability region (simultaneous stable oscillations in

the x- and y- directions) of a quadrupole is represented by plot of Mathieu parameters a and q **Figure II. 14**. A line with a slope $a/q = 2DC/RF$ that passes through the origin of the $a - q$ diagram is the operating line or mass-scan line. All ions that fit with points on this line will travel the entire length of the quadrupole without interaction. The optimum mass separation is obtained when the mass-scan line is made to intersect the tip of the stability diagram (m_2).

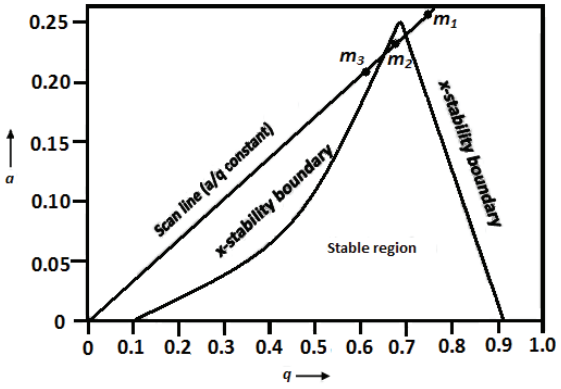

Figure II. 14: A plot of Mathieu parameters.

The **abundance sensitivity** is impacted by the combination of factors including design of the rods, frequency of the power supply and operating vacuum. The important impact on the abundance sensibility is the motion and kinetic energy of the ions as they enter and exit the quadrupole. The velocity, therefore the kinetic energy of the ions entering to the quadrupole will affect the ion motion and as a result will have direct impact on the abundance sensitivity. For that reason, the high plasma potential, and the use of lens to accelerate the ion beam (factors that affect the kinetic energy) will negatively affect the instrument´s abundance sensitivity.

The two used ICP-MS instrument are equipped with two stages **electron multiplier** as ion detector.

II.6.3 Operation conditions LA-ICP-MS

The ICP-MS 7500ce series from Agilent Technologies and ICP-MS X-series II from Thermo Electron were used for analysis. Conditions for each instrument were optimised and used during all measurements.

The mass analyser and their dwell time for each instrument are summarised in the **Table II. 2**.

Table II. 2: The m/z and dwell time used for both systems.

Element	Mass	Dwell time Agilent (sec)	Dwell time Thermo (ms)
P	31	0.1	10
Ca	44	0.01	0.1
V	51	0.1	10
Cr	52	0.1	10
Mn	55	0.1	10
Co	59	0.1	10
Ni	60, 61, 62	0.1	10
Cu	63, 65	0.1	10
Zn	66, 67, 68	0.1	10
As	75	0.1	10
Sr	84, 86, 87, 88	0.1	10
Ba	137, 138	0.1	10
Pb	206, 207, 208	0.1	10

In the case of ICP-MS X-series II from Thermo Electron the radiofrequency power was 1400 W. The gas flow of the makeup gas was 0.6 L/min and the reaction/collision gas flow of mixture of 2% H_2 in Helium was 3 mL/min. During the laser ablation, the Helium was used with the gas flow of 0.9 L/min and the laser operating conditions were 5 Hz repetition rate, scan speed of 15 µm/sec, spot size of 55 µm and the energy of 26 J/cm^2 (~70 %).

In the case of ICP-MS 7500ce series from Agilent Technologies the radiofrequency (rf) power of 1500 W was used during the measurements. The gas flow of the makeup gas was 0.6 L/min and the reaction/collision gas flow of Helium was 3 mL/min. During the laser ablation, the Helium was used with the gas flow of 1 L/min and the laser operating conditions were 5 Hz repetition rate, scan speed of 30 µm/sec, spot size of 80 µm and the energy of 18 J/cm^2 (~70 %).

II.7 SCANNING ELECTRON MICROSCOPY MEASUREMENTS

Scanning electron microscopy (SEM) coupled with EDX was used for the SEM observations and cartography of selected major elements. The SEM observations were performed using the JEOL scanning electron microscope (JEOL 5800LV Japan) operating at 15 kV and the data were treated by Spirit software version 1.07. The EDX was equipped by Si(Li) detector and the energy spectrums were obtained for Al, Ca, Fe and Mg. The EDX was calibrate with the pure Cu. The collection time for the spectra was 600s.

II.8 SAMPLE DESCRIPTION

II.8.1 Samples

In this work, six reference materials and six real samples were employed. Different laboratories already analyzed the six real samples.

The **CTA-FFA-1** (fine fly ash) is from Instytut Chemii I Techniki Jadrowej (Polish reference Material for multielement trace analysis); Ash No.3 – **CRM019-050** from RTC, Laramie, USA; Standard Reference Material **NIST1633b** – Constituent Elements in Coal Fly Ash from National Institute of Standards and Technology; **BE-1** (braunkohlenaschen) from Bergakademie Freiberg and **BCR038** (fly ash from pulverised coal) with **BCR176** (fly ash) are from Institute for Reference Materials and Measurements (IRMM).

Other three samples were from Analeach project [43]. It discusses samples with reference name **CW3** – sewage sludge chemical waste from Ludwig Shafen, Germany; **CW10** – fly ash from Calmova dumpsite, Slovak Republic and **CW11** – brown coal based power plant from Hungary.

Other samples are **L1** – brown coal based power plant which was homogenized in Research Institute of Inorganic Chemistry, Usti nad Labem, Czech Republic, **EPR1** from power plant Prunerov, Czech Republic, homogenization in UJEP Liberec (J.E. Purkyne University), Czech Republic and **ELE** from power plant Ledvice which was analysed by Accredited Test Laboratory (VUHU a.s., Most), Czech Republic.

II.8.2 Sample preparation

Because fly ash samples could not be pressed into the pellets without binder, the selection of mass ratio between the sample and binder and binder itself must be performed.

As it can be seen from **Figure II. 15 – A, B** and **Figure II. 16**, the shape of powder sample could be employed to divide samples into three groups.

In the first group (CTA-FFA-1, L1 and BCR038 fig1A) fly ash powder is mainly composed of spherical particles, second group presented on the 1B consists mostly individual particles with its size more than 30 μm in diameter (BE1, CRM 019-050, CW10, ELE and EPR1) and the third group consists compact assembly of amorphous particles (BCR176, CW3, CW11 and NIST1633b). There is no relation between the sample origin and its apparent structure.

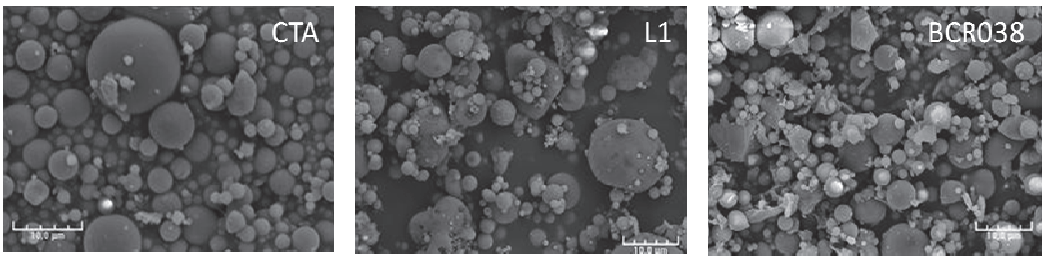

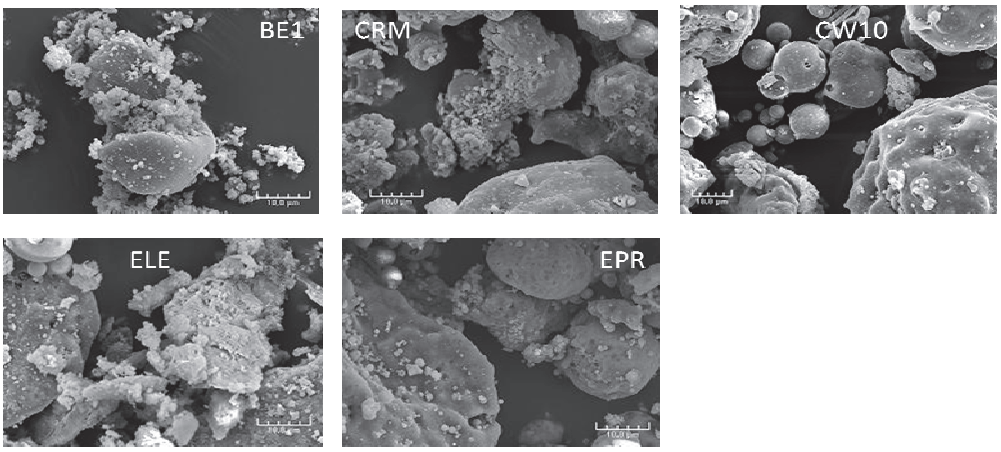

Figure II. 15 – A, B: SEM observations of fly ashes samples contained mostly spherical particles, magnification x2000.

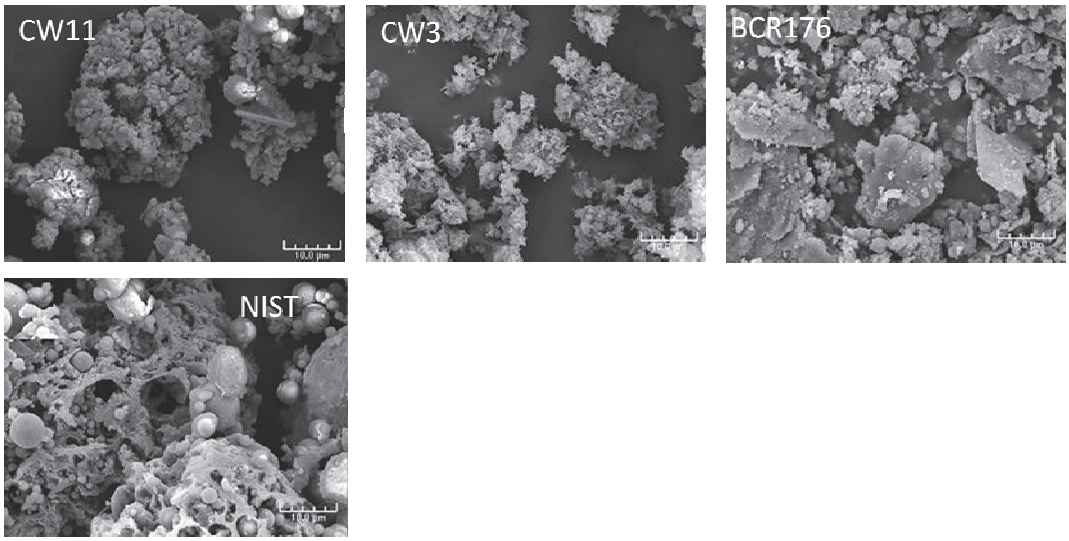

Figure II. 16: SEM observations of fly ashes samples contained mostly spherical particles, magnification x2000.

Due to this important variation in shape and structure, a binder was found necessary to efficiently prepare pellets from these very different powders. For the evaluation of the mass ratio, the cellulose as a binder was chose and pellets with different mass ratios were prepared. The aim of this procedure is the preparation of sufficiently compact pellets with the sample concentration high enough to obtain the signal response for all elements present in the sample. The mass ratios of

powder cellulose and NIST 1633b were: 1:5; 2:4; 3:3; 4:2 and 5:1. The pellets prepared in mass ratio cellulose: NIST163b 1:5 were not sufficiently resistant to the laser ablation. On the contrary the pellet prepared in mass ration 1:5 was too diluted, so the response of the trace elements was not satisfactory. With regard to pellets stability during laser ablation, signal response for trace elements and the quantity of sample used for pellets preparation, the mass ratio was chosen 1:1.
Pellets were prepared following the same procedure: 200 mg of the sample was mixed with 200 mg of binder, homogenization of the mixture was achieved or by centrifugal ball mill Retsch S1 (Retsch GmBH Germany). The optimum homogenization time was 15 minutes with 400 rpm. Or the homogenisation was performed by Planetary micro mill Pulverisette 7 Classic line (Fritsch, Germany) with 10 minutes homogenisation time with 400 rpm. Homogenized mixture was then pressed into 13 mm diameter pellets with resulting thickness of about 2 mm. Two presses were used for the pellets preparation. A hydraulic press (Lightpath Optical, CoLTD, Great Britain) at 10 MPa for 240 s was employed and second, the hydraulic press SP-1 (Mobiko, Pty, Czech Republic) at 10Mpa for 240 s was employed.

Lithium tetraborate fusion is suitable for preparation of soils, geological materials, slags and other silicates and resistant materials because it transforms the samples into homogeneous materials. This is because why this technique is suitable for x-ray spectroscopy and laser ablation. The fusion of oxide-based samples as fly ashes with alkaline borates (lithium tetraborate, sodium tetraborate, lithium metaborate or sometimes polymetaphosphates) is an effective and simple sample preparation for chemical analysis. In the fusion process, the mixture of alkaline compounds (flux) melts, and becomes a solvent for all the oxides of the sample, yielding an amorphous homogeneous solution of the cations of the sample constituents and the flux in a cloud of oxygen atoms. Using this means, the deleterious solubility and heterogeneity properties of the oxide compounds can be removed. Lithium tetraborate fusion was used in two cases, the first case was the lithium tetraborate alkali fusion with following digestion in the acid for the ICP analysis; the second case was the preparation of lithium tetraborate beads for the direct laser ablation. The reason why the lithium tetraborate beads are used is the stability of plasma due to the glass matrix, supposed homogeneity of the prepared bead and the fact that they are time-stable; it means that can be reused for recalibration or analysis. The disadvantage of fusion procedure is the high level of total dissolved solids introduced during sample preparation. The advantage of alkali fusion method is the possibility of determination of all major elements (including sodium and potassium) after alkali fusion in a single solution.

II.8.3 Description of the tested binders and chromophores

Several binders and absorption modifiers were tested. Seven different binders were tested for pellets preparation: PVDF (Polyvinylidene Difluoride), cellulose powder with particle size ~ 20 µm (Aldrich Chemical company, Inc, USA), Ag powder with particle size ~ 100 µm (Goodfellow, purity 99.99%, Goodfellow Cambridge Limited, Great Britain) or powdered silver (99.99%) with particle size diameter <15 µm from Safina, Co (Czech Republic), α-cyano-4-hydroxy-cinnamic acid with purity 97% (from Aldrich Chemical company, Inc, USA) vanillic acid, maleic acid (Fluka AG, Germany, purity > 99%) and caffeine (Sigma Chemicals Co., USA).

During the sample preparation, several **organic binders** were used as modifiers of absorption properties of the samples as it was presented by several authors [19-22]. For pellets preparation 60% of powder sample was mixed with 40% of organic binder and pressed. The pellets prepared with **chromophores** were prepared following this procedure: first the chromophores were compacted with fly ash samples, but prepared pellets were not mechanically stable. This is why cellulose must be added into the pellets: 60 mg of cellulose was mixed with 180 mg of fly ash sample and 160 mg of chromophore. This mixture was homogenised and compacted into pellets.

II.8.4 Description of internal standard

In this work several internal standards were used and several series of pellets were prepared. Several internal standards and procedures of internal standardization were performed and their preparation is summarized in the **Table II. 3**. Internal standard is used to achieve good precision, compensate the matrix effect produced during laser ablation or compensate the influence of the sample composition and is used to obtain good accuracy. There are several criteria which must be take account during the internal standard selection. The internal standard:

- ☑ Is not present in the sample or is present in low quantity;
- ☑ Are the major elements which do not interfere with the elements to be determined.
- ☑ In the case mass spectrometry is desirable, when the first ionisation potential of internal standard is similar to that of the analyte to be corrected;
- ☑ Does not produce any chemical incompatibilities with the analyte of interest;
- ☑ Behaves similarly to the analytes of interest such that it can correct for their signal changes in varying composition.

Table II. 3: Descriptions of internal standards and their concentrations.

	Internal standard (IS)	Procedure	Concentration
Preparation A	In (l)*	Addition in the binder	20 mg/kg in sample
Preparation B	Ag (s)*	Present as a binder	~ 1
Preparation C	C (s)*	Present as a binder	~ 1
Preparation D	Er (s) *, Sm (s)*, Be (l)*	Addition of IS in the mixture of binder and sample	~2.3 %w/w (Er, Sm) 100 mg/kg
Preparation E	Au (l)*	Addition in the binder	1000 mg/kg in sample
Preparation F	Au (l)*, Rh (l)*, Ir (l)*, Pt (l)*	Addition in the binder	500 mg/kg in sample
Preparation G	Ca	Present in the sample	Various (%w/w)
Preparation H	Lu (s)*	Addition during the preparation of fused beads	3 %w/w

* l – liquid, s – solid

The internal standards were generally added in the form of solution into the sample or into the binder, only in the case of Er and Sm, previous digestion of internal standard was necessary. Because Sm and Er were presents as oxides (Sm_2O_3 and Er_2O_3) in the powder form, the procedure of decomposition was performed. Several decomposition procedures were tested and finally for the Erbium 3 ml of HNO_3 was added; Samarium was decomposing with 3 ml of hot HNO_3. The internal standards were added in known amount into the binder, or sample and well homogenised with the sample. The concentrations of the ISs were calculated for each IS and each sample.

II.8.5 Preparation of alkali fusion solutions

To evaluate the accuracy of obtained results, the fused beads and the alkali fusion were performed.

The protocol for lithium tetraborate fusion will now be explained. 4 to 5 mg of alkali sample was mixed with 100 mg of lithium tetraborate (Sigma Aldrich, 99.995% + metal basis) in a platinum crucible. The fusion was performed in a programmed muffle furnace which involved 2 steps.

The first step was to increase the temperature by 5°C per minute to obtain a temperature of 550°C. This temperature was reached within 30 minutes. The second step was to increase the temperature by 5°C per minute to obtain 1100°C, shown in, **Figure II. 17**. After fusion, the melted solution was dissolved in 2 ml of nitric acid normapur and the solution was added to with deionised water, to the volume of 100 ml. The normally used acids for dissolution of melted solutions are hydrochloric acid

and nitric acid. The nitric acid commonly help to dissolve the remnants of organic matter [23]. A schematic diagram of sample preparation is shown in **Figure II. 18**.

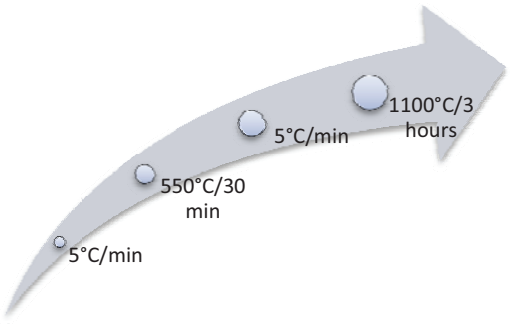

Figure II. 17: Temperature steps in the microwave furnace.

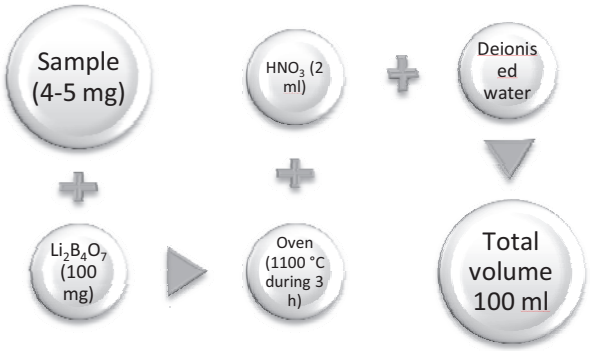

Figure II. 18: Scheme of lithium tetraborate fusion.

II.8.6 Preparation of fused beads

The preparation protocol for lithium tetraborate beads is as follows. 400 mg of sample material was mixed with 2.00 grams of lithium tetraborate and also mixed with the internal standard ($Lu_2 0_3$) with a concentration of 3 %w/w (0.08 g), all mixed in a platinum crucible as shown in, **Figure II. 19**. Induction heating was used for the fusion and then the beads were prepared with 2 cm diameters and a thickness of 2 mm. Spectroscopic blanks were prepared without adding any fly ash sample. The glass blank was prepared by fusing $Li_2B_4O_7$ to form the disk. The second blank was prepared by fusing $Li_2B_4O_7$ and Lu_2O_3 to form the disk.

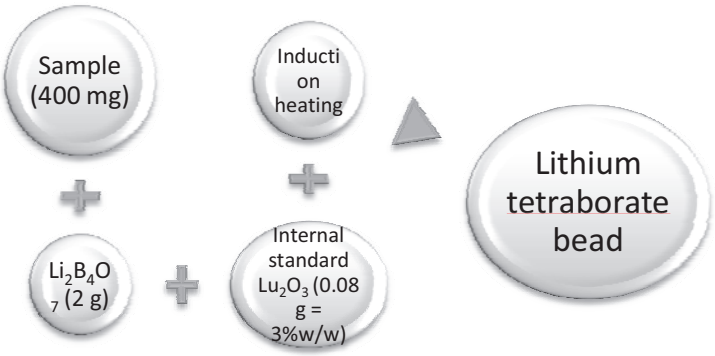

Figure II. 19: The preparation protocol for lithium tetraborate beads.

II.9 REFERENCES

1. Maiman, T.H., *Stimulated Optical Radiation in Ruby.* Nature, 1960. **187**(4736): p. 493-494.
2. Chang, W., *Principles of lasers and optics*. 2005: Cambridge Univ Pr.
3. Young, M., *Optics and lasers: including fibers and optical waveguides*. 2000: Springer Verlag.
4. Weber, M., *CRC Handbook of Lasers*. 2001, CRC Press LLC.
5. http://www.rp-photonics.com/. *Encyclopaedia of Laser Physics and Technology.* June 2009].
6. Cerullo, G., et al., *Problems in laser physics*. 2001: Kluwer Academic Pub.
7. Piepmeier, E., *Analytical applications of lasers*: John Wiley & sons.
8. Hecht, J., *The laser guidebook*. 1999: McGraw-Hill Professional.
9. Ready, J.F., *Industrial Applications of Lasers – Second Edition.* Academic Press, 1997.
10. Shultz, W.W., H. Poprawe, R., *Laser Physics and Applications, Subvolume B: Laser Systems, Part 2.* Springer, 2008.
11. Pedrotti, F. and L. Pedrotti, *Prentice-Hall, Introduction to Optics*. 1987, Inc., Englewood Cliffs, New Jersey.
12. Miziolek, A., V. Palleschi, and I. Schechter, *Laser-induced breakdown spectroscopy (LIBS): fundamentals and applications*. 2006: Cambridge Univ Press.
13. Cremers, D. and L. Radziemski, *Handbook of laser-induced breakdown spectroscopy*. 2006: John Wiley.
14. Motelica-Heino, M. and O.F.X. Donard, *Comparison of UV and IR laser ablation ICP-MS on silicate reference materials and implementation of normalisation factors for quantitative measurements.* Geostandards Newsletter-the Journal of Geostandards and Geoanalysis, 2001. **25**(2-3): p. 345-359.
15. Longerich, H.P., D. Gunther, and S.E. Jackson, *Elemental fractionation in laser ablation inductively coupled plasma mass spectrometry.* Fresenius Journal of Analytical Chemistry, 1996. **355**(5-6): p. 538-542.
16. Günther, D., et al., *Direct liquid ablation: a new calibration strategy for laser ablation-ICP-MS microanalysis of solids and liquids.* Fresenius'Journal of Analytical Chemistry, 1997. **359**(4): p. 390-393.
17. www.thermo.com. June 2009.
18. Taylor, H.E., *Inductively Coupled Plasma – Mass Spectrometry, Practice and Techniques.* Academic Press, 2001.

19. O Connor, C., M. Landon, and B. Sharp, *Absorption coefficient modified pressed powders for calibration of laser ablation inductively coupled plasma mass spectrometry.* Journal of Analytical Atomic Spectrometry, 2007. **22**(3): p. 273-282.
20. Boue-Bigne, F., et al., *A calibration strategy for LA-ICP-MS analysis employing aqueous standards having modified absorption coefficients.* Journal of Analytical Atomic Spectrometry, 1999. **14**(11): p. 1665-1672.
21. Connor, C., B. Sharp, and P. Evans, *On-line additions of aqueous standards for calibration of Laser Ablation Inductively Coupled Plasma Mass Spectrometry: theory and comparison of wet and dry plasma conditions.* Journal of Analytical Atomic Spectrometry, 2006. **21**(6): p. 556-565.
22. Masters, B. and B. Sharp, *Universal calibration strategy for laser ablation inductively coupled plasma mass spectrometry based on the use of aqueous standards with modified absorption coefficients.* Analytical Communications, 1997. **34**(9): p. 237-239.
23. Bettinelli, M., et al., *Determination of trace elements in power plant emissions by inductively coupled plasma mass spectrometry, comparison with other spectrometric techniques.* Microchemical Journal, 1998. **59**(2): p. 203-218.

III PART

RESULTS AND DISCUSSION

III.1 SAMPLE PREPARATION

III.1.1 Binder selection

The role of binder is to prepare compact, mechanically stable pellets resistant to the laser ablation. In some cases, the pellets without binder could not be compacted and would even "explode" during the laser firing [1]. One of the main interest of binder is also to provide a certain degree of matrix matching as it is added in a 1/1 ratio it may also allow a simple addition of internal standard to the solid samples [2]. The fly ash samples could not be pressed without binder addition, different binders: PVDF (Polyvinylidene Difluoride), cellulose powder, silver powder were evaluated and led to a good mechanical stability, pellets prepared using these binders could easily be handled and were resistant to laser firing.

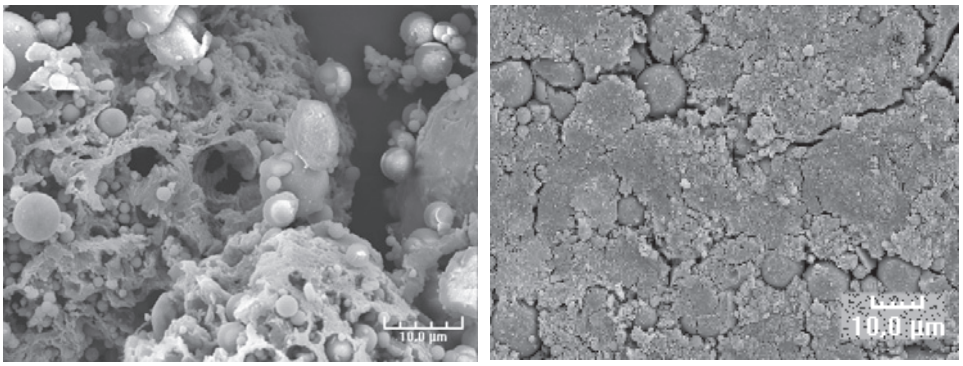

Figure III. 1: surface of a fly ash powder NIST 1633b and the pellet surface (NIST/cellulose).

As it can be seen from **Figure III. 1**, surface of the pellet is more homogeneous than that of the "free" powder. Consequently the laser beam of interacts with a more homogeneous surface when proceeding to laser sampling by LIBS or LA-ICP-MS spectroscopies.

III.1.2 Sample homogenisation

Since the fly ashes have complicated matrix with no uniform particles size, the first criteria was to select an efficient homogenisation procedure. Two mechanisms were tested, manual homogenisation using a grinding mortar and a ball mill homogenisation.

As it is shown on **Figure III. 2**, original shape of the fly ash particles and their granulometric distribution were rather different from one sample to the other. Powders are both originating from coal fired power plants; the L1 is produced after the combustion of brown coal while the NIST1633b originates from bituminous coal.

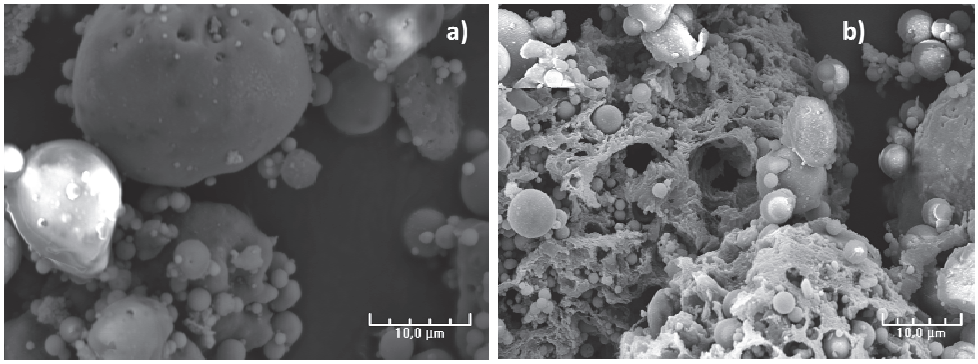

Figure III. 2: example of powders without homogenisation; a) – L1 x2500 magnification, b) – NIST1633b x2000 magnification.

To evaluate the efficiency of homogenisation, the particle size diameters of original samples was compared to that of the grinded powders (**Table III. 1**).

Table III. 1: Particle size diameter of selected sample (Particle Size Analyzer CILAS 1064).

Sample	L1	NIST1633b
Without homogenisation	10-55 µm	10-40 µm
grinding mortar	6-33 µm	5-23 µm
ball mill	4-17 µm	3-14 µm

As it can be seen, for the two fly ashes, a significant particle size reduction is observed for both procedures. Maximum particle size is at least divided by two. Furthermore, a narrow particle size distribution was obtained using ball mill homogenisation.

The narrower the particle size (and its distribution), the lower the RSDs should be. To compare effect of homogenisation, a comparison of signal stability was made using LIBS spectroscopy.

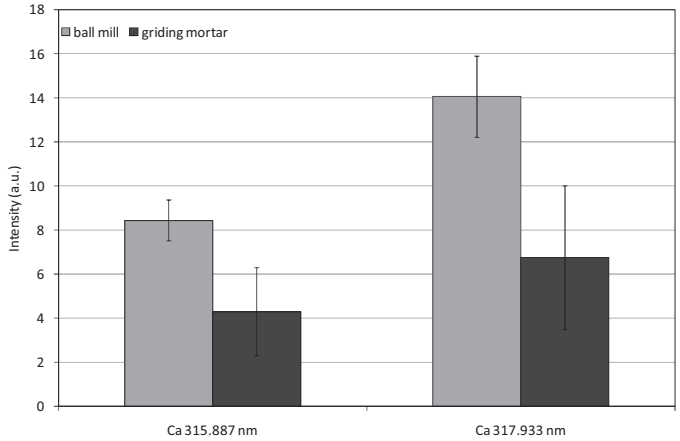

Figure III. 3: Signal intensities and relative standard deviation obtained by LIBS on NIST1633b mixed with α-cyano-4-hydroxy-cinnamic in mass ratio (1:1).

The Relative Standard Deviations of six repetitive LIBS analysis were higher for the pellets prepared from manually homogenised sample, **Figure III. 3**. A decrease of the RSD from 40 % to 10 % is obtained when the ball mill was employed.
This procedure was found to give best RSDs, and therefore was employed in the following work.

III.2 SENSITIVITY STUDY

Quantification of trace and major elements of the fly ashes is likely to be realized with a good accuracy only if some requirements are fulfilled:

- ☑ Sensitivity is high and measurements are stable;
- ☑ Sensitivity is comparable from one sample to the other;

In order to address these different points, careful optimizations of the LIBS and LA-ICP-MS setups were made. Classical optimization of laser and detection parameters was first achieved. Addition of chromophore was then evaluated to obtain an acceptable matrix matching between samples.
This chapter describes first the results obtained using LIBS spectroscopy III.2.1. In the following part results obtained using LA-ICP-MS will be described.

III.2.1 LIBS Study

III.2.1.1 Laser parameter optimisations

The laser pulse energy optimisation was performed to obtain the highest signal with acceptable RSDs and to avoid self-reversal phenomenon. The optimisations made on the LIBS setups employed in our work are presented on **Figure III. 4**.

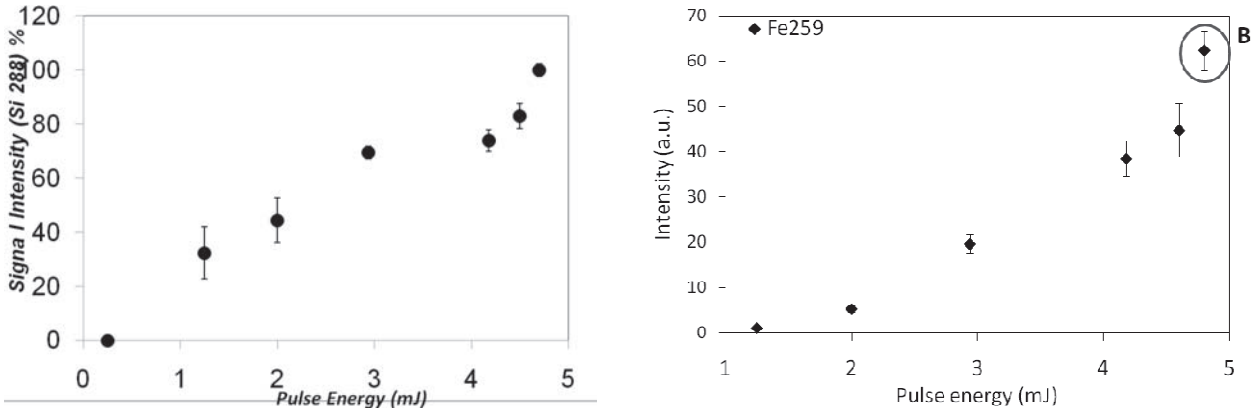

Figure III. 4: Signal intensity against pulse energy (mJ) of the laser for setup 1 for the Silica line (A) and iron analytical line (B). Tested sample was Nist1633b mixed with cellulose. RSD (%) are calculated from six replicates.

As it can be seen from both setups, a significant signal increase is obtained together with a drastic reduction of the RSD (%). For set-up1 (mininite laser) the maximum pulse energy was selected, while for set-up2 (using Brilliant laser) an intermediate energy was employed to avoid detector saturation.

III.2.1.2 Sensitivity as a function of binder nature

The objective of this work is to be able to detect a wide range of elements at low concentrations using, either using LIBS spectroscopy or LA-ICP-MS. The laser sampling is common to both methods and as a consequence, any improvement in laser/matter interaction should improve sensitivity.
One of the major advantages of powder analysis is that it facilitates the addition of internal standards or matrix modifiers. As it was made for the internal standard, a matrix modifier can be added to the powder as powder itself or through the addition of spiking solution to the binder. Many authors have already described the addition of matrix modifiers to improve ablation efficiency [3-5].

In our work a comparison of sensitivity obtained using different binders was made. The binder giving best sensitivity and a good mechanical stability of the pellets was then further selected to calculate figures of merits (LODs and accuracy).

III.2.1.2.1 Comparison of sensitivities

The pellets made from cellulose, powdered silver and their mixture were evaluated on the three laser setups. **Table III. 2** represents the sensitivity obtained for different binders only for the NIST1633b fly ash.

Table III. 2: Normalized sensitivities of iron and calcium in different binders (NIST1633b).

Binder	Fe 259.957 nm	Ca 315.887 nm	Ca 317.933 nm
Cellulose	13.5	19	19
Silver	100	100	100
Cellulose and silver (1/1)	17	13.5	16

A sensitivity increase was observed using a silver containing binder, to evaluate this phenomenon on the other fly ashes; sensitivity was measured in all samples using setup 1, 2 and 3. Sensitivity measured in different binders is reported to that measured in cellulose to facilitate comparison. Ratios are calculated from expression (1)

$$Ra = (S_{elt}/c_{elt})_{binder}/(S_{elt}/c_{elt})_{cellulose} \quad (1)$$

Where S net is the net signal of the element, c is the concentration (certified or measured after a wet digestion).

A ratio significantly superior to 1 indicates a sensitivity improvement when compared to cellulose binder. Results are presented in **Table III. 3**: A-D.

Table III. 3: A-D: Ratio comparison between different binders.

A: Al I 308.215 nm

	Set-up1			Set-up2			Set-up3
	Ag/Agcell	Ag/Cell	Agcell/Cell	Ag/Agcell	Ag/Cell	Agcell/Cell	Agcell/Cell
BE1	0.74	1.13	1.53	1.62	2.58	1.60	0.70
CTA	0.93	1.00	1.08	2.36	4.02	1.71	0.80
CRM	1.28	1.49	1.17	3.85	9.13	2.37	0.69
NIST	1.11	1.46	1.32	2.38	4.57	1.92	0.85

B: Ca II 317.933 nm.

	Set-up 1			Set-up 2			Set-up 3
	Ag/Agcell	Ag/Cell	Agcell/Cell	Ag/Agcell	Ag/Cell	Agcell/Cell	Agcell/Cell
BE1	0.85	1.13	1.34	1.67	3.22	1.93	1.12
CTA	0.64	0.84	1.31	2.07	4.05	1.96	0.77
CRM	1.60	1.15	0.72	3.80	10.49	2.76	0.91
NIST	1.12	2.03	1.81	1.91	3.81	1.99	0.84

C: Mg II 280.270 nm.

	Set-up 1			Set-up 2			Set-up 3
	Ag/Agcell	Ag/Cell	Agcell/Cell	Ag/Agcell	Ag/Cell	Agcell/Cell	Agcell/Cell
BE1	0.71	1.01	1.43	1.53	2.40	1.57	1.17
CTA	1.05	0.97	0.93	1.89	3.20	1.70	0.74
CRM	1.52	1.57	1.03	2.47	6.51	2.63	0.71
NIST	1.16	1.33	1.15	1.88	2.02	1.08	0.88

D: Fe I 259.957 nm.

	Set-up 1			Set-up 2			Set-up 3
	Ag/Agcell	Ag/Cell	Agcell/Cell	Ag/Agcell	Ag/Cell	Agcell/Cell	Agcell/Cell
BE1	0.90	1.17	1.30	1.84	3.68	2.00	0.71
CTA	1.07	0.86	0.81	2.00	3.72	1.86	1.02
CRM	1.66	1.29	0.78	2.98	7.64	2.57	0.75
NIST	1.23	1.71	1.39	2.36	4.31	1.83	1.00

A significant increase was obtained adding silver to the classical cellulose binder. And especially when **set-up 1** and **2** were employed, no improvement was observed on **set-up 3**.

The mean improvement is roughly 20% when using a cellulose silver binder. This phenomenon was found to be sample dependant and more important on **set-up 2**.

To explain this sensitivity increase, three hypotheses were tested:

- ☑ Increase of LIP plasma temperature leading to an increased signal intensity;
- ☑ Low crater grinding leading to a better detection efficiency (especially on set-up 1 and 2);
- ☑ A thermal effect more important on pellets containing silver.

III.2.1.2.2 Silver effect

Best sensitivity was obtained for silver containing pellets; several investigations were made to explain this result. Micro-plasma temperature and crater drilling were suspected to be significantly different when either silver or cellulose binder is employed.

To clearly evaluate the effect of silver content on the electronic excitation temperature, mixtures of titanium oxide, silver and cellulose were prepared. TiO_2 mass was kept constant (50% w/w) and percentage of silver varied from 0 to 50%. Ti was selected as it is a common element for plasma temperature estimation [6-9]; it could easily be mixed with cellulose and silver and had also sensitive lines on the spectral window accessible with set-up 1. The estimated temperature is the electronic excitation temperature; to admit it represents the plasma temperature one should consider a Local Thermodynamic Equilibrium to exist in the LIP plasma, therefore assuming that all particles of the plasma have the same temperature. This LTE hypothesis is commonly assumed in ICP or LIBS for plasma temperature measurements [10-16] but is not fully established. The objective here was only to estimate differences of electronic excitation temperatures between two plasmas obtained from slightly different targets.

Table III. 4 presents the Ti (II) 301.72nm intensity and the estimated electronic excitation temperature. Excitation temperature of the plasma was determined using the Boltzmann method, using the Ti (II) 301.72 nm, Ti (II) 302.97 nm Ti (II) 305.81 nm Ti (II) 306.62 nm Ti (II) 307.52 nm Ti (II) 307.86 nm and Ti (II) 311.77 nm lines. A plot of $Ln\ (I_i\lambda_i/g_iA_i)$ as a function of E_i, should give a linear curve with a slope of $-1/kT$. Where the Boltzmann is constant k, I is the line intensity, $A, g\ and\ \lambda$ are transition probability, degeneracy, and wavelength, respectively, of one spectral line and E is the excitation energy of the line of interest.

Table III. 4: Temperatures measured from boltzman plot and Ti 301.72 nm intensity as a function of increasing silver % in the "model" pellet.

Silver percentage (%)	Temperature (K)	Ti 301.72 nm Intensity
0	15122	354
10	15054	279
20	15108	450
30	15600	510
40	15994	575
50	16071	735

As it can be seen and even with the uncertainty due to the lack of precision of intensity measurements, and that of g_i, A_i coefficients, a temperature rise is observed with an increased silver concentration of the "model" pellets. Similarly, the net intensity of Ti lines also increased rapidly with the silver concentration (mean 70% increases) with the exception of pellets containing 10% of silver which gave intensity 20-30% smaller.

The Boltzmann method was also employed on Fly ash pellets mixed with silver, cellulose and the silver / cellulose (1/1) mixture. In this case iron lines could be employed because iron is present in large concentration in the fly ashes; measurements were achieved using **set-up 3** as on **set-up** 1 these wavelengths could not be measured. Temperature was calculated from the most classical [17-18] iron lines; Fe (I) 373.332 nm, Fe (I) 373.532 nm, Fe (I) 374.693 nm, Fe (I) 383.338 nm, Fe (I) 386.552 nm and Fe (I) 387.25 nm [11, 19-21].

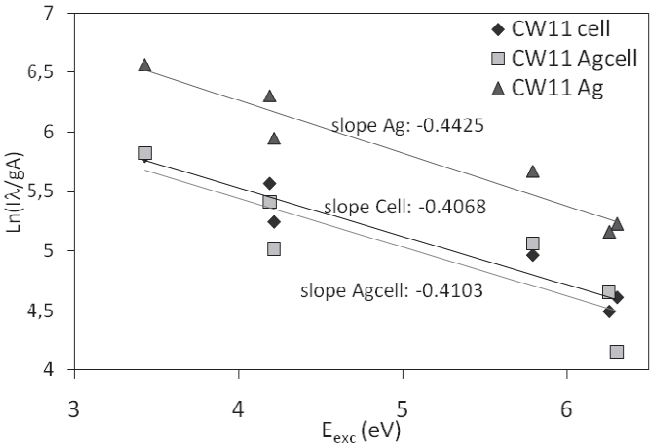

Figure III. 5: The Boltzmann plot for six Fe I emission lines measured on fly ash samples.

According to the slopes measured from **Figure III. 5**, the temperature was 10000 K for cellulose, 10500 K for the silver /cellulose mixture and 11200 K for silver.

Either on the model or on the fly ash pellets, the temperature difference is small and does not fully explain the sensitivity improvement when using silver pellets. The temperature variation is common to both setups and as the sensitivity increase was not observed on both systems another hypothesis was evaluated.

It was noticed, that on the cellulose pellets laser ablation rapidly drilled a "deep" crater leading to a signal quenching. Assuming the plasma observation was made with an angle of 30° from the sample surface on set-up 1 and 2 only, this phenomenon was likewise. On the contrary the crater observed on silver pellets was not as deep and subsequently, the signal was higher.

The profiles shown on figures (**Figure III. 6**; **Figure III. 7**, and **Figure III. 8**) exhibits the differences in the craters obtained for different binders.

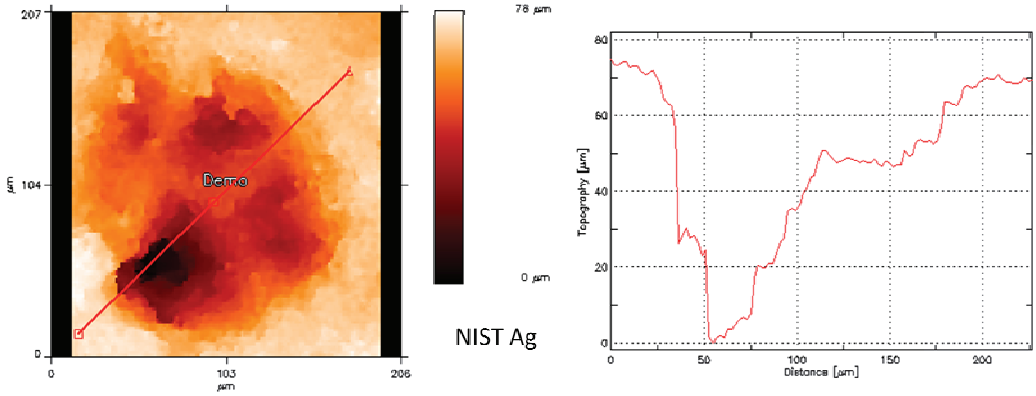

Figure III. 6: Crater profile after LIP ablation for Ag binder, crater depth 75 µm

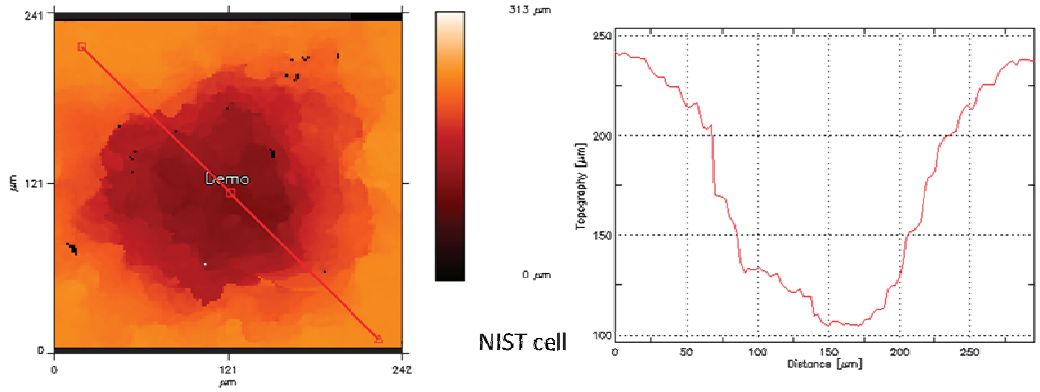

Figure III. 7: Crater profile after LIP ablation for cellulose binder, crater depth 145 µm.

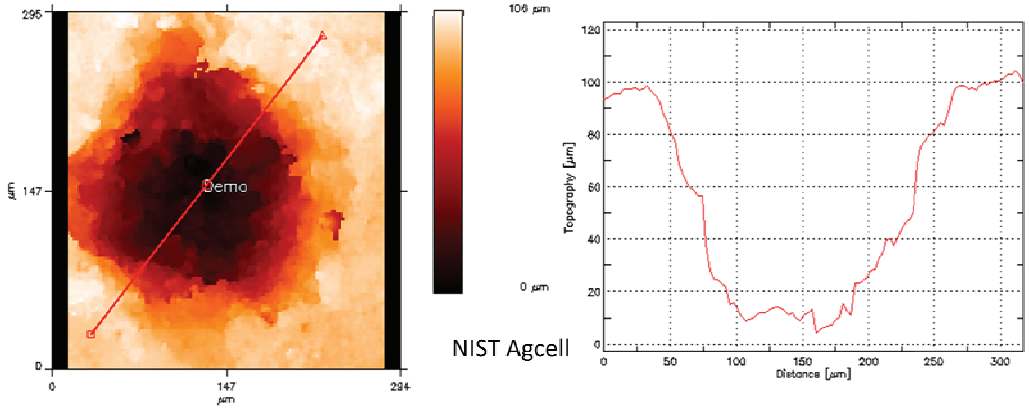

Figure III. 8: Crater profile after LIP ablation for mixture of cellulose and powder silver binder, crater depth 100 µm.

Crater depth was measured using an optical profilometer and led to 3.6 µm/pulse for silver pellets, 6.2-9.6 µm/pulse for Ag/cellulose binder and 12-17.2 µm/pulse for the cellulose binder. This difference was consistent with the hypothesis of a signal quenching due to a rapid crater drilling. This second observation was also consistent with the sensitivity improvement obtained using a silver containing binder.

A third hypothesis was also likewise: a thermal effect was observed on silver containing pellets while in the case of pellets with cellulose there is no thermal interaction with the sample surface. In the case of pellets with silver we can observe (**Figure III. 9**) a large "burned" surface around the crater, the laser created micro-plasma expands rather at the sample surface and a higher signal is obtained. In the case of cellulose pellets plasma is employed to create a crater and the collected emission is lower.

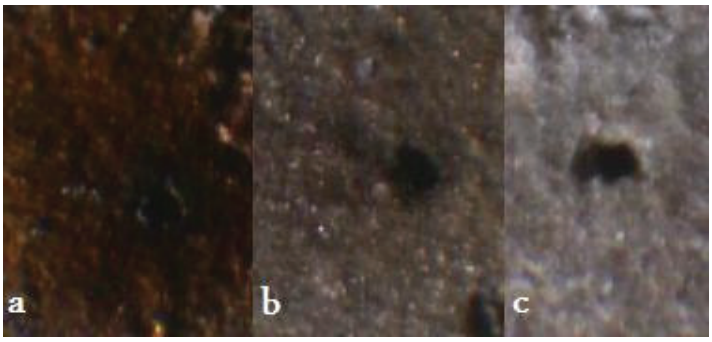

Figure III. 9: CRM 019-050 sample surface after laser ablation; a- silver binder, b- silver/cellulose binder, c- cellulose binder.

Only the combination of the three phenomenons could explain the benefic effect of silver on LIBS signal. Addition of silver to the cellulose binder ensured a higher sensitivity and provided as well good mechanical stability, but silver alone was not appropriate as RSDs were worse. This is why the cellulose powder and the mixture of cellulose and silver powder were used for the future work.

III.2.2 LA-ICP-MS study

Compared to LIBS spectroscopy, Laser ablation hyphenated to inductively coupled plasma mass spectrometry allows improving significantly the sensitivity. The main interest of LA-ICP-MS is therefore to obtain detection of elements at very low concentrations and to easily identify interferences using isotopic ratios.

Different strategies were evaluated in order to increase sensitivity and to obtain a certain degree of matrix matching. As mentioned before fly ashes are pelletized with either a mixture of cellulose and silver or with cellulose in a 1/1 mass ratio. As a consequence 50% of the ablated target is made of similar composition. To increase this degree of similarity and reduce so called matrix effects, chromophores were added to the cellulose.

The different strategies tested to improve sensitivity and reduce matrix effects are presented in the following parts: laser sampling optimization, optimisation of ICP-MS conditions (use of collisions cell technology) and the comparison of different chromophores added to the binder.

Finally, a comparison of sensitivity obtained from the different fly-ash samples was made in order to select conditions giving low matrix effects and best detection capabilities.

III.2.2.1 Laser sampling optimisation

As it was made for the LIBS study, pulse energy was optimised to obtain high elemental sensitivity together with an acceptable repeatability. The optimum was found with a fluency of 26 J/cm2. A frequency of 5 Hz with a scan speed of 15 µm/sec was selected to provide higher quantity of ablated matter without degradation of RSDs. The frequency was optimised to determinate the quantity of ablated material which goes to the plasma. As it can be seen on the **Figure III. 10 - A**, in the case of 5 Hz repetition rate, there is no important differences between the intensity obtained for 65% of fluency and those obtained for 70% of fluency. It can be also concluded that the values of standard deviations are decreasing in the increasing fluency. As it can be seen on the **Figure III. 10 – B**, the optimum conditions for the laser system were found with the repetition rate equal 10 Hz, spot size diameter of 80 µm, 70% of fluency (≈ 18 J/cm2) and the scan speed 30 µm/sec.

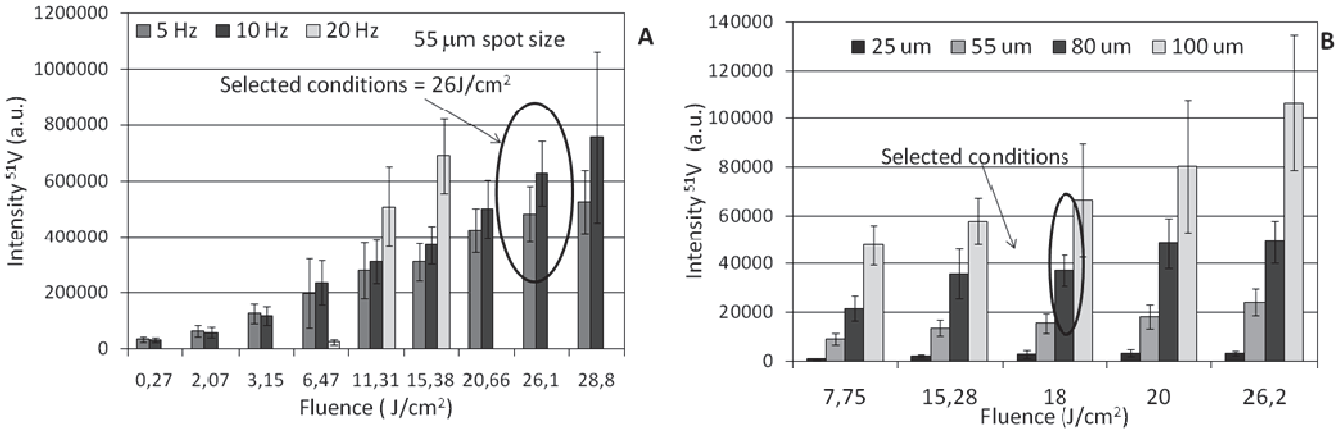

Figure III. 10: A – Optimised condition for the LA-ICP-MS Thermo analysis; 55 µm spot size diameter, 5 Hz repetition rate and increasing fluency, scan speed 15 µm/sec. **B** – Optimised condition for the LA-ICP-MS Agilent analysis were 80 µm spot size diameter, 10 Hz repetition rate and increasing fluency, scan speed 30 µm/sec, sample ^{51}V.

Spot size study was carried out on both systems to evaluate the degree of improvement that could be obtained in measurements repeatability. Using a large spot size one can theoretically smooth sample in-homogeneity. A comparison between different laser spot sizes was evaluated for both systems. Results are presented on **Figure III. 11**, using the same laser (UP 213) associated to two different ICP-MS.

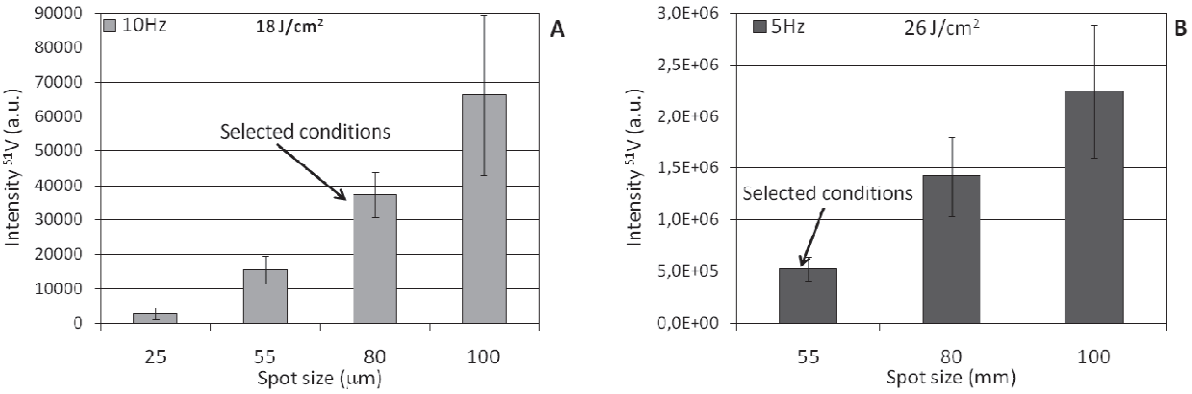

Figure III. 11: ^{51}V signal intensity using different spot size.(A UP213– Agilent system, B UP213– Thermo system).

Experimentally, there is no tendency in the size spot and the RSD values. For the LA-ICP-MS (UP 213-Thermo system), the RSD increase with increasing spot size, with an RSD ranging from 22 to 29 %. In the case of LA-ICP with the Agilent system (**Figure III. 11 – A**) the RSD variations was greater, from 61

to 17 %, the lower RSD was obtained for an 80 µm spot size. In both cases, the optimal conditions with regard to the intensity and the lowest RSD were selected for measurements. In the table below, the optimum conditions are summarized.

Table III. 5: Working conditions for the laser on the two LA-ICP-MS systems.

Parameter	LA-ICP-MS Agilent	LA-ICP-MS Thermo
Repetition rate (Hz)	10	5
Spot size (µm)	80	55
Fluence (J/cm^2)	18	26
Scan speed (µm/sec)	30	15

III.2.2.2 Addition of chromophores

To improve sensitivity and also to improve sample/laser interaction an addition of chromophores to the selected binders was made. Following the work of O´Connor *et al*. [3], it was expected that organic chromophores absorbing at the lasing wavelength could also act as binders for the fly ash sample.

The objective is to improve sensitivity to detect "difficult" elements like selenium, arsenic, lead or cadmium. It was also expected that organic absorbing binders should homogenize sensitivity between the different samples due to a more "sample independent" ablation process [3]. In the work of O´Connor the addition of organic modifiers improved analytical data and especially when using external calibration it was explained by the unification of absorption properties.

Unfortunately the binding properties of the selected chromophores were not appropriate to efficiently prepare pellets with fly-ash. Consequently, the organic modifiers were first added to the cellulose binder before mixing with the fly ash (detailed preparation is presented in experimental part). The organic chromophores selected for this purpose were: maleic acid ($C_4H_4O_4$), caffeine ($C_8H_{10}N_4O_2$), cinnamic acid and vanillic acid.

Vanillic acid was first tested as it was the selected chromophore in the work of O´Connor. Pellets prepared from mixture of fly-ashes and vanillic acid added to cellulose were not mechanically stable so that no further experiment could be made using this preparation. Maleic acid ($C_4H_4O_4$) and caffeine ($C_8H_{10}N_4O_2$) are water soluble, and the absorption maximum was measured on a UV/VIS

spectrophotometer; λ_{max} for maleic acid was close to 210 nm and for caffeine it was 205 nm. These two values are indicating both maleic acid and caffeine absorbs at the lasing wavelength i.e. 213 nm. The molar absorption coefficients at 213 nm were calculated from the Beer-Lambert law: $A = \varepsilon . c . l$. For maleic acid E was 1.6 10^5 $Lmol^{-1}cm^{-1}$ and for caffeine E was 2.810^5 $Lmol^{-1}cm^{-1}$.

As sensitivity was different from one sample to the other, the comparison is made on an average sensitivity calculated from sensitivities obtained from the four reference materials: NIST, CTA, CRM and BE1.

An example of this comparison is shown for ^{51}V, ^{75}As, ^{86}Sr and ^{206}Pb on **Figure III. 12**.

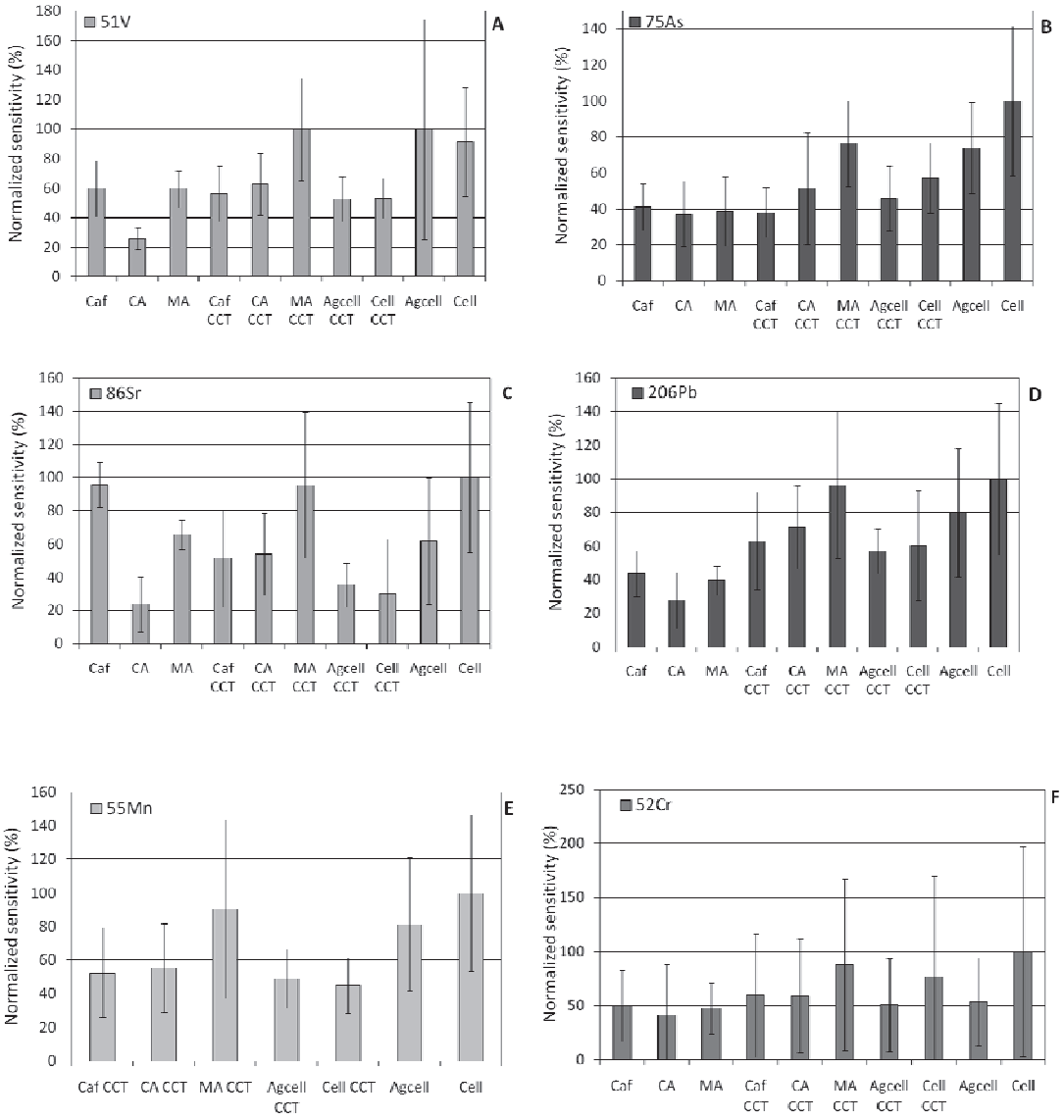

Figure III. 12: Comparison of sensitivities using different chromophores added to the binder.

From the first six elements selected for comparison it can be seen that addition of maleic acid to the cellulose binder gave increased sensitivity.

For arsenic, the addition of caffeine gave also good results but sensitivity with no chromophore was better, in this case 25 to 30% higher. For vanadium, again maleic acid gave interesting results. But the cellulose gave also a good sensitivity. In all case, the binder mixture: silver and cellulose gave an elevated sensitivity but often very large uncertainty.

The high sensitivity obtained when the powder cellulose is employed is in the contrary from that obtained for LIBS. It can be explained by the difference in lasing wavelength and also by the larger ablated mass observed using cellulose. As mentioned before, the laser drills a deeper crater releasing a high quantity of particles while ablation of silver containing pellets led to lower amount of ablated matter. The volume of total ablated material was calculated for the NIST1633b sample assuming that the crater was ring shaped and the profile was conical. At 213nm craters drilled in pellets prepared from NIST mixed with cellulose and mixed with silver cellulose mixture were observed and crater depth and diameter were measured. The ablated volume was twice when using cellulose without silver.

In the case of selenium and cadmium, only a few samples were concentrated enough to be able to detect elements. Sensitivity is therefore calculated on these samples.

Addition of caffeine brought no sensitivity improvement at all for this element and Se was no detected. In maleic acid pellets, sensitivity is 184cts/mg/kg while for classical cellulose the sensitivity was better 305 cts/mg/kg when not using the collision cell and only 135 cts/mg/kg when using it. Uncertainty evaluated for the different selenium containing samples was high, from 64% in maleic acid to 82% in cellulose. For cadmium detection results were similar for the maleic acid containing binder and the cellulose with a 320 cts/mg/kg sensitivity for 110Cd and best sensitivity was obtained for cellulose without the CCT (614 cts /mg/kg). Caffeine gave poorer sensitivity (180 cts /mg/kg). Again dispersion of the values is high ranging from 74 to 89%.

For the other elements, it could be seen from **Figure III. 12** that a better sensitivity is obtained when the CCT was employed.

III.2.2.3 Effect of collisions/reactions cell

Although main interest of the collisions/reactions cells is to neutralise polyatomic it was found in our study that sensitivity could be increased even when using classical isotopes.

Evaluation of the effect of collisions/reactions cells is on polyatomic in laser ablation is not an easy task. To evaluate the interest of CCT in this objective we have compared the isotopic ratios of some

elements using CCT and without using CCT. This experiment was carried out using pellets mixed with cellulose; results are presented in **Table III. 6**.

Table III. 6: Isotopic ratios without utilisation of collision cell.

	$^{52}Cr/^{53}Cr$	$^{63}Cu/^{65}Cu$	$^{60}Ni/^{61}Ni$	$^{66}Zn/^{67}Zn$	$^{66}Zn/^{68}Zn$	$^{88}Sr/^{87}Sr$	$^{88}Sr/^{86}Sr$	$^{137}Ba/^{138}Ba$	$^{208}Pb/^{207}Pb$	$^{206}Pb/^{207}Pb$
	8.8	**2.2**	**23.1**	**6.80**	**1.5**	**11.8**	**8.4**	**6.4**	**2.4**	**1.1**
BCR038	8.6	2.0	21.0	6.3	1.6	1.0	7.9	6.8	2.4	1.2
BCR176	10.4	2.2	15.7	7.0	1.5	3.0	8.4	7.1	2.5	1.2
Be1	9.4	2.1	12.0	4.9	1.2	12.5	8.9	7.5	2.8	1.3
CRM	8.8	2.1	9.7	7.5	1.6	3.7	8.1	6.8	2.6	1.3
CTA	9.5	2.3	15.6	7.4	1.7	1.8	8.5	7.1	2.6	1.2
CW10	10.1	2.1	7.3	10.2	1.8	2.5	8.6	6.9	2.7	1.3
CW11	10.5	2.0	1.0	22.8	3.5	11.5	8.6	6.5	2.7	1.3
ELE	8.9	2.1	18.3	47.9	1.7	5.3	8.5	6.6	2.5	1.3
EPR	9.1	2.1	13.8	11.6	2.0	2.4	8.8	6.4	2.6	1.3
L1	8.7	2.1	14.8	12.0	2.0	1.8	8.6	6.6	2.6	1.3
NIST	8.7	2.1	17.5	8.1	1.6	5.6	8.4	6.5	2.4	1.3

In classical ICP-MS conditions, isotopic ratios of copper and lead were close to theoretical value indicating no interference on the corresponding m/z. On the contrary, most Ni and Zn ratios were significantly different from the expected values. For Sr, Ba and Cr a few sample exhibited significant departures from theoretical isotopic ratios.

Table III. 7: Isotopic ratios with utilisation of collision cell.

CCT	$^{52}Cr/^{53}Cr$	$^{63}Cu/^{65}Cu$	$^{60}Ni/^{61}Ni$	$^{66}Zn/^{68}Zn$	$^{66}Zn/^{67}Zn$	$^{88}Sr/^{87}Sr$	$^{88}Sr/^{86}Sr$	$^{138}Ba/^{137}Ba$	$^{208}Pb/^{207}Pb$	$^{206}Pb/^{207}Pb$
BCR038	8.3	2.2	23.1	1.5	7.2	0.9	8.9	6.0	2.4	1.3
BCR176	9.3	2.2	65.7	1.5	6.8	3.1	9.0	6.0	2.7	1.2
Be1	8.5	2.2	17.6	1.2	5.6	12.1	8.8	6.2	2.7	1.2
CRM	7.9	2.2	22.5	1.6	7.7	3.3	8.7	6.1	2.6	1.3
CTA	8.4	2.2	21.4	1.6	7.9	1.6	9.0	6.3	2.4	1.3
CW10	8.8	2.2	12.8	1.8	11.2	2.4	8.9	5.8	3.0	1.2
CW11	9.1	2.2	13.7	2.4	32.2	12.0	9.3	6.4	2.8	1.4
Ele	8.8	2.1	22.3	2.0	10.1	5.0	8.9	6.5	2.8	1.4
EPR	8.4	2.2	18.7	1.9	10.7	2.2	9.0	6.0	2.9	1.2
L1	9.0	2.4	21.4	2.0	11.2	1.8	8.9	6.6	2.8	1.2
Nist	8.2	2.2	18.5	1.8	8.5	5.7	8.9	6.3	2.7	1.3

When the CCT is employed a sample dependant effect was observed. For chromium isotopic ratios, an improvement was observed for the three samples: CW10, CW11 and BCR176. Both 52 and 53

isotopes of chromium could be interfered either by ArC^+ or by ClO^+ polyatomic. No indication of the carbon or chlorine content of the three samples was available, so that the correlation between poly atomics neutralisation and isotopic ratio accuracy could not be clearly established.

In the case of barium, initially: only three samples gave erroneous isotopic ratios (BCR176, BE1 and CTA), using the collision cell isotopic ratios were closer to the theoretical value.

With regard to the Strontium, two ratios are reported in **Table III. 6** and **Table III. 7**, $^{86}Sr/^{88}Sr$ gave good results while $^{88}Sr/^{87}Sr$ was correct only when the amount of Sr in the sample is high (i.e. for BE1 and CW11) and the polyatomic or isobaric interference negligible. The use of collision cell did not improve isotopic ratios and only 88Sr could be used for quantification.

Isotopic ratios for copper and lead were all verified, no interference on the m/z concerned was created within the collision cell.

A very slight improvement was obtained for Nickel leading to the hypothesis that Ni pollution could be present in cellulose or within the laser ablation setup itself.

III.2.2.4 Sensitivity homogeneity

To obtain a good accuracy the sensitivity should not be sample dependant, to evaluate this question, the signal to concentration ratios were compared between the different sample and for each element. **Table III. 8** presents the results obtained for ^{51}V, ^{75}As, ^{88}Sr and ^{206}Pb with and without use of collision cell.

Table III. 8: Normalized sensitivity and RSD (%).

	^{51}V						^{75}As					
	cell	cell CCT	MA CCT	Caf CCT	MA	Caf	cell	cell CCT	MA CCT	Caf CCT	MA	Caf
NIST	**84**	**100**	**84**	**102**	**88**	**76**	**144**	**149**	**137**	**200**	**123**	**118**
CRM	**170**	**147**	**148**	**156**	**92**	**140**	**125**	**114**	**111**	**91**	**57**	**111**
CTA	**78**	**85**	**69**	**75**	**64**	**76**	**63**	**77**	**52**	**57**	**37**	**52**
Be1	**93**	**96**	**108**	**89**	**109**	**122**	**65**	**74**	**94**	**77**	**81**	**107**
CW10	113	117	126	127	224	133	120	107	139	113	281	130
CW11	73	65	76	81	68	86	59	83	84	96	61	88
EPR	99	96	115	90	83	96	51	46	48	45	42	47
L1	73	76	74	81	72	71	115	111	135	120	118	147
RSD(%)	**35**	**26**	**28**	**28**	**52**	**28**	**45**	**34**	**37**	**48**	**36**	**80**

^{86}Sr	^{206}Pb

	cell	cell CCT	MA CCT	Caf CCT	MA	Caf	cell	cell CCT	MA CCT	Caf CCT	MA	Caf
NIST	**56**	**60**	**54**	**65**	**61**	**200**	**75**	**92**	**103**	**144**	**118**	**93**
CRM	**232**	**185**	**172**	**195**	**116**	**136**	**115**	**93**	**211**	**176**	**95**	**168**
CTA	**57**	**64**	**54**	**65**	**54**	**44**	**47**	**58**	**70**	**71**	**77**	**88**
Be1	**178**	**191**	**203**	**194**	**239**	**194**	**145**	**215**	**141**	**118**	**127**	**127**
CW10	56	57	71	56	113	51	74	60	63	74	146	75
CW11	94	105	136	118	125	97	162	173	90	85	92	110
EPR	59	54	58	52	49	38	59	48	51	49	60	48
L1	44	45	52	54	43	41	48	45	72	83	87	90
RSD(%)	**72**	**63**	**61**	**62**	**69**	**65**	**50**	**59**	**53**	**43**	**36**	**28**

The compared conditions were: addition of maleic acid, caffeine as chromophores, the simple cellulose binder without any chromophore added and the binder composed of a cellulose and silver mixture. The CCT was used in this study as sensitivity was better in this condition. For comparison, results without the CCT are also presented.

From the **Table III. 8** can be seen that lower RSD (%), (i.e. a good sensitivity homogeneity) could be obtained using of collision cell for a majority of evaluated elements (V, As and Sr). Only in the case of lead, the sensitivity homogeneity was better without the use of collision cell.

The RSD (%) values obtained for other evaluated elements and selected conditions with the use of collision cell are present on the **Table III. 9**.

Table III. 9: Sensitivity relative standard deviations.

RSD (%)	51V	52Cr	55Mn	59Co	60Ni	63Cu	66Zn	75As	86Sr	137Ba	206Pb
cell	69	80	51	91	70	37	32	35	56	66	158
cell CCT	31	86	45	85	54	46	30	38	51	67	87
MA CCT	28	107	54	88	68	51	28	37	61	100	53
Caf CCT	28	134	60	77	71	50	34	48	62	79	43

In the case of LA-ICP-MS analysis, cellulose, maleic acid and caffeine with the use of collision cell gave the best results in the term of sensitivity. Cellulose binder, cellulose binder with the use of collision cell and maleic acid with caffeine also with the use of collision cell were selected as optimal conditions for further evaluations – for the detection limit (LODs) calculation and accuracy calculations.

Nevertheless, the lack of sensitivity homogeneity was important and was depending on the element. To overcome this problem, two strategies were evaluated; the use of an internal standard and a different preparation of the sample using fusion beads. The first objective was to compare the signal to concentration ratios in a homogeneous sample (the fusion is generally employed in this purpose) and further to add an internal standard as it was mentioned in the preceding part of this work.

III.3 UTILISATION OF AN INTERNAL STANDARD

As previously demonstrated the improvement in analytical data obtained by the addition of chromophores to the binder was moderate. As a consequence use of an internal reference: an element already present at known concentration or added to the sample again at a known concentration, was tested to improve analytical data.

An internal standard is usually employed in laser ablation to compensate for matrix effects produced during laser ablation, particle transport or during vaporisation / atomisation /ionisation process within the ICP plasma. One of the advantages of powder analysis is the possibility to add easily an internal standard, as a powder itself or as spiking solution mixed with the binder. Elements present in the binder itself are also likely to be employed as internal reference.

In our work several internal standards were evaluated for LIBS and LA-ICP-MS measurements. Requirements are similar for the selection of an ideal internal standard. **Table III. 10** summarize the selected internal standards tested in our work.

Table III. 10: Selected internal standards.

Type of internal standard	Element	Origin
Present in sample or binder		
Major element in the pellets	Ag, C	Present in constant concentration from the binder
Major element in the sample	Ca	Concentration must be known before analysis
Added as spiking solution to the binder		
ICP classical internal standards	Be, In, Er, Sm	Rare elements present at low concentration in sample
Internal standards	Au, Ir, Lu, Rh	Rare elements present at very low concentration in sample

For each internal standard, new series of pellets were prepared and to avoid interaction of internal standards with each other.

It must be mentioned, that during the evaluation of influence of internal standard, the calibration curves are plotted with and without the use of an internal reference for a more precise comparison.

III.3.1 Internal standards present as major element in the pellets

As presented previously, fly ash powder was mixed with cellulose or silver to obtain stable pellets. As a consequence, large concentrations of Ag and C are brought through the binder addition and could be considered as almost constant from one sample to the other (mass ratio between sample and binder was 1:1).

For optical spectroscopy, Ag and C are interesting because of their simple spectrum. In order to obtain efficient matrix effects compensation a homogeneous distribution in the pellets was verified. SEM-EDS cartography was realised for each pellet prepared with measurements of carbon and silver distribution. As shown on **Figure III. 13** the distribution of these elements was quite homogeneous.

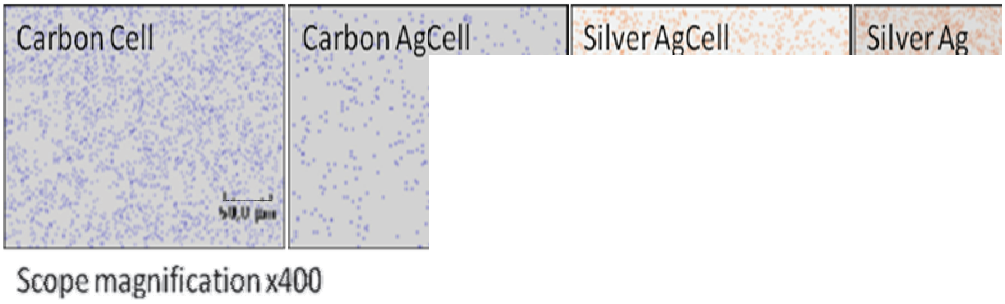

Figure III. 13: Carbon and silver mapping using SEM-EDS, sample is NIST1633b mixe cellulose (cell), cellulose and silver (agCell), silver (Ag).

III.3.1.1 LIBS analysis

Silver and carbon could be measured in pellets prepared with the silver/cellulose bind relatively simple spectrum in the wavelength region employed, but self absorption occ sensitive lines, the Ag 243.778 nm line was employed in our work.

An example of the calibration curves obtained for the four reference materials with a internal standard is presented on **Figure III. 14** for calcium and magnesium in **Figure III**

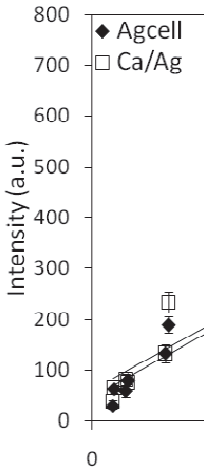

Figure III. 14: LIBS – Calibration curves obtained for Ca II 317.933 nm (mixed binder).

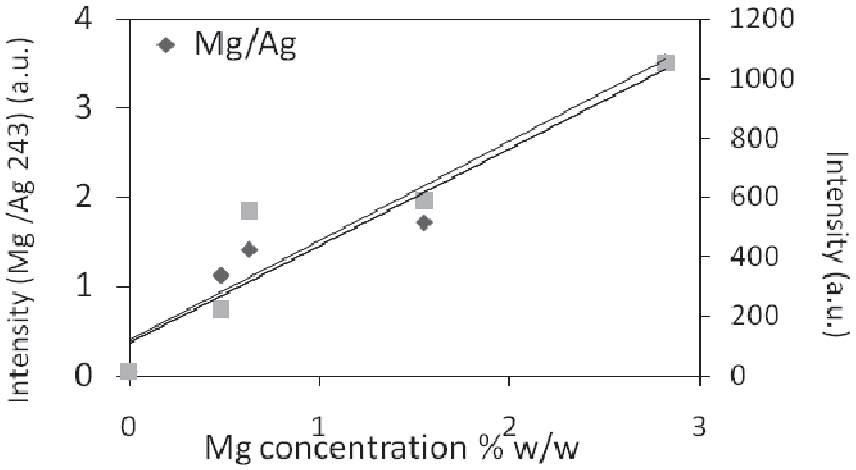

Figure III. 15: LIBS – Calibration curves obtained for Mg 280 nm, I.S. is Ag 243 nm (AgCell binder).

As it can be seen a moderate improvement is obtained and this improvement appeared to be element dependent. Similar results are observed for carbon as an internal standard. A similar study was made using carbon as an internal standard. In this study only C 247 nm could be measured on the LIBS set-up 1. To obtain a full comparison, for the elements of interest (Fe, Mg, Al and Ca) the determination coefficients were calculated for both silver and mixture of silver and cellulose binders and these are presented in **Table III. 11**.

Table III. 11: Determination coefficients (r2) obtained for two different binders with and without internal standard.

	Al 308	Fe 259	Mg 280	Ca 317
External calibration (r^2)	0.30	0.10	0.56	0.89
Carbon int. Std. (r^2)	0.75	0.77	0.65	0.87
Silver Int. Std. (r^2)	0.03	0.67	0.75	0.91

An improvement is obtained for all elements with the use of either carbon (C 247 nm) or silver (Ag 243 nm). The use of silver did improve linearity in the case of Al. Nevertheless, an evaluation of accuracy of the method using C and Ag will be presented further as linear calibration curves were obtained in these conditions.

III.3.1.2 LA-ICP-MS analysis

Silver and carbon are present at very high concentrations (50% for some sample), so that no measurement of Ag, even on the low abundance isotopes could be made.

Carbon as ^{13}C could be measured only on the LA ICP MS set-up 2 (Brno). The evaluation of carbon internal standard was performed on the series of pellets containing the cellulose binder and the mixture of cellulose and silver binder.

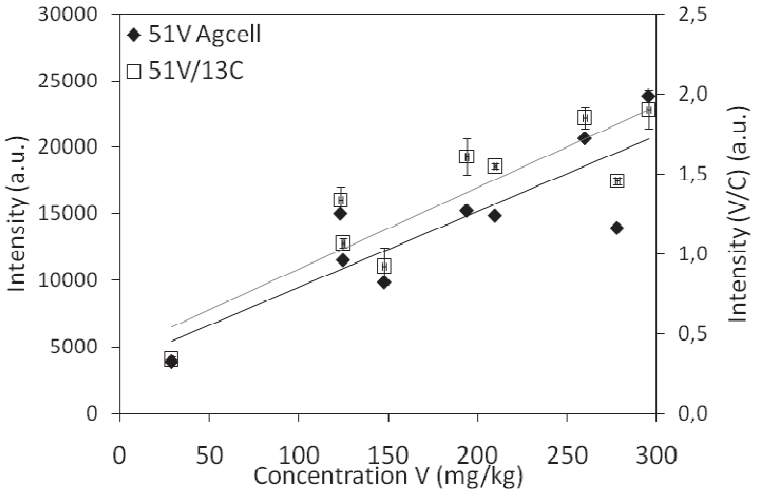

Figure III. 16: Calibration curve obtained for ^{51}V using ^{13}C as an internal standard.

As it can be seen from **Figure III. 16** no improvement was observed, on the contrary, deterioration in the calibration behaviour was observed in the case of cellulose binder and the utilisation of carbon internal standard – the determination coefficient r^2 decreased from 0.97 without internal standard to 0.32. In the case of the mixture of cellulose and silver binder, there is no significant difference between utilisation with and without internal standard. The determination coefficient without internal standard r2 = 0.89 and with internal standard the determination coefficient was r2 = 0.85.

In ICP-MS, the use of a major matrix component as an internal reference, was not successful, neither using Ag nor ^{13}C.

III.3.2 Internal standards present at low concentration in the sample

III.3.2.1 Classical ICP internal standards for LIBS analysis

Classical elements employed in ICP as internal standards are rare elements such as Indium or Erbium and Beryllium. In this work, due to low sensitivity of In and other classical internal standards in LIBS spectroscopy, only Beryllium and Erbium could be evaluated using set-up 3. Samarium was not evaluated because of lack of sufficiently intense analytical line. Results are presented in the **Table III. 12**.

Table III. 12: Determination coefficients (r^2) obtained for LIBS measurement with and without the use of beryllium and erbium as internal standards.

Determination coefficient (r^2)	Ca II 317.933 nm	Fe I 259.957 nm	Al I 308.215 nm	Mg II 280.270 nm
Agcell	1.00	0.49	0.50	0.85
Agcell /Be313	0.99	0.60	0.47	0.79
Agcell/Er323	0.99	0.69	0.32	0.75
Cell	0.99	0.48	0.52	0.75
Cell / Be313	0.97	0.86	0.76	0.56
Cell/Er323	0.99	0.78	0.83	0.80

In the case of both tested internal standards, deterioration in calibration trends was observed for aluminium and magnesium while no influence was observed for calcium and an improvement was obtained for iron.

III.3.2.2 Classical ICP internal standards for LA-ICP-MS analysis

Indium is commonly used as internal standard in ICP-MS spectroscopy. It was also described in geological analysis [22-24] using LA-ICP-MS. Indium was added in constant concentration into the powder cellulose, homogenised, and then mixed with samples.

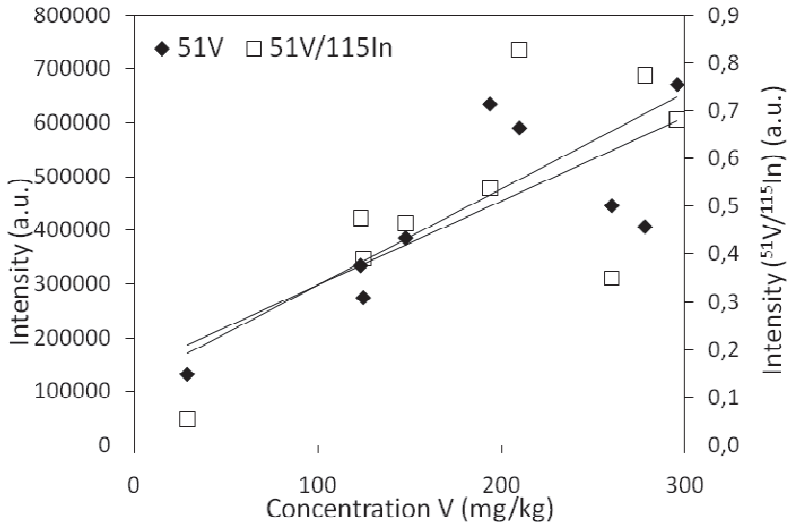

Figure III. 17: Influence of internal standard ^{115}In on the calibration tendency of ^{51}V, mixture of cellulose and powder silver as a binder.

As shown on **Figure III. 17**, the use of indium internal standard was not successful. The values of determination coefficients in the case of powder cellulose binder obtained on the **set-up 2** (Brno) were 0. 78 without internal standard and 0.30 with the use of internal standard, **Figure III. 18**. In the case of mixture of powder cellulose and powder silver binder measured on the **set-up 1** (Lyon), the determination coefficient for the calibration tendency without utilisation of internal standard was r^2 = 0.77 and with internal standard r^2 = 0.73.

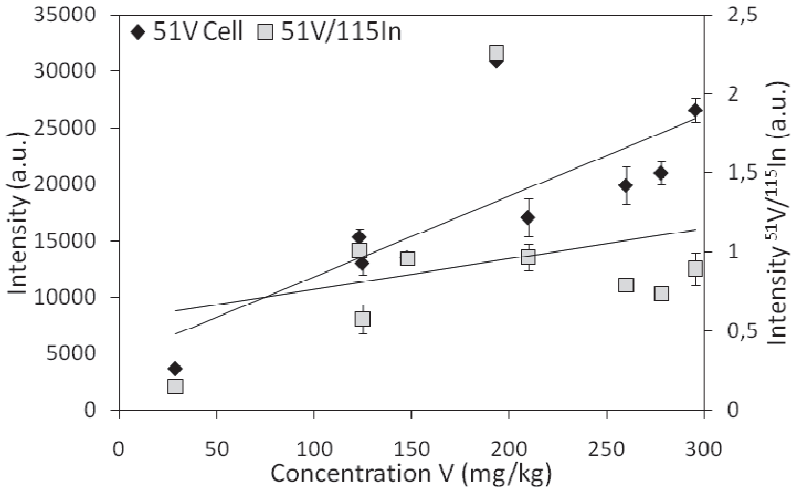

Figure III. 18: Influence of internal standard ^{115}In on the calibration tendency of ^{51}V, cellulose binder and the set-up 2 (Brno) was used for measurement.

Other commonly employed internal standards in ICP are Be, Er and Sm, these elements are used generally to compensate for ICP related matrix effects. Their interest is also to cover a large mass range. Beryllium (ionisation potential = 9.3 eV) and was used for As, Se, Sb, Cd, Hg, Zn, S and P. Samarium (5.6 eV) was used for Ba and Sr, while Erbium (6.08 eV) was employed for Ca, V, Cr, Mn, Co, Ni and Cu. **Figure III. 19** presents the calibration curves obtained with and without the use of the internal standards**.**

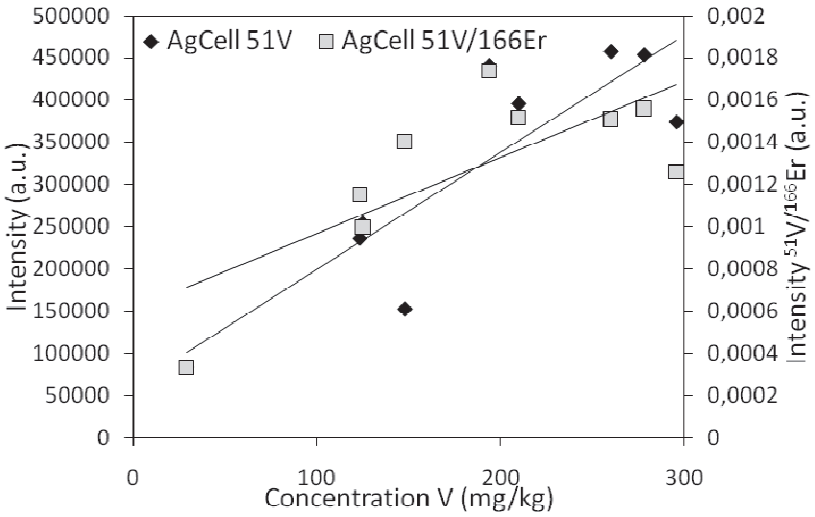

Figure III. 19: Influence of internal standard ^{166}Er on the calibration tendency of ^{51}V, mixture of powder cellulose and powder silver used as binder. Set-up 2 (Lyon) was used for measurement.

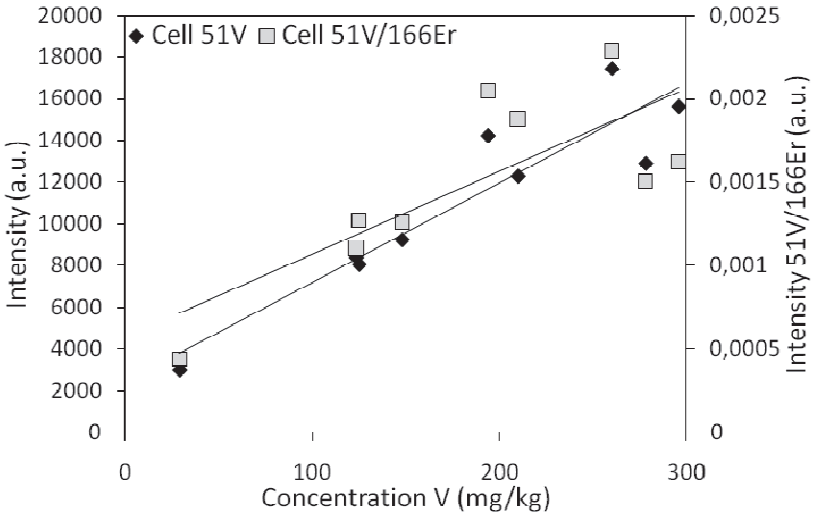

Figure III. 20: Influence of internal standard ^{166}Er on the calibration tendency of ^{51}V, cellulose powder used as binder. Set-up 1 (Brno) was used for measurement.

During homogenisation, after the IS addition, several samples with silver binder reacted (effervescence of the samples) after the Erbium oxide addition (CTA-FFA-1, NIST1633b, L1). Neither these internal standards did not bring the improvement of calibration tendency, on the contrary, the deterioration in calibration tendencies was observed. This deterioration can be explained partially by the reaction with the samples with silver binder (samples CTA-FFA-1, NIST1633b and L1).

The significant deterioration of the linearity when the Erbium as internal standard was used can be observed on the **Figure III. 19** and **Figure III. 20** for both evaluated experimental set-ups (Lyon and Brno); and this trend was confirmed by the values of determination coefficients (**Table III. 13**) where the values of determination coefficients are presented. Only in the case of arsenic determination, improvement in calibration trends was observed for both evaluated binders and experimental set-ups.

Table III. 13: Determination coefficient obtained for different binders with erbium as internal standard.

Determination coefficient (r^2)	^{51}Vanadium	^{75}Arsenic	^{206}Lead
Agcell Set-up1	0.87	0.72	0.91
Agcell /^{166}Er Set-up1	0.75	0.93	0.86
Cell Set-up1	0.92	0.67	0.97
Cell/^{166}Er Set-up1	0.47	0.92	0.73
Agcell Set-up2	0.92	0.98	0.96
Agcell /^{166}Er Set-up2	0.88	0.96	0.98
Cell Set-up2	0.93	0.94	0.92
Cell/^{166}Er Set-up2	0.78	0.98	0.92

Set-up1 – Lyon, Set-up2 - Brno

In the case of Samarium and Beryllium, the calibration trends using these internal standards were rapidly decreasing and no linear plot could be obtained.

To find an appropriate internal standard appeared as a difficult task. As described in part 1, fly ashes concentrate a wide range of elements. Therefore, some experiments were carried out to check occurrence of all elements likely to be measured using ICP.

First a qualitative method was established on the LA-ICP-MS system to evaluate occurrence of signal on the m/z ratios of interest. As the mass filter of this system is a quadrupole only a limited range of

mass was explored, a second experiment was then built on the ICP/SFMS to fully explore the mass range.

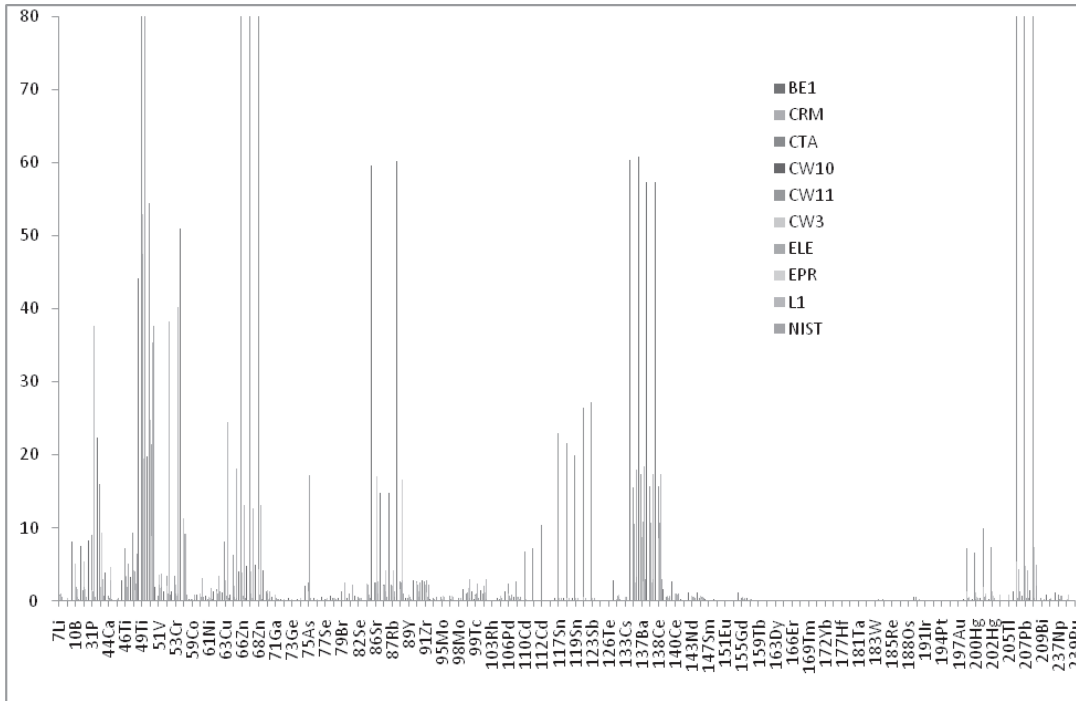

Figure III. 21: LA-ICP-MS analysis of all elements present in samples.

Signal measured in the fly ashes was compared to that recorded for NIST 612 glass sample. This reference material is well known for its low content of a variety of trace elements. As it can be seen from **Figure III. 21**, elements are generally present (or more sensitive) in fly ashes compared to the glass sample.

A few elements gave lower signals: calcium that is present at 12% in NIST 612.

In the 143 to 197 mass (m/z) range, where the lanthanides are detected the signal measured in fly ashes is comparable or inferior to that measured in NIST 612 but very intense signals were obtained in this region. Low signal was obtained only on platinum, gold, irridium, rhodium and lutetium this was confirmed by measurements achieved after sample digestion and measurements on ICP-SFMS.

These elements are not classical internal standards but were tested; two separated solutions gold, iridium and rhodium with two different concentrations were tested. In both cases the ISs were added into the binder, homogenised and compacted with the samples. These internal standards were tested both LIBS (only for gold) and LA-ICP-MS techniques.

III.3.2.3 LIBS analysis

Gold signal was measured on LIBS set-up 3 as it had a better sensitivity. Signals obtained for Rh and Ir were too low to be correctly employed for internal standardisation. Adding more IS to the sample was difficult due to the cost of internal standard solutions. The influence of gold internal standard to the selected binders is present on the next figure, **Figure III. 22**.

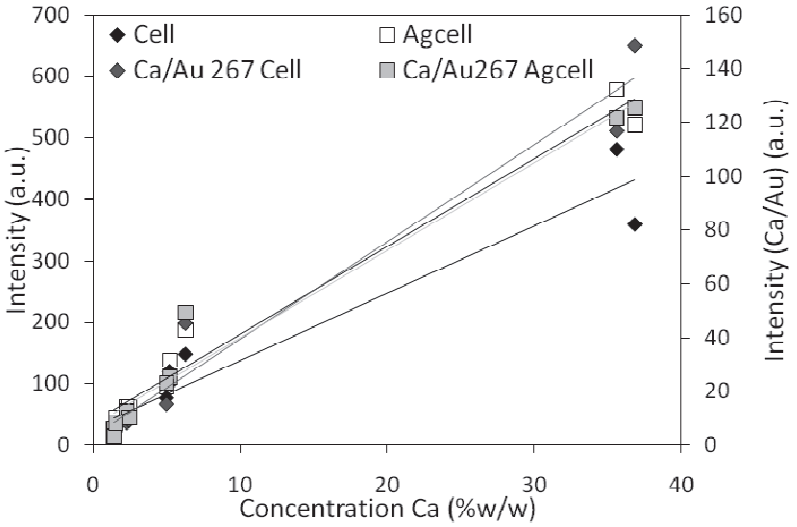

Figure III. 22: Influence of gold internal standard on the calibration tendency of Ca 317.994 nm, gold Au I 267 nm was used for measurements; LIBS analysis.

The determination coefficients are presented on the **Table III. 14**. As it can be seen from the table, there is no significant influence of the gold internal standard to the calibration trends. Only slight improvement was observed for calcium determination when cellulose was used as binder. In the case of the rest of selected elements, the deterioration in calibration trends was observed for both evaluated binders.

Table III. 14: Determination coefficient of LIBS measurements obtained for different binders with and without internal standard.

Determination coefficient (r^2)	Ca II 317.933 nm	Fe I 259.957 nm	Al I 308.215 nm	Mg II 280.270 nm
Agcell	0.99	0.91	0.84	0.91
Agcell /Au267	0.98	0.70	0.41	0.88
Cell	0.97	0.63	0.57	0.91
Cell /Au267	0.98	0.51	0.30	0.85

In LIBS spectroscopy, the improvement observed is very small either using mixed binder or a simple cellulose binder. There is therefore no interest to use gold as internal standard in comparison to the results obtained by silver or carbon.

III.3.2.4 LA-ICP-MS analysis

Gold, iridium and rhodium signals could be easily measured on LA-ICP-MS system. A comparison of Intensity ratios against concentration ratios is presented in **Figure III. 23**. The regression coefficients are summarised in the **Table III. 15**.

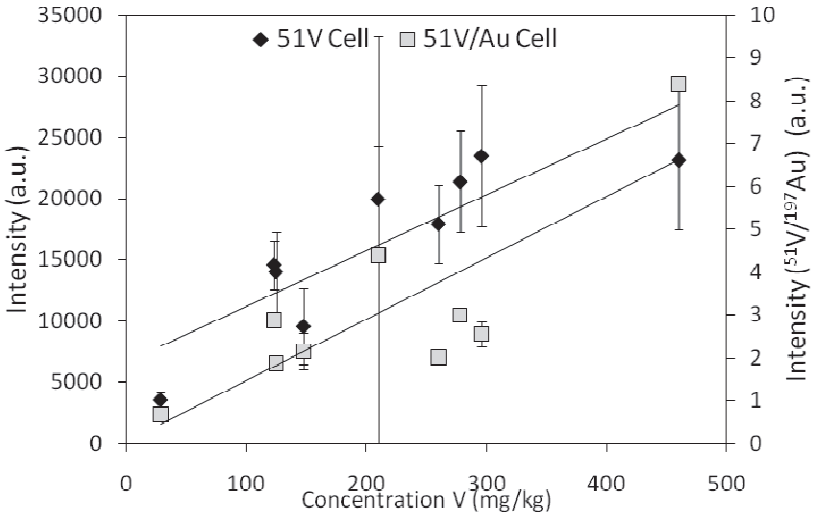

Figure III. 23: ^{51}V signal with and without the internal standard (cellulose pellets).

The gold as internal standard was evaluated on both LA ICP MS systems, in Lyon and Brno and their calibration trends are presented on the **Figure III. 23** and **Figure III. 24**, respectively. As it can be seen, high RSD values were obtained for the cellulose binder with the use of internal standard, also the deterioration in calibration trend was observed for the cellulose binder using both systems.

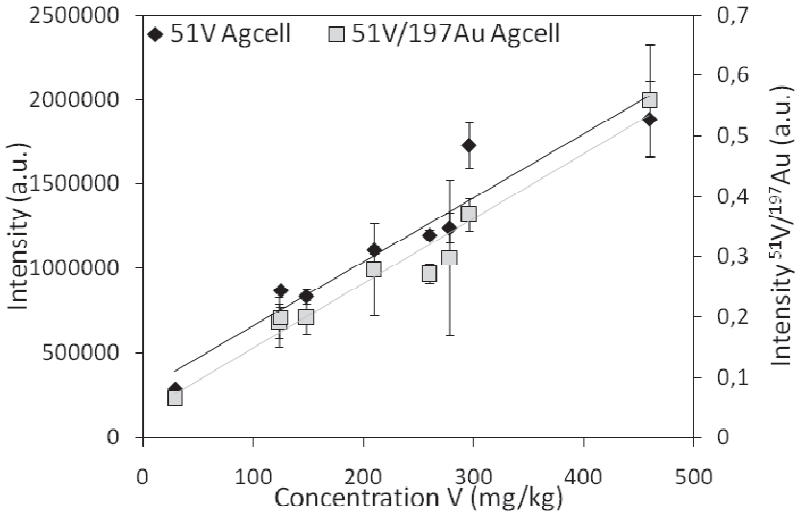

Figure III. 24: Calibration for ^{51}V with and without an internal standard.

The values of determination coefficients for both experimental set-ups and selected elements are present on the **Table III. 15**.

Table III. 15: Determination coefficients for different binders with and without internal standard.

Determination coefficient (r^2)	^{51}V	^{52}Cr	^{55}Mn	^{66}Zn	^{75}As	^{206}Pb
Agcell Set-up1	0.96	0.15	0.89	0.98	0.98	0.98
Agcell/^{197}Au Set-up1	0.97	0.22	0.58	0.89	0.99	0.95
Cell Set-up1	0.98	0.36	0.89	0.66	0.98	0.95
Cell/^{197}Au Set-up1	0.87	0.44	0.74	0.46	1.00	0.83
Cell Set-up2	0.86	0.39	0.88	0.61	0.99	0.97
Cell/^{197}Au Set-up2	0.82	0.37	0.88	0.45	0.99	0.71
Agcell Set-up2	0.90	0.55	0.83	0.97	0.98	0.93
Agcell/^{197}Au Setup2	0.82	0.55	0.85	0.96	0.99	0.70

From the **Table III. 15** it can be seen that determination coefficients are extremely close to 1 for V, As and Pb even using no internal standard. For those elements there is no use adding an internal

standard. On the contrary, low determination coefficients were obtained for Zn, Mn and Cr, and even using an internal standard, linearity was not improved.

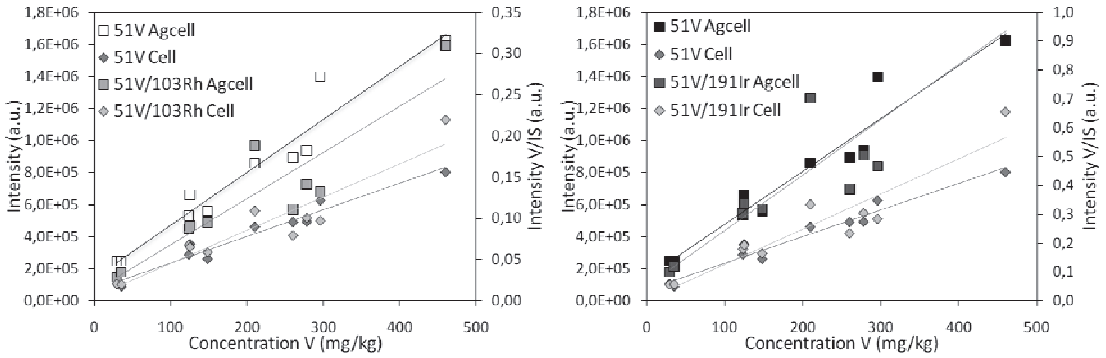

Figure III. 25: Calibration plots with and without Ir internal standard.

The determination coefficients were calculated for iridium and rhodium internal standard and their values are present on the **Table III. 16**.

Table III. 16: Comparison of determination coefficients obtained for two studied binders and different internal standards – Au, Ir and Rh with concentration 500 mg/kg.

Determination coefficient (r^2)	^{51}V	^{52}Cr	^{55}Mn	^{66}Zn	^{75}As	^{206}Pb
Agcell	0.97	0.94	0.52	0.92	0.98	0.94
Agcell /^{191}Ir	0.90	0.97	0.72	0.85	0.99	0.96
Agcell /^{103}Rh	0.91	0.96	0.68	0.85	0.99	0.96
Cell	0.98	0.94	0.64	0.69	0.99	0.99
Cell /^{191}Ir	0.94	0.96	0.68	0.54	0.99	0.94
Cell /^{103}Rh	0.94	0.95	0.62	0.48	0.99	0.93

The calibration tendency shows nearly the same evolution with and without Ir and Rh as internal standards, (**Figure III. 25**). We can conclude that both for the two studied binders, the internal standards tested gave no improvement of analytical data.

III.3.3 Internal standard present as major element with known concentration

Elements added through the binder (Ag/C) or spiked to the cellulose powder gave no improvements. One of the elements present in large concentration and measured before the LA-ICP-MS or LIBS study could be used as an internal standard. The difficulty is to determine the elements concentration before a quantification can be made using LA-ICP-MS or LIBS, the advantage is that this element is correctly mixed to the matrix.

In this purpose calcium was tested. It was present in large concentration range in all samples. SEM-EDS cartography of calcium in the different pellets prepared with silver/cellulose binder was first established to verify the homogeneity of Ca distribution in the pellet, **Figure III. 26**. With the exception of ELE all sample had a satisfactory surface homogeneity for this element.

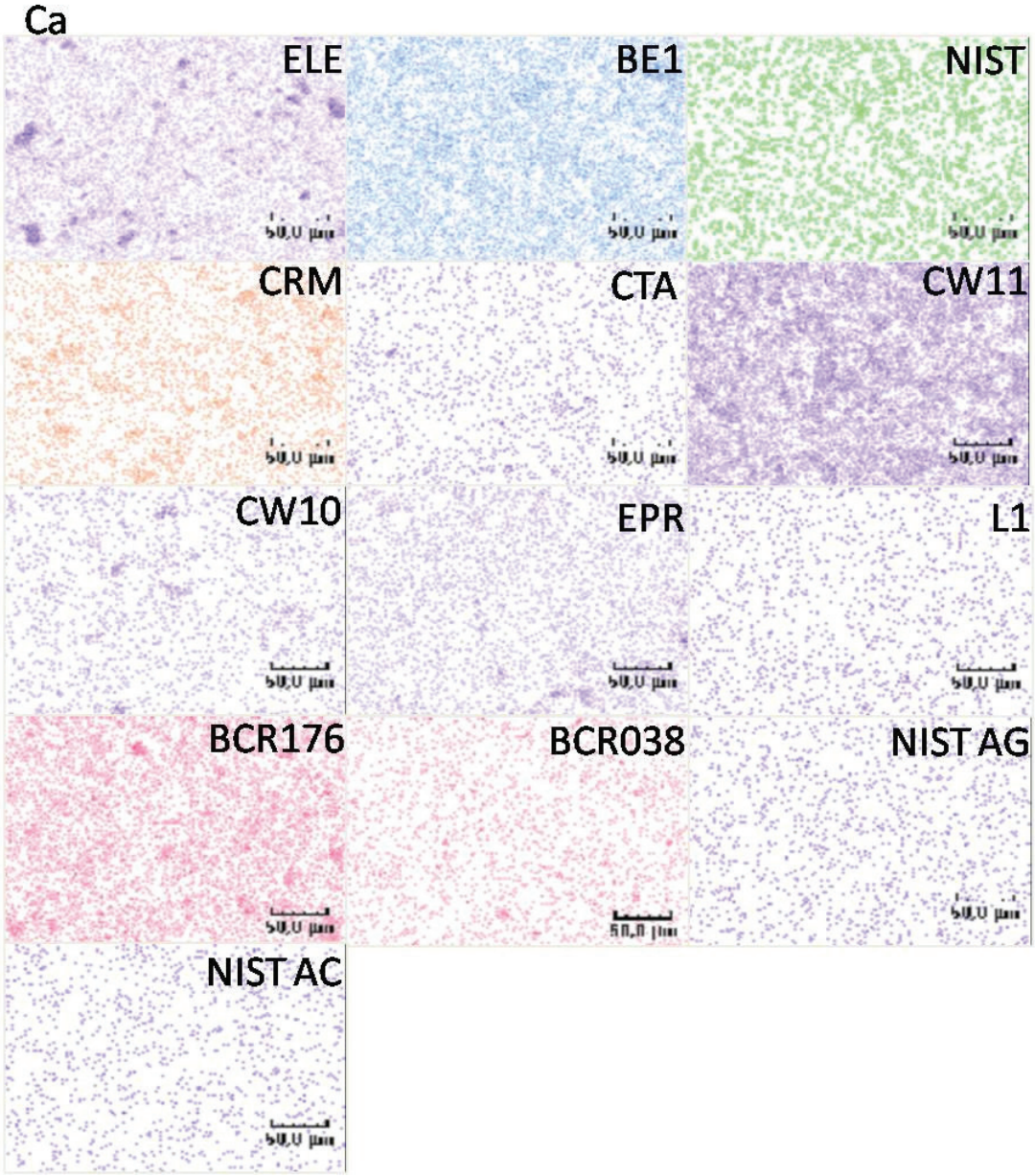

Figure III. 26: Cartography observation made by SEM-EDS obtained for calcium in different pellets with cellulose binder and two NIST pellets with mixed and silver binders.

III.3.3.1 LIBS analysis

The internal standard evaluation was performed for LIBS analysis, where the influence of calcium (Ca II 317.933 nm) as internal standard was tested on the iron (Fe I 259.957 nm) line. Better results were obtained when silver as binder was used and the worst results were obtained for cellulose binder. The calibration tendencies for LIBS analysis, Fe I 259.957 nm was measured and calcium line Ca II 317.933 nm was used as internal standard line. On the **Figure III. 27** the improvement in linearity can

be observed when the internal standard is used. Better results were obtained for silver binder with internal standard, the determination coefficients are summarised in the **Table III. 17**.

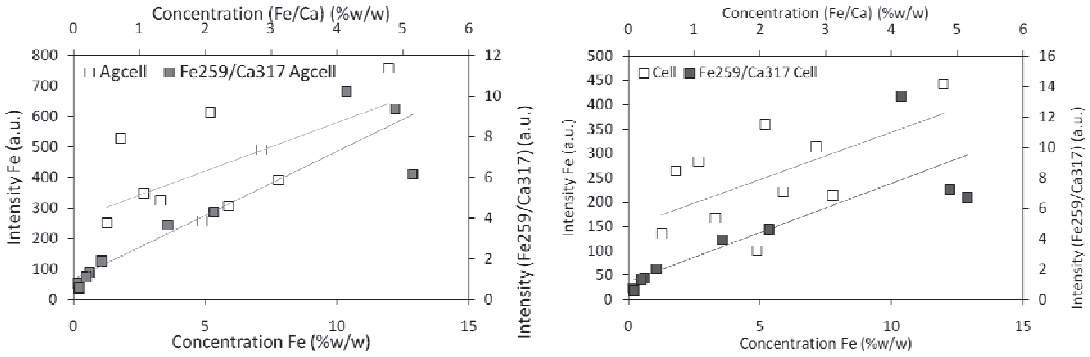

Figure III. 27: Calibration tendencies obtained for two selected binders for Fe I 259.957 nm with and without internal standard (Ca II 317.933 nm).

Table III. 17: Determination coefficient obtained with and without Ca (Ca II 317.933 nm) as internal standard.

Determination coefficient (r^2)	Fe 259.957 nm	Al 308.215 nm	Mg 280.270 nm
Agcell	0.61	0.59	0.72
Agcell/Ca	0.92	0.95	0.91
Cell	0.60	0.45	0.25
Cell/Ca	0.84	0.94	0.83

As seen on the **Table III. 17** linearity was improved using Ca as an internal standard. Determination coefficients were slightly better that using carbon or silver internal standards. But in this case, the determination of Ca has to be made by an alternative method before the LIBS measurement. Accuracy calculation will be made, selecting reference materials as standards and using L1, CW11, CW10 and EPR as real samples. The results obtained will be compared to the results obtained using Ag and C as internal standards.

III.3.3.2 LA-ICP-MS analysis

Calcium is difficult to measure using ICP MS as it is present in large concentrations, a reduced dwell time and a minor isotope were employed to do so. An example of calibration plot is presented on **Figure III. 28** and the obtained determination coefficients are shown in **Table III. 18**.

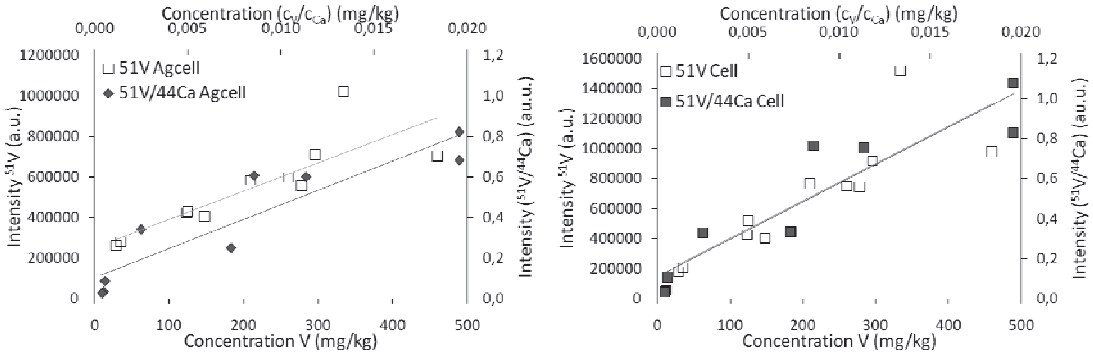

Figure III. 28: Effect of calcium internal standard on the calibration tendencies for cellulose and mixture of cellulose and silver binders, LA-ICP-MS analysis of ^{51}V, dwell time 10 ms.

Table III. 18: Determination coefficient obtained with and without Ca as internal standard for two studied binders, LA-ICP-MS analysis.

Determination coefficient (r^2)	^{51}V	^{75}As	^{206}Pb
Agcell	0.84	0.98	0.60
Agcell/^{44}Ca	0.91	0.95	0.91
Cell	0.85	0.99	0.94
Cell/^{44}Ca	0.91	0.98	0.99

The utilisation of calcium brought improvement in calibration strategies, the linear calibration tendency were obtained for nearly all tested elements (except cobalt). This improvement was confirmed by determination coefficient r^2, **Table III. 18**.

Calculation of concentrations found in real samples will be made using reference materials as standards using this internal standard. The results will be compared to the concentrations obtained on the same elements using an addition of chromophores to the binder. The calcium as major element presented in the samples was chosen as internal standard. Calcium was the only one element for which the improvement in the calibration trends was observed. This can be done by the fact which was mentioned before – its presence as a major element in the sample and also by the fact that the same sample treatment was performed. The disadvantage of this internal standard is the obligatory knowledge of its concentration before the analysis. So, the second analytical technique must be used for the calcium concentration determination.

The results will be compared to the concentrations obtained on the same elements using an addition of chromophores to the binder.

III.4 FUSION BEADS

All these evaluations of different internal standards showed the difficulties with the choice of appropriate internal standards and their addition into the pellets. Internal standard could be inhomogeneous, except in the case of Ca where SEM-EDS mapping exhibited a good homogeneity of the element, for this reason, fused beads were prepared. In this case the sample represents only 16% of the target; the flux (lithium tetraborate) represents major part of the bead. Mixing of fly ash and flux is made using a fusion at high temperature so that, theoretically, a good homogenisation and reduced sample dependant ablation process. Lutetium was tested as internal standard only in the fused beads. It was added before the fusion of lithium tetraborate fused beads, so the well homogenisation was assured and the internal standard could be taken as a part of matrix. The measurements of fused beads on two different ablation and detection system were performed and examples of calibration tendency for LIBS and LA-ICP-MS measurements is shown on the example of ^{51}V, (**Figure III. 29**). There was neither improvement nor deterioration in calibration tendency observed. This can be due the high concentration of lutetium in fused beads and consequently shorter dwell time (0.1 ms for ^{176}Lu, 100 ms for ^{51}V).

Regression coefficient for fused bead without internal standard was $r^2 = 0.94$, with internal standard the regression coefficient was $r^2 = 0.94$.

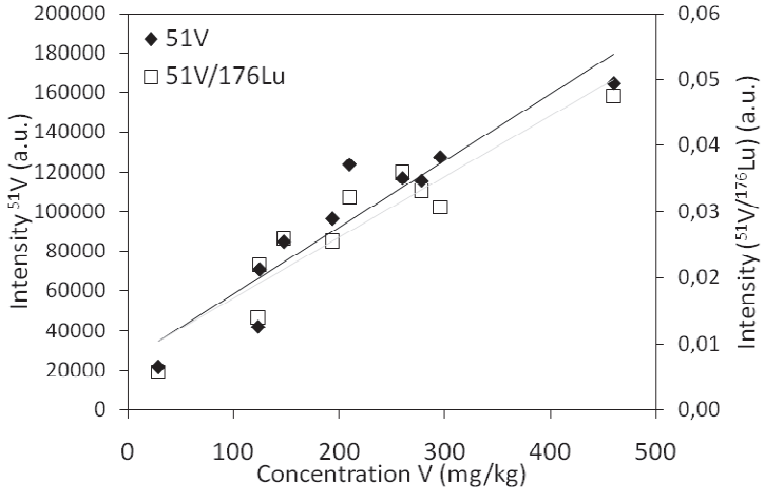

Figure III. 29: Effect of lutetium as internal standard to the fused bead measurements; LA-ICP-MS measurement, ^{51}V as analyte, ^{176}Lu was used as internal standard.

Before mentioned internal standards did not present big improvements, except the case of lutetium in the LIBS analysis, in calibration tendencies and did not compensate the matrix effect. For this

reason, the choice of internal standard present in the sample matrix was tested. Calcium as a major element with sufficiently intense lines on the LIBS spectrum, high concentration in the samples and isotopes with absence of interference was chosen.

The lutetium was added only into the fused beads, and its influence as internal standard was evaluated. The example of calibration tendency is present on the **Figure III. 30**.

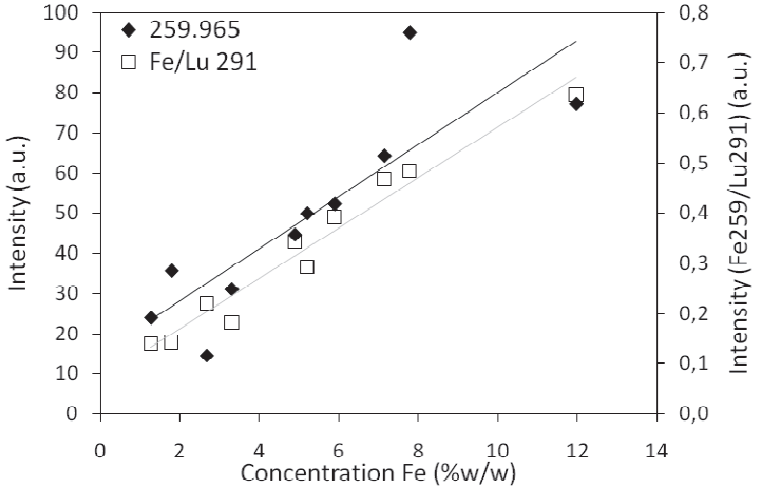

Figure III. 30: Effect of lutetium as internal standard to the fused bead measurements; LIBS measurement, Fe I 259.957 nm as determinate element, Lu I 291.118 nm was used as internal standard.

The regression coefficient for fused bead without internal standard was r^2 = 0.85, with internal standard the regression coefficient was r^2 = 0.98.

It can be conclude that neither sample homogenisation, nor the way how the internal standard was added into the pellets plays role.

III.5 LIMIT OF DETECTION

To obtain the reliable results, sensitivity should be optimised to obtain the low RSD results. To achieve this low RSD, the pellets must be mechanically stable. The laser pulse energy optimisation was performed to obtain the highest signal with acceptable RSDs and to avoid self-reversal phenomenon.

III.5.1 LIBS Study

To evaluate the efficiency of the experimental set-up, the accuracy and detection limits for different series of pellets were calculated. One sample with the concentration in the middle of concentrations range was chosen as unknown and its concentration was calculated and compared with the declared value. Limits of detection were calculated as $LOD = \frac{3 \times SD_{bkg}}{sensitivity}$ and their values for all experimental set-ups are present on the **Table III. 19**. As it can be seen from the tables, the detection limits for different experimental set-ups and series of pellets varies for different elements and different analysed lines. The lowest detection limits were obtained for magnesium Mg II 279.553 nm and Mg II 280.27 nm lines, where the detection limits varies from 0.003 % w/w to 0.41 %w/w. The highest detection limits were calculated for the aluminium lines, especially for Al I 308.215 nm line (values from 0.61 %w/w to 5.44 %w/w). The important role plays the experimental set-up – set-up 1, set-up 2 and set-up 3 (Quantel Brilliant laser system). The comparison of detection limits between horizontal and vertical experimental set-ups did not show big differences, only in the case of Ca II 315.887 nm and Al I 308.215 nm the lowest limits of detection were obtained for horizontal experimental set-up, **Table III. 19**.

Table III. 19: Limit of detection % m/m calculated for different experimental set-ups.

Element	Wavelength (nm)	LODs %w/w *(setup 1)*		LODs %w/w *(setup 2)*		LODs %w/w *(setup 3)*	
Binder		*Silver /Cellulose*	*Cellulose*	*Silver /Cellulose*	*Cellulose*	*Silver /Cellulose*	*Cellulose*
Ca	315.887	0.27	0.64	0.25	0.6	0.12	0.1
	317.933	0.20	0.30	0.25	0.55	0.28	0.3
Mg	279.553	0.006	0.01	0.07	0.03	0.02	0.41
	280.270	0.009	0.016	0.03	0.03	0.11	0.37
Fe	259.957	0.29	0.65	0.13	0.12	0.32	0.39
Al	308.215	0.69	0.47	1.57	0.70	2.19	5.4
	309.271	0.27	0.24	0.76	0.67	1.67	4.4

From the **Table III. 19** can be seen that all detection limits are in the same concentration range (hundred of mg/kg) for all tested experimental set-ups.

III.5.2 LA-ICP-MS measurements

Detection limits were calculated as in previous case of LIBS determination as 3 times standard deviation of the background divided by the sensitivity of the element with the lowest concentration. For LODs calculations, the isotopes with the highest abundance were chosen and the obtained values are presented in Tables (**Table III. 20**).

As the pellets were prepared in mass ratio 1:1, the LODs were calculated for this ratio. This is because pellets containing fly ashes could not be pressed without use of binder (they were not mechanically stable). All values are presented in mg/kg range. Better LODs were obtained for cellulose binder.

Table III. 20: Detection limits calculated for LA-ICP-MS measurements.

	mg/kg ^{31}P	mg/kg ^{51}V	mg/kg ^{52}Cr	mg/kg ^{55}Mn	mg/kg ^{59}Co	mg/kg ^{60}Ni	mg/kg ^{63}Cu	mg/kg ^{66}Zn	mg/kg ^{75}As	mg/kg ^{78}Se	mg/kg ^{88}Sr	mg/kg ^{110}Cd	mg/kg ^{118}Sn	mg/kg ^{121}Sb	mg/kg ^{137}Ba	mg/kg ^{202}Hg	mg/kg ^{208}Pb
cell CCT	84.55	0.62	0.28	3.15	0.18	1.30	0.32	2.03	1.86	1.21	0.72	0.04	N/M	0.20	1.18	4.18	0.06
cell	37.86	0.63	0.54	1.00	0.04	0.33	1.34	5.13	3.04	1.20	5.17	0.13	0.33	0.18	2.22	2.60	0.09
MA CCT	168.67	1.59	2.55	3.52	0.23	6.15	0.54	2.26	2.10	2.16	8.64	0.13	N/M	0.15	4.68	5.37	1.42
Caf CCT	372.68	0.96	5.01	4.45	0.33	1.69	3.52	4.69	3.11	4.30	9.81	0.21	N/M	0.38	5.78	2.59	0.15

N/M – not measured

The very small amount of material ablated is responsible for some of the high detection limits obtained. As a comparison a laser ablation system operated at similar fluence but sampling on a surface a hundred times larger and associated to an ICP-OES (JAAS 2005) gave similar detection limits. From the **Table III. 20** the detection limits were in hundred of ppb values or in units of mg/kg values.

For comparison, detection limits for several elements were calculated also after LA-ICP-OES measurement, **Table III. 21**, to verify the difficulties with determination of several elements by the LIBS and LA-ICP-MS measurements.

Table III. 21: Detection limits obtained for LA-ICP-OES measurements.

	%w/w Mg280	%w/w Al396	%w/w Fe238	mg/kg Ba455	mg/kg Cd228	mg/kg Cr267	mg/kg Cu327	mg/kg Mn259	mg/kg Sr407	mg/kg Zn206
Cell	0.00102	0.0232	0.0030	3.65	0.034	2.60	2.40	2.16	7.12	51.51

As it can be seen, LIBS and LA-ICP methods are fully complementary. And to improve detection limits using LA-ICP-MS, a larger amount of sample should be analysed. A higher repetition rate of the use of fs laser is advisable in this objective.

III.6 ACCURACY

The accuracy was calculated both for LIBS and LA-ICP-MS measurements on the selected conditions and for selected series of pellets. For the LIBS measurements, three experimental set-ups were evaluated while for LA ICP MS only the results obtained on the system Thermo are discussed. Accuracy is one of the most important figures of merit during a validation procedure.

III.6.1 LIBS analysis

The binder giving best sensitivity and mechanically stable pellets selected in Part III.1, was employed to evaluate accuracy using the three LIBS experimental set-ups. As mentioned in Part III.3, the linearity was found better when using an internal standard (C, Ag and Ca). The concentrations or major elements (Ca, Mg, Fe and Al) were calculated using reference materials (CTA, NIST, BE1 and CRM) as standards. LIBS determination was compared to measurements obtained from alkali fusion and wet digestion. Concentrations of the samples (i.e. L1, EPR, CW3, CW10 and CW11) were first calculated from external calibration, results are shown in **Table III. 22**.

Table III. 22: Determination of Ca, Mg, Fe and Mg in fly ash samples by LIBS: comparison of different setups using external calibration.

			L1	EPR	CW3	CW10	CW11
Al	1	LIBS	21.6	8.85	29 .0	14.5	0.4
	2	LIBS	11.1	28 .2	13.8	14.7	<LOD
	3	LIBS	21.0	36.6	NA	14.5	<LOD
	** D	ICP-OES	17.6	13.8	7.13	10.53	4.45
Ca	1	LIBS	1.36	1.79	21.1	3.8	20.0
	2	LIBS	0.06	2.1	21.2	4.2	21.6
	3	LIBS	<LOD	<LOD	NA	3.7	24.3
	** D	ICP-OES	1.42	2.45	26.5	4.99	36.84
Fe	1	LIBS	16.2	10.9	4.41	30.4	35.9
	2	LIBS	3.1	29.0	20.7	13 .7	4.2
	3	LIBS	2.7	10.8	NA	6.9	<LOD
	** D	ICP-OES	6.26	11.9	5.18	7.13	3.29
Mg	1	LIBS	0.6	0.7	1.6	1.1	2.1
	2	LIBS	<LOD	2.2	2.8	1.8	2.6
	3	LIBS	0.4	0.86	NA	1.13	2.2
	** D	ICP-OES	0.96	1.4	1.29	2.13	3.3

As it can be seen the accuracy is not good. The three set-ups employed gave similar poor analytical data.

The accuracy using external calibration for all the elements evaluated is presented on the **Figure III. 31**.

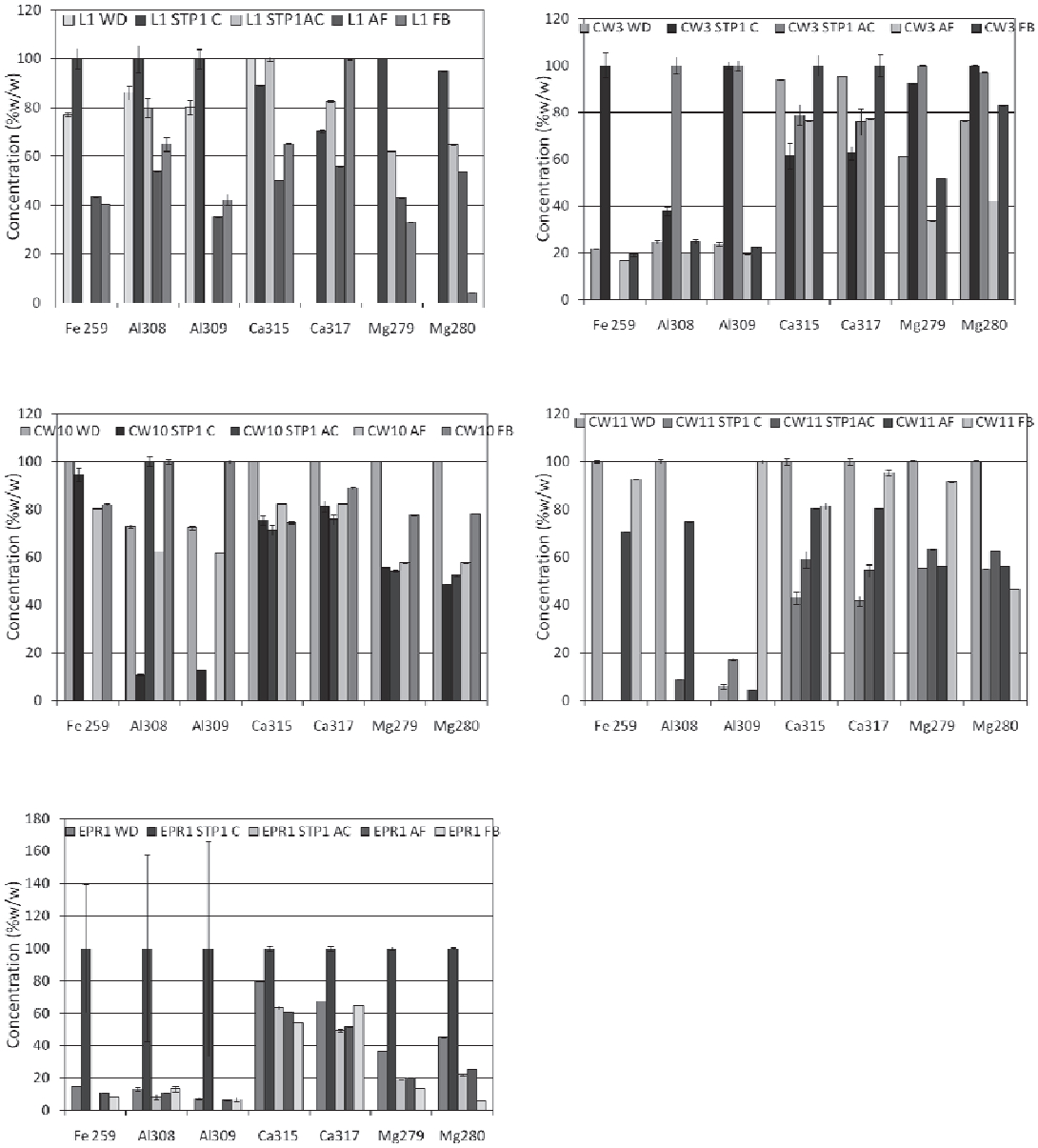

Figure III. 31: Normalized concentrations obtained for all evaluated analytical lines.

The use of an internal standard is compulsory in this case. The following table compares concentration found using LIBS set-up 1 when employing internal standards as recommended in part

III.3. The results using C, Ag and Ca are presented and a comparison is made with wet digestion/ICP-AES analysis, and alkali fusions/ICP-AES analysis, **Table III. 23**.

Table III. 23: Determination of Ca, Mg, Fe and Mg in fly ash samples: comparison of different procedures using internal standards C, Ag and Ca.

			L1	$\sigma_{n=5}$	EPR	$\sigma_{n=5}$	CW3	$\sigma_{n=5}$	CW10	$\sigma_{n=5}$	CW11	$\sigma_{n=5}$
Al	C int. ref.	LIBS	17.2	1.2	13.8	3.1	11.5	0.7	14.1	1.4	4.3	0.4
	Ag int. ref.	LIBS	15.1	3.0	12.9	3.2	10.1	2.0	11.8	1.4	4.6	0.4
	Ca int. ref.	LIBS	13.7	3.9	14.2	2.3	8.5	0.8	13.6	4	3.3	1.0
	*Fusion	ICP-OES	**14.6**	**0.1**	**11.6**	**0.05**	**5.8**	**0.04**	**9.0**	**0.04**	**3.3**	**0.03**
	** Digestion	ICP-OES	**17.6**	-	**13.8**	-	**7.13**	-	**10.53**	-	**4.45**	-
Ca	C int. ref.	LIBS	1.64	0.09	2.2	0.6	24.5	0.7	4.47	0.7	20.93	3.6
	Ag int. ref.	LIBS	2.37	0.30	2.94	1.0	27.6	4.1	4.03	0.7	23.98	3.7
	-	-	-		-		-		-		-	
	*Fusion	ICP-OES	**0.92**	**0.01**	**1.87**	**0.02**	**21.5**	**0.11**	**4.11**	**0.1**	**27.8**	**0.16**
	** Digestion	ICP-OES	**1.42**	-	**2.45**	-	**26.5**	-	**4.99**	-	**36.84**	-
Fe	C int. ref.	LIBS	7.3	1.1	15.5	2.7	13.5	1.1	11.1	1.2	3.4	0.46
	Ag int. ref.	LIBS	5.7	0.4	24.3	4.5	14.9	0.3	10.7	1.2	4.7	0.5
	Ca int ref	LIBS	11.5	3	20.4	6	-		9.6	1.9	-	
	*Fusion	ICP-OES	**5.18**	**0.02**	**8.86**	**0.02**	**4.04**	**0.04**	**5.73**	**0.03**	**2.33**	**0.02**
	** Digestion	ICP-OES	**6.26**	-	**11.9**	-	**5.18**	-	**7.13**	-	**3.29**	-
Mg	C int. ref.	LIBS	0.94	0.18	1.16	0.2	1.44	0.08	1.63	0.09	1.72	0.2
	Ag int. ref.	LIBS	0.92	0.20	1.45	0.27	1.4	0.22	1.33	0.02	2.13	0.03
	Ca int ref	LIBS	1.02	0,29	1.25	0,37	-		1.09	0,33	-	
	*Fusion	ICP-OES	**0.52**	**0.01**	**0.78**	**0.006**	**0.71**	**0.004**	**1.23**	**0.01**	**1.86**	**0.02**
	** Digestion	ICP-OES	**0.96**	-	**1.4**	-	**1.29**	-	**2.13**	-	**3.3**	-

As it can be seen the accuracy obtained using an internal standard was far better. When calcium was employed mean accuracy ranged from 82 % recovery for Mg to 101 % and 166 % for Al and Fe respectively. These results are very sample dependant and as calcium had to be measured first, this procedure was not found ideal for fast and nevertheless accurate determination of major elements in fly ash samples.

Other internal standards, brought by the binder were silver and carbon. Using silver as an internal reference, the mean recovery (calculated from the 5 sample) was 107% for Al and Ca 175 for Fe and

89 % for Mg. When carbon is employed the values are slightly higher with: 118% for Al, 89% for Ca, 153 for Fe and 84% for Mg. A significant degradation of the recovery is obtained for iron measurements. The mapping of this element was therefore made using SEM-EDS to verify its homogeneity at the sample surface.

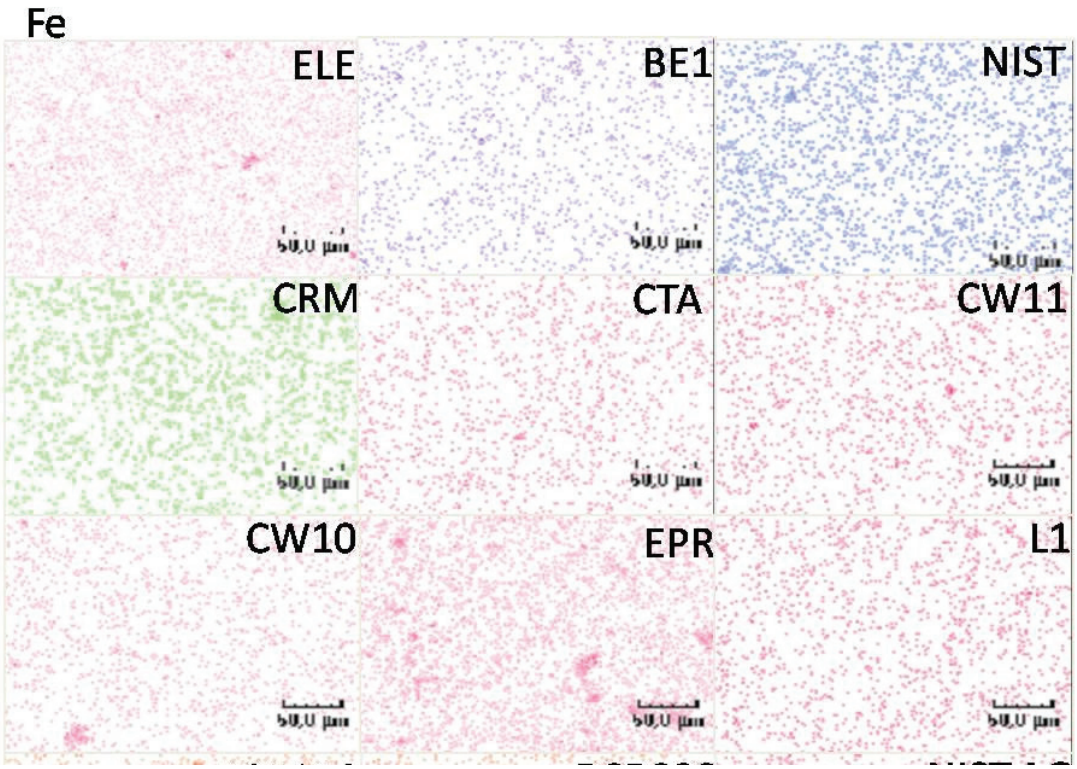

Figure III. 32: SEM-EDS cartography observation of iron in the pellets with 50 µm step.

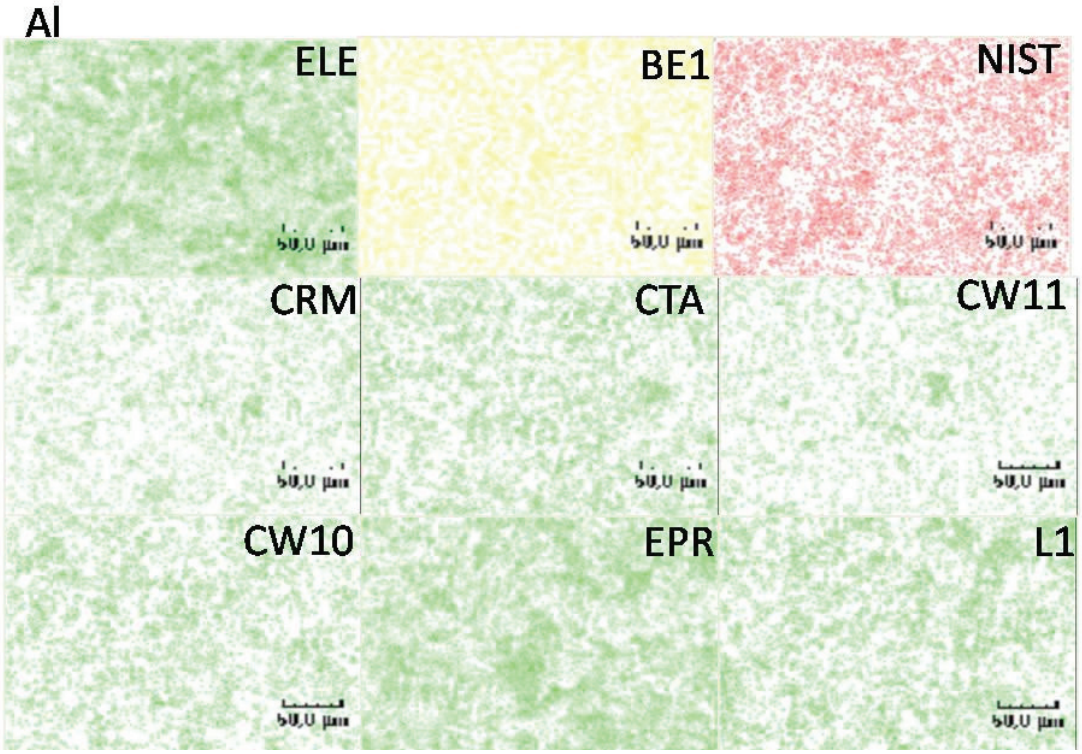

Figure III. 33: The SEM-EDS mapping characterisation of aluminium presence in the samples; set of pellets with cellulose binder.

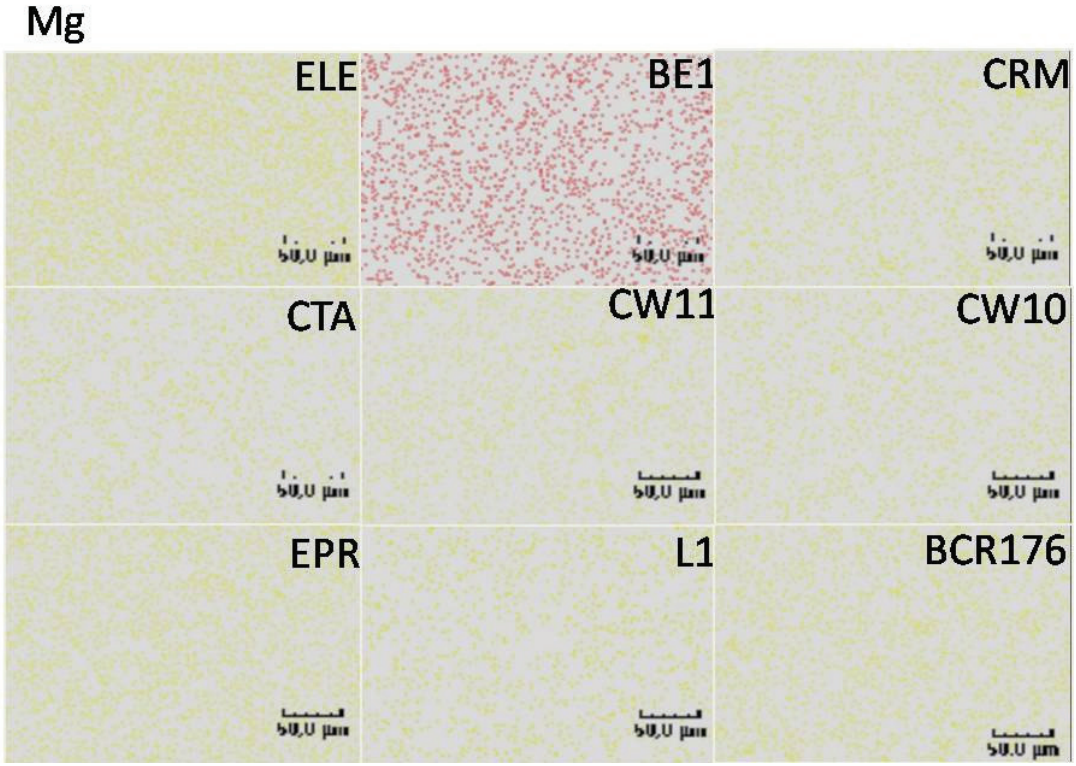

Figure III. 34: The SEM-EDS mapping on the pellets surface of magnesium presence in the samples.

With a comparison of element mapping, it can be seen that only iron in certain sample (CW10 and EPR) is not homogeneous. This phenomenon could partially explain the lack of accuracy obtained for this element.

The LIBS measurement is made on a restricted surface (i.e. 150µm diameter spot) while sampling for wet digestion or alkali fusion is made on a larger part of the sample.

III.6.2 LA-ICP-MS analysis

The accuracy of the measurements was calculated also for the LA-ICP-MS measurements for the series of pellets and conditions which were found to have the highest sensitivity. The maleic acid, caffeine and cellulose binder with the use of collision cell were used for this purpose. The cellulose binder without use of collision cell was used as a standard condition and the accuracy results were compared. The arsenic, chromium, copper, manganese, lead, strontium, vanadium and zinc were analyse and the concentration of real samples was calculated. As in the case of LIBS measurements, four reference materials were used as standards and the five other samples were used as real samples, **Table III. 24** A and B.

Table III. 24-A: Comparison of concentrations found using wet digestion and LA ICP MS.

	Arsenic mg/kg			Chromium			Copper			Manganese		
	WD*	LA ICP MS	Recov (%)	WD	LA ICP MS	Recov (%)	WD	LA ICP MS	Recov (%)	WD	LA ICP MS	Recov (%)
CW10												
C		517	88		83	93		77	114		377	43
M		591	101		-	-		70	104		563	64
caf	585	472	81	88	-	-	67	51	76	881	569	65
CT		444	76		11	13		70	105		433	49
CW11												
C		21	95	85	83	93		53	107		320	72
M		32	145		-	-		56	113		609	137
caf	22	48	217		-	-	50	36	73	443	541	122
CT		28	126		-	-		44	88		417	94
EPR												
C		42	51		121	60		100	52		534	34
M		59	47		-	-		102	53		731	47
caf	82	59	49	202	-	-	192	75	39	1558	760	49
CT		41	50		55	27		83	43		482	31
L1												
C		204	88		133	55		87	87		112	33
M		260	112		-	-		82	82		341	99
caf	233	206	88	240	-	-	99	63	64	345	318	92
CT		191	82		79	45		74	74		180	52

WD* are results obtained after wet digestion.

Table III. 25-B: Comparison of concentrations found using wet digestion and LA ICP MS.

	Lead			Strontium			Vanadium			Zinc		
	WD*	LA ICP MS	Recov (%)	WD	LA ICP MS	Recov (%)	WD	LA ICP MS	Recov (%)	WD	LA ICP MS	Recov (%)
CW10												
C	57	114	201	391	197	50	125	173	138	162	-	-
M		113	199		410	105		207	166		206	127
caf		113	200		420	107		185	148		187	115
CT		80	141		222	57		163	131		-	-
CW11												
C	24	112	475	1573	927	59	148	113	77	53	-	-
M		113	480		1192	76		121	82		150	284
caf		107	453		1291	82		120	81		80	152
CT		86	364		983	63		89	60		-	-
EPR												
C	66	112	171	340	186	55	210	294	140	228	-	-
M		117	178		381	112		259	124		251	110
caf		112	171		383	113		310	148		168	74
CT		78	119		201	59		243	116		-	-
L1												
C	73	110	150	387	169	44	278	284	102	220	-	-
M		124	171		375	97		280	101		245	111
caf		121	167		386	100		256	92		194	88
CT		79	108		196	51		259	93		-	-

WD* are results obtained after wet digestion.

On the tables (**Table III. 24-A** and **Table III. 25-B:**) the accuracy of selected elements was calculated. Because of big differences in certified and found values for several elements, the possibility of use of internal standard was evaluated for the same elements and the same conditions, **Table III. 26-A** and **B**.

Table III. 26-A: Accuracy calculations for selected elements and real samples with the use of calcium as internal standard.

Calcium used as internal standard												
	Arsenic mg/kg			**Chromium**			**Copper**			**Manganese**		
	WD*	LA ICP MS	Recov (%)	WD	WD*	LA ICP MS	Recov (%)	WD	WD*	LA ICP MS	Recov (%)	WD
CW10												
C		1018	174		90	103.7		75	112		838	95
M	584	1023	174	90	105	119	65	405	83	878	981	111
caf		424	73		60	68		22	70		815	93
CT		848	145		40	48		26	133		912	104
CW11												
C		136	612		-	-		59	121		-	-
M	22	111	576	85	-	-	48	-	-	442	-	-
caf		221	1015		-	-		1	3		-	-
CT		184	877		-	-		111	204		-	-
EPR												
C		61	74		257	127		135	71		1514	97
M	81	81	100	203	228	113	191	162	84	1558	1766	113
caf		34	42		147	73		88	46		1485	95
CT		71	88		191	94		127	67		1325	85
L1												
C		383	165		366	153		102	103		251	73
M	233	507	218	240	351	146	99	119	120	345	254	74
caf		158	68		149	62		68	69		162	47
CT		473	203		294	123		116	117		361	105

Table III. 276-B: Accuracy calculations for selected elements and real samples with the use of calcium as internal standard.

Calcium used as internal standard												
	Lead			**Strontium**			**Vanadium**			**Zinc**		
	WD*	LA ICP MS	Recov (%)	WD*	LA ICP MS	Recov (%)	WD*	LA ICP MS	Recov (%)	WD*	LA ICP MS	Recov (%)
CW10												
C	55	130	226	389	254	65	125	309	250	160	200	124
M		140	246		404	104		2321	253		299	184
caf		75	129		274	70		91	149		-	-
CT		40	70		264	67		67	187		28	12
CW11												
C	24	280	1185	1573	-	-	147	-	-	52	-	-
M		774	3325		-	-		-	-		958	1779
caf		332	1386		-	-		2	55		-	-
CT		-	-		-	-		6	155		-	-
EPR												
C	66	88	134	341	453	134	211	424	202	228	235	103
M		96	144		446	131		404	193		328	143
caf		51	77		296	87		284	135		27	12
CT		56	85		492	145		363	172		289	127
L1												
C	72	88	121	386	565	146	278	469	169	220	264	120
M		98	134		592	153		500	180		328	149
caf		57	78		364	94		236	85		111	50
CT		97	132		639	165		426	153		521	237

WD* are results obtained after wet digestion; C – cellulose binder, M – Maleic acid CCT, caf – caffeine with CCT, CT – cellulose binder with CCT

Generally results are in good agreement between LA-ICP and wet digestion, using external calibration. Some elements are overestimated in the pellets containing chromophores indicating a possible contamination or an enhanced fractionation effect. As an example, difficulties were observed for the chromium determination and especially for the CW11 sample.

As shown in **Table III. 26-A, B** results obtained using internal standard are not significantly different. As a conclusion a calibration made form reference materials was found perfectly adapted for the

determination of minor elements in most fly ash samples, even if their origin was drastically different (bituminous coal, brown coal or domestic waste fly ash).

III.6.3 Conclusion accuracy

In this chapter, accuracy was calculated for both evaluated analytical systems – LIBS and LA-ICP-MS systems for all series of pellets. In the case of LIBS system, only the major elements were evaluated, while LA-ICP-MS system was employed for trace element determination. For major elements a good agreement was found between the alkali fusion, wet digestion and LIBS measurements.

The accuracy was calculated also for the LA-ICP-MS measurements for selected conditions – cellulose binder with the use of collision cell, maleic acid and caffeine also with the use of collision cell. For minor elements a good agreement was also obtained.

III.7 REFERENCES

1. Ito, K., et al., *LA-ICP-MS analysis of pressed powder pellets to luminescence geochronology.* Chemical Geology, 2009. **262**(3-4): p. 131-137.
2. Vanheuzen, A.A. and J.B.W. Morsink, *Analysis of Solids by Laser Ablation Inductively Coupled Plasma Mass-Spectrometry (La-Icp-Ms) .2. Matching with a Pressed Pellet.* Spectrochimica Acta Part B-Atomic Spectroscopy, 1991. **46**(14): p. 1819-1828.
3. O´Connor, C., M. Landon, and B. Sharp, *Absorption coefficient modified pressed powders for calibration of laser ablation inductively coupled plasma mass spectrometry.* Journal of Analytical Atomic Spectrometry, 2007. **22**(3): p. 273-282.
4. Lee, Y.L., C.C. Chang, and S.J. Jiang, *Laser ablation inductively coupled plasma mass spectrometry for the determination of trace elements in soil.* Spectrochimica Acta Part B-Atomic Spectroscopy, 2003. **58**(3): p. 523-530.
5. Weis, P., H. Beck, and D. Günther, *Characterizing ablation and aerosol generation during elemental fractionation on absorption modified lithium tetraborate glasses using LA-ICP-MS.* Analytical and Bioanalytical Chemistry, 2005. **381**(1): p. 212-224.
6. Qi, H., et al., *Spatial spectroscopic diagnose of the plasma produced from laser ablation of a KTA crystal.* Laser Physics Letters, 2007. **4**(3): p. 212-217.
7. De Giacomo, A., *Experimental characterization of metallic titanium-laser induced plasma by time and space resolved optical emission spectroscopy.* Spectrochimica Acta Part B: Atomic Spectroscopy, 2003. **58**(1): p. 71-83.
8. Estupinan, H., et al., *Stoichiometry analysis of titanium oxide coating by LIBS.* European Physical Journal D, 2009. **53**(1): p. 69-73.
9. Estupinan, H., et al., *Analysis of the composition of titanium oxide coating by Laser Induced Breakdown Spectroscopy.* Riao/Optilas 2007, 2008. **992**: p. 1213-1216.
10. Aguilera, J.A. and C. Aragon, *Characterization of a laser-induced plasma by spatially resolved spectroscopy of neutral atom and ion emissions. Comparison of local and spatially integrated measurements.* Spectrochimica Acta Part B-Atomic Spectroscopy, 2004. **59**(12): p. 1861-1876.
11. Aguilera, J.A. and C. Aragon, *Multi-element Saha-Boltzmann and Boltzmann plots in laser-induced plasmas.* Spectrochimica Acta Part B-Atomic Spectroscopy, 2007. **62**(4): p. 378-385.
12. Aragon, C. and J.A. Aguilera, *Characterization of laser induced plasmas by optical emission spectroscopy: A review of experiments and methods.* Spectrochimica Acta Part B-Atomic Spectroscopy, 2008. **63**(9): p. 893-916.

13. Aragon, C., J. Bengoechea, and J.A. Aguilera, *Influence of the optical depth on spectral line emission from laser-induced plasmas.* Spectrochimica Acta Part B-Atomic Spectroscopy, 2001. **56**(6): p. 619-628.
14. De Giacomo, A., et al., *ns- and fs-LIBS of copper-based-alloys: A different approach.* Applied Surface Science, 2007. **253**(19): p. 7677-7681.
15. Fantoni, R., et al., *Methodologies for laboratory Laser Induced Breakdown Spectroscopy semi-quantitative and quantitative analysis-A review.* Spectrochimica Acta Part B-Atomic Spectroscopy, 2008. **63**(10): p. 1097-1108.
16. Gornushkin, I.B., et al., *Radiation dynamics of post-breakdown laser induced plasma.* Spectrochimica Acta Part B-Atomic Spectroscopy, 2004. **59**(4): p. 401-418.
17. Aydin, Ü., et al., *Spectral line selection for time-resolved investigations of laser-induced plasmas by an iterative Boltzmann plot method.* Spectrochimica Acta Part B: Atomic Spectroscopy, 2008. **63**(10): p. 1060-1065.
18. Lacroix, D., C. Boudot, and G. Jeandel, *Spectroscopic studies of GTA welding plasmas. Temperature calculation and dilution measurement.* European Physical Journal-Applied Physics, 1999. **8**(1): p. 61-69.
19. Aguilera, J., et al., *Application of calibration-free laser-induced breakdown spectroscopy to radially resolved spectra from a copper-based alloy laser-induced plasma.* Spectrochimica Acta Part B: Atomic Spectroscopy, 2009. **64**(7): p. 685-689.
20. Aragon, C., F. Penalba, and J.A. Aguilera, *Curves of growth of neutral atom and ion lines emitted by a laser induced plasma.* Spectrochimica Acta Part B-Atomic Spectroscopy, 2005. **60**(7-8): p. 879-887.
21. Hill, S., *Inductively coupled plasma spectrometry and its applications*. 1999: Blackwell.
22. Nagaishi, K. and T. Ishikawa, *A simple method for the precise determination of boron, zirconium, niobium, hafnium and tantalum using ICP-MS and new results for rock reference samples.* Geochemical Journal, 2009. **43**(2): p. 133-141.
23. Warnken, K.W., H. Zhang, and W. Davison, *Analysis of polyacrylamide gels for trace metals using diffusive gradients in thin films and laser ablation inductively coupled plasma mass spectrometry.* Analytical Chemistry, 2004. **76**(20): p. 6077-6084.
24. Gravel, J.F.Y., et al., *Multielemental laser-enhanced ionization spectrometry for the determination of lead at the trace level in pelletized coal using laser ablation and internal standard signal normalization.* Applied Spectroscopy, 2004. **58**(6): p. 727-733.

IV CONCLUSIONS

In this work, two methods based on laser ablation were optimized for fly ash analysis. Laser Induced Breakdown Spectroscopy (LIBS) was used for quantitative determination of major elements in fly ash samples and Laser Ablation Inductively Coupled Plasma Mass Spectrometry (LA-ICP-MS) was used for quantitative minor and trace element determination.

The following conclusions can be drawn from this study:

- ☑ Sample homogenisation is important parameter to obtain homogeneous element distribution in the samples. Binder evaluation showed that silver as a binder improved signal intensities obtained for LIBS measurements, but this binder did not allow preparing sufficiently mechanically stable pellets. From all tested binders cellulose and mixture of powder silver and cellulose were selected for LIBS measurements. Mixed binder was found to be compromise between the maximal signal intensities and mechanical stability of pellets.

- ☑ To improve sensitivity on LA-ICP-MS, organic modifiers were tested as it was reported by several authors. The use of a collision cell to eliminate polyatomic interferences was also evaluated. Addition of maleic acid and caffeine, as chromophores, with the use of collision cell were found to give best results.

- ☑ Because external calibration was found difficult for several evaluated elements, the possibility of utilisation of internal standard was evaluated. Several internal standards were tested – carbon and silver were selected because they were present in the binders, so it can be supposed that they were homogeneously distributed within the samples and their concentrations can be supposed as constant in all samples. The homogeneous binder distribution was verified using SEM-EDS measurements Calcium, naturally present in samples in high concentrations, gave significant improvements in calibration trends for all evaluated elements. The disadvantage of this internal standard is that its concentration must be known before analysis.

- ☑ After selection of optimised conditions and binders, the detection limits were calculated for both evaluated techniques and for LIBS measurements the detection limits were in range of hundreds of mg/kg for all evaluated major elements (Al, Ca, Fe and Mg). In the case of LA-ICP-MS measurements, the detection limits were lower than mg/kg range for a majority of evaluated minor and trace elements.

- ☑ The LIBS spectroscopy was employed to determine Fe, Mg, Ca, Si and Al in selected samples. A multi-matrix calibration curve built using reference materials gave good results when using an internal standard (carbon or silver). Determination of Fe, Mg, Ca, Si and Al was in good agreement with classical determination by ICP-OES after a wet digestion or an alkali fusion. The method developed in this study is quite promising as the sample preparation of the fly ashes is simple and fast and the LIBS spectra recorded in a few seconds. The obtained calibration curves may be employed for the determination of Ca, Al, Mg and Fe in different fly ashes samples (i.e. from coal based power plant to chemical waste incinerator). One of the problems encountered during this work was the homogeneity at the sample surface. Even if ball mill grinding was found efficient aggregates of iron could be observed on a sample.

- ☑ The LA-ICP-MS system was employed for the same selected sampleto determine minor elements. A four points calibration using reference materials as standards was appropriate for quantification of As, Ni, Pb, Zn, Cu, Ba, Sr and V. Accuracy was acceptable for most elements when using LA-ICP-MS (or LA-ICP-OES). The difficulty of such a procedure is to adapt the calibration range to the determined concentrations, a careful selection of the CRMs employed for calibration has to be made. Use of an internal standard, added or already present in the sample was appropriate.

A major finding of this work reveals that analysis of fly ash samples using laser ablation methods is possible for both major and minor elements.